THE EUROPEAN
PHYSICAL JOURNAL C

CrossMark

Regular Article - Experimental Physics

Constraints on the off-shell Higgs boson signal strength in the high-mass ZZ and WW final states with the ATLAS detector

ATLAS Collaboration[*]

CERN, 1211 Geneva 23, Switzerland

Abstract Measurements of the ZZ and WW final states in the mass range above the $2m_Z$ and $2m_W$ thresholds provide a unique opportunity to measure the off-shell coupling strength of the Higgs boson. This paper presents constraints on the off-shell Higgs boson event yields normalised to the Standard Model prediction (signal strength) in the $ZZ \rightarrow 4\ell$, $ZZ \rightarrow 2\ell2\nu$ and $WW \rightarrow e\nu\mu\nu$ final states. The result is based on pp collision data collected by the ATLAS experiment at the LHC, corresponding to an integrated luminosity of 20.3 fb^{-1} at a collision energy of $\sqrt{s} = 8$ TeV. Using the CL_s method, the observed 95 % confidence level (CL) upper limit on the off-shell signal strength is in the range 5.1–8.6, with an expected range of 6.7–11.0. In each case the range is determined by varying the unknown $gg \rightarrow ZZ$ and $gg \rightarrow WW$ background K-factor from higher-order quantum chromodynamics corrections between half and twice the value of the known signal K-factor. Assuming the relevant Higgs boson couplings are independent of the energy scale of the Higgs boson production, a combination with the on-shell measurements yields an observed (expected) 95 % CL upper limit on Γ_H/Γ_H^{SM} in the range 4.5–7.5 (6.5–11.2) using the same variations of the background K-factor. Assuming that the unknown $gg \rightarrow VV$ background K-factor is equal to the signal K-factor, this translates into an observed (expected) 95 % CL upper limit on the Higgs boson total width of 22.7 (33.0) MeV.

1 Introduction

The observation of a new particle in the search for the Standard Model (SM) Higgs boson at the LHC, reported by the ATLAS [1] and CMS [2] Collaborations, is a milestone in the quest to understand electroweak symmetry breaking. Precision measurements of the properties of the new boson are of critical importance. Among its key properties are the couplings to each of the SM fermions and bosons, for which ATLAS and CMS presented results in Refs. [3,4],

and spin/CP properties, studied by ATLAS and CMS in Refs. [5,6].

The studies in Refs. [7–10] have shown that the high-mass off-peak regions beyond $2m_V$ ($V = Z, W$), well above the measured resonance mass of about 125 GeV [4,11], in the $H \rightarrow ZZ$ and $H \rightarrow WW$ channels are sensitive to Higgs boson production through off-shell and background interference effects. This presents a novel way of characterising the properties of the Higgs boson in terms of the off-shell event yields, normalised to the SM prediction (referred to as signal strength μ), and the associated off-shell Higgs boson couplings. Such studies provide sensitivity to new physics that alters the interactions between the Higgs boson and other fundamental particles in the high-mass region [12–18]. This approach was used by the CMS Collaboration [19] to set an indirect limit on the Higgs boson total width. The analysis presented in this paper is complementary to direct searches for Higgs boson to invisible decays [20,21] and to constraints coming from the Higgs boson coupling tests [3,4].

This paper presents an analysis of the off-shell signal strength in the $ZZ \rightarrow 4\ell$, $ZZ \rightarrow 2\ell2\nu$ and $WW \rightarrow e\nu\mu\nu$ final states ($\ell = e, \mu$). It is structured as follows: Sect. 2 discusses the key theoretical considerations and the simulation of the main signal and background processes. Sections 3–5 give details for the analysis in the $ZZ \rightarrow 4\ell$, $ZZ \rightarrow 2\ell2\nu$ and $WW \rightarrow e\nu\mu\nu$ final states, respectively. The dominant systematic uncertainties are discussed in Sect. 6. Finally the results of the individual analyses and their combination are presented in Sect. 7.

The ATLAS detector is described in Ref. [22]. The present analysis is performed on pp collision data corresponding to an integrated luminosity of 20.3 fb^{-1} at a collision energy of $\sqrt{s} = 8$ TeV.

2 Theoretical predictions and simulated samples

The cross-section $\sigma_{\text{off-shell}}^{gg \rightarrow H^* \rightarrow VV}$ for the off-shell Higgs boson production through gluon fusion with subsequent decay into

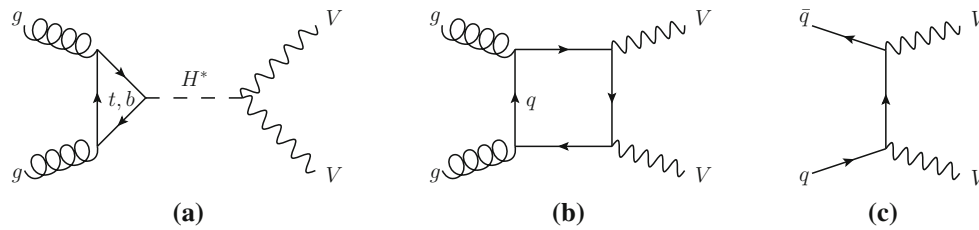[*] e-mail: atlas.publications@cern.ch

Fig. 1 The leading-order Feynman diagrams for **a** the $gg \to H^* \to VV$ signal, **b** the continuum $gg \to VV$ background and **c** the $q\bar{q} \to VV$ background

vector-boson pairs,[1] as illustrated by the Feynman diagram in Fig. 1a, is proportional to the product of the Higgs boson couplings squared for production and decay. However, unlike the on-shell Higgs boson production, $\sigma_{\text{off-shell}}^{gg \to H^* \to VV}$ is independent of the total Higgs boson decay width Γ_H [7,8]. Using the framework for Higgs boson coupling deviations as described in Ref. [23], the off-shell signal strength in the high-mass region selected by the analysis described in this paper at an energy scale $\hat{s}$, $\mu_{\text{off-shell}}(\hat{s})$, can be expressed as:

$$\mu_{\text{off-shell}}(\hat{s}) \equiv \frac{\sigma_{\text{off-shell}}^{gg \to H^* \to VV}(\hat{s})}{\sigma_{\text{off-shell, SM}}^{gg \to H^* \to VV}(\hat{s})} = \kappa_{g,\text{off-shell}}^2(\hat{s}) \cdot \kappa_{V,\text{off-shell}}^2(\hat{s}),$$
(1)

where $\kappa_{g,\text{off-shell}}(\hat{s})$ and $\kappa_{V,\text{off-shell}}(\hat{s})$ are the off-shell coupling scale factors associated with the $gg \to H^*$ production and the $H^* \to VV$ decay. Due to the statistically limited sensitivity of the current analysis, the off-shell signal strength and coupling scale factors are assumed in the following to be independent of $\hat{s}$ in the high-mass region selected by the analysis. The off-shell Higgs boson signal cannot be treated independently from the $gg \to VV$ background, as sizeable negative interference effects appear [7]. The interference term is proportional to $\sqrt{\mu_{\text{off-shell}}} = \kappa_{g,\text{off-shell}} \cdot \kappa_{V,\text{off-shell}}$.

In contrast, the cross-section for on-shell Higgs boson production allows a measurement of the signal strength:

$$\mu_{\text{on-shell}} \equiv \frac{\sigma_{\text{on-shell}}^{gg \to H \to VV}}{\sigma_{\text{on-shell, SM}}^{gg \to H \to VV}} = \frac{\kappa_{g,\text{on-shell}}^2 \cdot \kappa_{V,\text{on-shell}}^2}{\Gamma_H / \Gamma_H^{\text{SM}}},$$
(2)

which depends on the total width Γ_H. Assuming identical on-shell and off-shell Higgs boson coupling scale factors, the ratio of $\mu_{\text{off-shell}}$ to $\mu_{\text{on-shell}}$ provides a measurement of the total width of the Higgs boson. This assumption is particularly relevant to the running of the effective coupling $\kappa_g(\hat{s})$ for the loop-induced $gg \to H$ production process, as it is

---

[1] In the following the notation $gg \to (H^* \to)VV$ is used for the full signal + background process for $VV = ZZ$ and WW production, including the Higgs boson signal (S) $gg \to H^* \to VV$ process, the continuum background (B) $gg \to VV$ process and their interference. For vector-boson fusion (VBF) production, the analogous notation VBF $(H^* \to)VV$ is used for the full signal plus background process, with VBF $H^* \to VV$ representing the Higgs boson signal and VBF VV denoting the background.

sensitive to new physics that enters at higher mass scales and could be probed in the high-mass m_{VV} signal region of this analysis. More details are given in Refs. [12–16]. With the current sensitivity of the analysis, only an upper limit on the total width Γ_H can be determined, for which the weaker assumption

$$\kappa_{g,\text{on-shell}}^2 \cdot \kappa_{V,\text{on-shell}}^2 \leq \kappa_{g,\text{off-shell}}^2 \cdot \kappa_{V,\text{off-shell}}^2,$$
(3)

that the on-shell couplings are no larger than the off-shell couplings, is sufficient. It is also assumed that any new physics which modifies the off-shell signal strength $\mu_{\text{off-shell}}$ and the off-shell couplings $\kappa_{i,\text{off-shell}}$ does not modify the predictions for the backgrounds. Further, neither are there sizeable kinematic modifications to the off-shell signal nor new, sizeable signals in the search region of this analysis unrelated to an enhanced off-shell signal strength [18,24].

While higher-order quantum chromodynamics (QCD) and electroweak (EW) corrections are known for the off-shell signal process $gg \to H^* \to ZZ$ [25], which are also applicable to $gg \to H^* \to WW$, no higher-order QCD calculations are available for the $gg \to VV$ background process, which is evaluated at leading order (LO). Therefore the results are given as a function of the unknown K-factor for the $gg \to VV$ background. QCD corrections for the off-shell signal processes have only been calculated inclusively in the jet multiplicity. The experimental analyses are therefore performed inclusively in jet observables, and the event selections are designed to minimise the dependence on the boost of the VV system, which is sensitive to the jet multiplicity.

The dominant processes contributing to the high-mass signal region in the $ZZ \to 4\ell$, $ZZ \to 2\ell2\nu$ and $WW \to e\nu\mu\nu$ final states are: the $gg \to H^* \to VV$ off-shell signal, the $gg \to VV$ continuum background, the interference between them, VV production in association with two jets through VBF and VH-like production modes $pp \to VV + 2j$ (s-, t- and u-channel) and the $q\bar{q} \to VV$ background. The LO Feynman diagrams for the $gg \to H^* \to VV$ signal, the continuum $gg \to VV$ background and the dominant irreducible $q\bar{q} \to VV$ background are depicted in Fig. 1. The $WW \to e\nu\mu\nu$ channel also receives sizeable background contributions from $t\bar{t}$ and single-top production. In the following a Higgs boson mass of $m_H = 125.5$ GeV, close to the ATLAS-measured Higgs boson mass value of
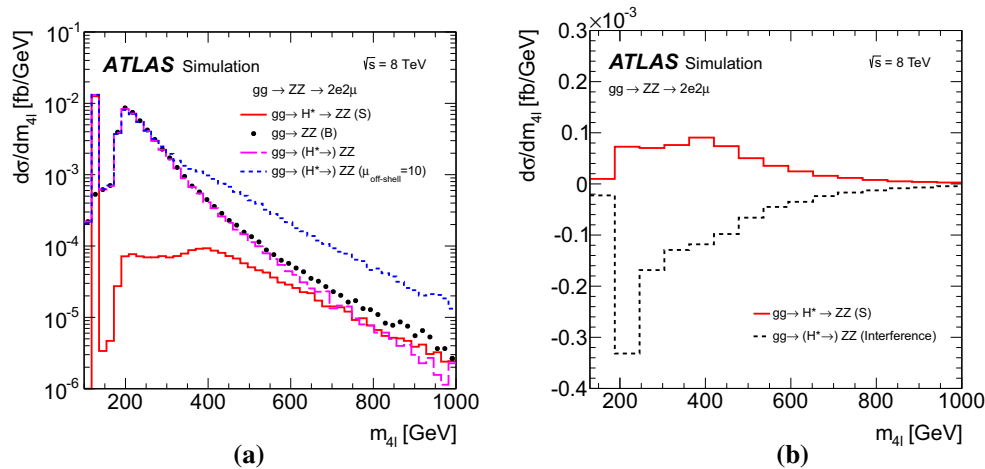
(a)   **(b)**

Fig. 2 a Differential cross-sections as a function of the four-lepton invariant mass $m_{4\ell}$ in the range of 100 GeV $< m_{4\ell} <$ 1000 GeV for the $gg \rightarrow (H^* \rightarrow)ZZ \rightarrow 2e2\mu$ channel at the parton level, for the $gg \rightarrow H^* \rightarrow ZZ$ signal (*solid line*), $gg \rightarrow ZZ$ continuum background (*dots*), $gg \rightarrow (H^* \rightarrow)ZZ$ with SM Higgs boson couplings (*long-dashed line*, including sig-nal plus background plus interference) and $gg \rightarrow (H^* \rightarrow)ZZ$ with $\mu_{\text{off-shell}} = 10$ (*dashed line*). **b** Differential cross-section as a function of $m_{4\ell}$ in the range of 130 GeV $< m_{4\ell} <$ 1000 GeV for the SM $gg \rightarrow H^* \rightarrow ZZ \rightarrow 2e2\mu$ signal (*solid line*) and its interference with the $gg \rightarrow ZZ \rightarrow 2e2\mu$ continuum background (*dashed line*)

125.36 GeV [11], is assumed for the off-shell signal processes. This small difference has a negligible impact on the predicted off-shell production yields.

Figure 2 illustrates the size and kinematic properties of the gluon-induced signal and background processes by showing the four-lepton invariant mass ($m_{4\ell}$) distribution for the $gg \rightarrow (H^* \rightarrow)ZZ \rightarrow 2e2\mu$ processes after applying the event selections in the $ZZ \rightarrow 4\ell$ channel (see Sect. 3) on generator-level quantities. The process $gg \rightarrow (H^* \rightarrow)ZZ \rightarrow 2e2\mu$ is shown for the SM $\mu_{\text{off-shell}} = 1$ case and for an increased off-shell signal with $\mu_{\text{off-shell}} = 10$. For low masses $m_{ZZ} < 2m_Z$ the off-shell signal is negligible, while it becomes comparable to the continuum $gg \rightarrow ZZ$ background for masses above the $2m_t$ threshold. The interference between the $gg \rightarrow H^* \rightarrow ZZ$ signal and the $gg \rightarrow ZZ$ background is neg-ative over the whole mass range. A very similar relation between the $gg \rightarrow H^* \rightarrow VV$ signal and the $gg \rightarrow VV$ background is also seen for the $gg \rightarrow (H^* \rightarrow)ZZ \rightarrow 2\ell2\nu$ and $gg \rightarrow (H^* \rightarrow)WW \rightarrow e\nu\mu\nu$ processes.

The detector simulation for most generated Monte Carlo (MC) event samples is performed using Geant4 [26,27]. Some background MC samples in the $WW \rightarrow e\nu\mu\nu$ analysis for processes with large cross-sections are simulated with the fast detector simulation package Atlfast-II [27].

2.1 Simulation of $gg \rightarrow (H^* \rightarrow)VV$

To generate the $gg \rightarrow H^* \rightarrow VV$ and $gg \rightarrow VV$ processes, including the interference, the LO MC generators gg2VV [7, 28] and MCFM [9,10] together with PYTHIA8 [29] and SHERPA+OpenLoops [30–33] are used. The QCD renor-malisation and factorisation scales are set to $m_{VV}/2$ [9]. The CT10 next-to-next-to-leading-order (NNLO) PDF set [34] is used, as the LO $gg \rightarrow VV$ process is part of the NNLO cal-culation for $pp \rightarrow VV$. The default parton showering and hadronisation option for the events processed with the full detector simulation is PYTHIA8 with the "power shower" parton shower option [29].

For the $gg \rightarrow H^* \rightarrow VV$ signal, a NNLO/LO K-factor[2] including the next-to-leading-order (NLO) electroweak cor-rections, $K^{H^*}(m_{VV}) = \sigma^{\text{NNLO}}_{gg \rightarrow H^* \rightarrow VV}/\sigma^{\text{LO}}_{gg \rightarrow H^* \rightarrow VV}$, is applied. The K-factor and associated uncertainties are cal-culated in Ref. [25] as a function of the Higgs boson virtual-ity m_{VV} for $m_H \sim 125.5$ GeV, using the MSTW2008 PDF set [35]. Additional corrections are used to re-weight the pre-dictions to the CT10 NNLO PDF set used in the simulation.

For the $gg \rightarrow VV$ background and the interference with the $gg \rightarrow H^* \rightarrow VV$ signal, no higher-order QCD calcula-tions are available. However, these corrections are studied for the WW final state in Ref. [36] in the soft-collinear approx-imation, which is considered suitable for high-mass Higgs boson production. In this approximation, the signal K-factor is found to provide a reliable estimate for the higher-order QCD corrections to the signal-background interference term.

The K-factor for the $gg \rightarrow VV$ background process, $K(gg \rightarrow VV)$, remains unknown. Therefore, the results in this note are given as a function of the unknown K-factor ratio between the $gg \rightarrow VV$ background and the $gg \rightarrow H^* \rightarrow VV$ signal, defined as

---

[2] The shorter $gg \rightarrow X$ notation is used also in the context of higher-order QCD calculations where qg and qq initial states contribute to the full $pp \rightarrow X$ process.

$$R_{H^*}^B = \frac{K(gg \to VV)}{K(gg \to H^* \to VV)} = \frac{K^B(m_{VV})}{K_{gg}^{H^*}(m_{VV})}, \tag{4}$$

where $K^B(m_{VV})$ is the unknown mass-dependent K-factor for the $gg \to VV$ background, and $K_{gg}^{H^*}(m_{VV})$ is the gluon-initiated K-factor [25] for the signal[3] as motivated by the soft-collinear approximation in Ref. [36]. Because the K-factor $K_{gg}^{H^*}(m_{VV})$ changes by less than 10 % as a function of m_{VV} in the relevant region of phase space, no mass dependence on $R_{H^*}^B$ is assumed. The range 0.5–2 is chosen for the variation of the K-factor ratio $R_{H^*}^B$ in order to include the full correction from the signal K-factor $K_{gg}^{H^*}(m_{VV}) \sim 2$ in the variation range. With respect to the LO $gg \to VV$ process, this corresponds to an absolute variation in the approximate range 1–4. Using the K-factors discussed above, the cross-section for the $gg \to (H^* \to) VV$ process with any off-shell Higgs boson signal strength $\mu_{\text{off-shell}}$ can be parameterised as:

$$\sigma_{gg \to (H^* \to) VV}(\mu_{\text{off-shell}}, m_{VV})$$
$$= K^{H^*}(m_{VV}) \cdot \mu_{\text{off-shell}} \cdot \sigma_{gg \to H^* \to VV}^{\text{SM}}(m_{VV})$$
$$+ \sqrt{K_{gg}^{H^*}(m_{VV}) \cdot K^B(m_{VV}) \cdot \mu_{\text{off-shell}}} \cdot \sigma_{gg \to VV, \text{Interference}}^{\text{SM}}(m_{VV})$$
$$+ K^B(m_{VV}) \cdot \sigma_{gg \to VV, \text{cont}}(m_{VV}). \tag{5}$$

More details are given in Appendix A.1.

In addition, higher-order QCD corrections to the transverse momentum[4] p_T and the rapidity y of the VV system are studied using SHERPA+OpenLoops, which includes matrix-element calculations for the first hard jet emission. A difference of order 20 % in the ratio of the p_T of the VV system in the relevant kinematic region is observed when comparing the LO generators with parton shower to SHERPA+OpenLoops, while the difference in the rapidity y of the VV system is small. This difference in the p_T of the VV system can modify the kinematic observables used in the analyses, leading to variations in both the kinematic shapes and acceptance which are not covered by the m_{VV} dependent systematic uncertainties derived in Ref. [25]. To account for these effects, the LO generators are re-weighted

to SHERPA+OpenLoops in the p_T of the VV system. Due to the different jet emission mechanisms in the signal and the background processes, different re-weighting functions are derived for the $gg \to H^* \to VV$ signal, the $gg \to VV$ background, and the total $gg \to (H^*) \to VV$, respectively. The impact of the re-weighting on the acceptance is below 1 % for the signal and at the level of 4–6 % for the background. In the $ZZ \to 4\ell$ channel, the re-weighting procedure is only used to account for the acceptance effects, as the matrix-element-based discriminant is insensitive to the p_T of the ZZ system. For the $ZZ \to 2\ell2\nu$ channel, the re-weighting is used in both the transverse mass shape and acceptance as the m_T depends on the p_T of the ZZ system. For the $WW \to e\nu\mu\nu$ channel, the re-weighting affects only the acceptance.

2.2 Simulation of electroweak VV production through VBF and VH-like processes

The electroweak[5] $pp \to VV + 2j$ processes contain both VBF-like events and VH-like events, which are simulated using MadGraph5 [37] and cross-checked using PHANTOM [38]. The QCD renormalisation and factorisation scales are set to m_W following the recommendation in Ref. [39] and the CTEQ6L1 PDF set [40] is used. PYTHIA6 [41] is used for parton showering and hadronisation.

The high-mass range selected by this analysis includes Higgs boson signal events arising from:

- the off-shell VBF $H \to VV$ process, which scales with $\kappa_{V,\text{off-shell}}^4$ and is independent of Γ_H,
- VBF-like VV processes with a t-channel Higgs boson exchange, which scale with $\kappa_{V,\text{off-shell}}^4$ and are independent of Γ_H,
- WH and ZH processes with an on-shell Higgs boson, with decays $Z \to 2\ell$ or $W \to \ell\nu$ and $H \to 2\ell2j$ or $H \to \ell\nu2j$, which scale with $\kappa_{V,\text{on-shell}}^4 / \Gamma_H$,

where we assume the same coupling strength $\kappa_{V,\text{off-shell}}$ in the two VBF-like contributions, although the energy scale of the Higgs boson propagator is different between the two cases. Due to the different Γ_H dependence, the on-shell and off-shell Higgs boson production processes are separated in the analysis by requiring that the generated Higgs boson mass satisfies $|m_H^{\text{gen.}} - 125.5\,\text{GeV}| < 1\,\text{GeV}$. This requirement is fully efficient in selecting the on-shell VH process. The NNLO QCD corrected cross-section in Ref. [23] is used for the on-shell VH production process. The cross-section $\sigma_{pp \to VV+2j}(\mu_{\text{off-shell}})$ for the electroweak $pp \to VV + 2j$ process for any off-shell Higgs boson signal strength $\mu_{\text{off-shell}}$

---

[3] Numerically, $K_{gg}^{H^*}(m_{VV})$ differs from $K^{H^*}(m_{VV})$ by ~ 2 % as the higher-order QCD contribution from qg and qq production is small. However, $K_{gg}^{H^*}(m_{ZZ})$ has substantially larger uncertainties than $K^{H^*}(m_{ZZ})$. Therefore $K^{H^*}(m_{ZZ})$ is substituted here, ignoring the 2 % shift in central value, but taking the difference in the systematic uncertainty into account.

[4] ATLAS uses a right-handed coordinate system with its origin at the nominal interaction point (IP) in the centre of the detector, and the z-axis along the beam line. The x-axis points from the IP to the centre of the LHC ring, and the y-axis points upwards. Cylindrical coordinates (r, ϕ) are used in the transverse plane, ϕ being the azimuthal angle around the beam line. Observables labelled "transverse" are projected into the x–y plane. The pseudorapidity is defined in terms of the polar angle θ as $\eta = -\ln\tan(\theta/2)$.

[5] Electroweak means in this context that QCD diagrams that enter through the QCD NNLO corrections to $pp \to VV$ are not included.

is parameterised in the same way as for the $gg \rightarrow (H^* \rightarrow) VV$ process. Details are given in Appendix A.2.

2.3 Simulation of $q\bar{q} \rightarrow ZZ$, WW and WZ backgrounds

The $q\bar{q} \rightarrow ZZ$, $q\bar{q} \rightarrow WW$, and $q\bar{q} \rightarrow WZ$ backgrounds are simulated at NLO in QCD using POWHEG-BOX [42] with dynamic QCD renormalisation and factorisation scales of $m_{VV^{(')}}$ and the CT10 NLO PDF set. In addition, SHERPA is used as a cross-check for the $q\bar{q} \rightarrow WZ$ background. Parton showering and hadronisation are done with PYTHIA8 for $q\bar{q} \rightarrow VZ$ and PYTHIA6 for $q\bar{q} \rightarrow WW$. The interference between the $q\bar{q} \rightarrow WW$ and $q\bar{q} \rightarrow ZZ$ processes for the $2\ell2\nu$ final state is negligible [42] and thus not considered.

The cross-sections for the $q\bar{q} \rightarrow ZZ$ and $q\bar{q} \rightarrow WW$ processes are calculated in Refs. [43,44], respectively, for two on-shell Z or W bosons in the final state at NNLO QCD accuracy. As these calculations include the $gg \rightarrow VV$ processes as part of the NNLO calculation, a different K-factor is provided by the authors of the Refs. [43,44] excluding the $gg \rightarrow VV$ component and using a QCD renormalisation and factorisation scale μ_{QCD} of $m_{VV}/2$ in order to consistently match the simulation of the $gg \rightarrow (H^* \rightarrow) VV$ process:

$$
\begin{aligned}
\text{K}_{q\bar{q}}(m_{VV}) = \big[&\sigma^{\text{NNLO}}_{q\bar{q}\rightarrow VV}(m_{VV}, \mu_{\text{QCD}} = m_{VV}/2) \\
 &- \sigma^{\text{LO}}_{gg\rightarrow VV}(m_{VV}, \mu_{\text{QCD}} = m_{VV}/2) \big] \\
 &\big/ \sigma^{\text{NLO}}_{q\bar{q}\rightarrow VV}(m_{VV}, \mu_{\text{QCD}} = m_{VV})
\end{aligned}
\tag{6}
$$

Electroweak higher-order corrections are not included in POWHEG-BOX. These corrections are calculated in Refs. [45,46] for on-shell outgoing vector bosons and found to be about -10% in the high-mass VV region of this analysis. To account for these corrections, the POWHEG-BOX events are re-weighted using a procedure comparable to the one described in Ref. [47], based on the kinematics of the diboson system and the initial state quarks.

2.4 Simulation of top-quark backgrounds

In the $WW \rightarrow e\nu\mu\nu$ channel, the $t\bar{t}$ and single-top (s-channel and Wt) backgrounds are simulated with POWHEG-BOX [48,49] with parton showering and hadronisation done with PYTHIA6, using the CT10 NLO PDF set. The t-channel single-top background is simulated using AcerMC [50]+PYTHIA6 and uses the CTEQ6LI PDF set. The relative rates of $t\bar{t}$ and single-top production are evaluated with Top++2.0 [51] and the calculations in Refs. [52–54] respectively.

3 Analysis of the $ZZ \rightarrow 4\ell$ final state

The analysis for the $ZZ \rightarrow 4\ell$ final state closely follows the Higgs boson measurements in the same final state described in Ref. [55], with the same physics object definitions, trigger and event selections, and background estimation methods. A matrix-element-based discriminant (ME-based discriminant) is constructed to enhance the separation between the $gg \rightarrow H^* \rightarrow ZZ$ signal and the $gg \rightarrow ZZ$ and $q\bar{q} \rightarrow ZZ$ backgrounds, and is subsequently used in a binned maximum-likelihood fit for the final result.

3.1 Event selection

To minimise the dependence of the $gg \rightarrow ZZ$ kinematics on higher-order QCD effects, the analysis is performed inclusively, ignoring the number of jets in the events.

The analysis is split into four lepton channels ($2\mu2e$, $2e2\mu$, $4e$, 4μ) as in Ref. [55]. Each electron (muon) must satisfy $E_{\text{T}} > 7\,\text{GeV}$ ($p_{\text{T}} > 6\,\text{GeV}$) and be measured in the pseudorapidity range $|\eta| < 2.47$ ($|\eta| < 2.7$). The highest-p_{T} lepton in the quadruplet must satisfy $p_{\text{T}} > 20\,\text{GeV}$, and the second (third) lepton in p_{T} order must satisfy $p_{\text{T}} > 15\,\text{GeV}$ ($p_{\text{T}} > 10\,\text{GeV}$). Lepton pairs are formed from same-flavour opposite-charge leptons. For each channel, the lepton pair with the mass closest to the Z boson mass is referred to as the leading dilepton pair and its invariant mass, m_{12}, is required to be between 50 and 106 GeV. The second (subleading) pair is chosen from the remaining leptons (more than four leptons are allowed per event) as the pair closest in mass to the Z boson and in the range of $50\,\text{GeV} < m_{34} < 115\,\text{GeV}$. The off-peak region is defined to include the range from $220\,\text{GeV} < m_{4\ell} < 1000\,\text{GeV}$.

Figure 3a shows the observed and expected distributions of $m_{4\ell}$ combining all lepton channels in the full off-peak region. The data are in agreement with the SM predictions, with a small deficit of the order of one standard deviation (1σ). Table 1 shows the expected and observed number of events in the signal-enriched region, $400\,\text{GeV} < m_{4\ell} < 1000\,\text{GeV}$, combining all lepton channels. This mass region was chosen since it is optimal for a $m_{4\ell}$ cut-based analysis.

3.2 Matrix-element-based kinematic discriminant

The matrix-element kinematic discriminant fully exploits the event kinematics in the centre-of-mass frame of the 4ℓ system, based on eight observables: $\{m_{4\ell}, m_{12}, m_{34}, \cos\theta_1, \cos\theta_2, \phi, \cos\theta^*, \phi_1\}$, defined in Refs. [5,55]. These observables are used to create the four-momenta of the leptons and incoming partons, which are then used to calculate matrix elements for different processes, provided by the MCFM pro-
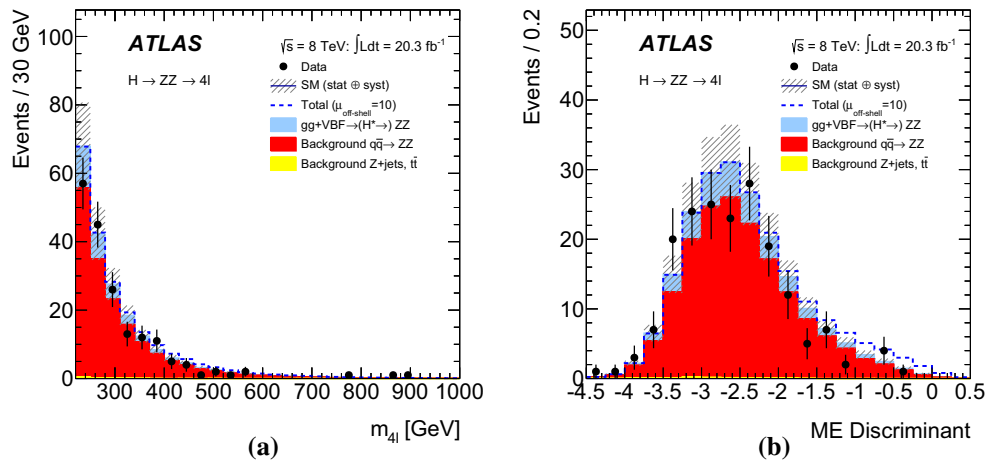
(a)

(b)

Fig. 3 Observed distributions for **a** the four-lepton invariant mass $m_{4\ell}$ in the range of $220\,\text{GeV} < m_{4\ell} < 1000\,\text{GeV}$ and **b** the ME-based discriminant combining all lepton final states for the ME-based analysis signal region, compared to the expected contributions from the SM including the Higgs boson (*stack*). The *dashed line* corresponds to the total expected event yield, including all backgrounds and the Higgs boson with $\mu_{\text{off-shell}} = 10$. A relative $gg \to ZZ$ background K-factor of $\text{R}^B_{H^*} = 1.0$ is assumed. The Z+jets and top-quark backgrounds are barely visible in the *plot* since they are very small (<1 % of the total background)

Table 1 Expected and observed numbers of events in the signal region for all final states in the cut-based approaches. For the $ZZ \to 4\ell$ analysis a mass range of $400 < m_{4\ell} < 1000\,\text{GeV}$ is used. The other backgrounds in the $ZZ \to 4\ell$ final state include contributions from Z+jets and top-quark processes. For the $ZZ \to 2\ell 2\nu$ analysis the range $380\,\text{GeV} < m_{\text{T}}^{ZZ} < 1000\,\text{GeV}$ is considered. For the $WW \to e\nu\mu\nu$ analysis, the region $\text{R}_8 > 450\,\text{GeV}$ is used and background event yields are quoted after the likelihood fit was performed. The expected events for the $gg \to (H^* \to)VV$ and VBF $(H^* \to)VV$ processes (ZZ or WW), including the Higgs boson signal, background and interference, are reported for both the SM predictions (in bold) and $\mu_{\text{off-shell}} = 10$. A relative $gg \to VV$ background K-factor of $\text{R}^B_{H^*} = 1$ is assumed. The uncertainties in the number of expected events include the statistical uncertainties from MC samples and systematic uncertainties. The entries with a $-$ are for processes with event yields < 0.1

Process	$ZZ \to 4\ell$	$ZZ \to 2\ell 2\nu$	$WW \to e\nu\mu\nu$
$gg \to H^* \to VV$ (S)	1.1 ± 0.3	3.2 ± 1.0	1.5 ± 0.4
$gg \to VV$ (B)	2.8 ± 0.8	5.3 ± 1.6	3.6 ± 1.1
$\boldsymbol{gg \to (H^* \to)VV}$	$\mathbf{2.4 \pm 0.7}$	$\mathbf{3.9 \pm 1.2}$	$\mathbf{2.4 \pm 1.2}$
$gg \to (H^* \to)VV$ ($\mu_{\text{off-shell}} = 10$)	9.2 ± 2.5	24.0 ± 7.3	10 ± 4
VBF $H^* \to VV$ (S)	0.12 ± 0.01	0.48 ± 0.04	0.42 ± 0.05
VBF VV (B)	0.71 ± 0.04	1.2 ± 0.2	1.6 ± 0.2
$\mathbf{VBF\ (H^* \to)VV}$	$\mathbf{0.59 \pm 0.03}$	$\mathbf{0.7 \pm 0.1}$	$\mathbf{1.1 \pm 0.1}$
VBF $(H^* \to)VV$ ($\mu_{\text{off-shell}} = 10$)	1.17 ± 0.06	2.9 ± 0.2	2.8 ± 0.3
$q\bar{q} \to ZZ$	21.3 ± 2.1	31.5 ± 3.5	\} 2.0 ± 0.2
$q\bar{q} \to WZ$	$-$	10.6 ± 1.4	
$q\bar{q} \to WW$	$-$	\} 0.4 ± 0.2	40 ± 5
$t\bar{t}$, Wt, and $t\bar{b}/tq\bar{b}$	$-$		35 ± 4
$Z \to \tau\tau$	$-$		1.4 ± 0.2
$Z \to ee, \mu\mu$	$-$	3.5 ± 3.0	$-$
Other backgrounds	$-$	0.8 ± 0.2	8.7 ± 1.3
Total Expected (SM)	24.4 ± 2.2	51 ± 6	90 ± 4
Observed	18	48	82

gram [9]. The following matrix elements are calculated for each event in the mass range $220\,\text{GeV} < m_{4\ell} < 1000\,\text{GeV}$:

- $P_{q\bar{q}}$: matrix element squared for the $q\bar{q} \to ZZ \to 4\ell$ process,

- P_{gg}: matrix element squared for the $gg \to (H^* \to)ZZ \to 4\ell$ process including the Higgs boson ($m_H = 125.5\,\text{GeV}$) with SM couplings, continuum background and their interference,

- P_H: matrix element squared for the $gg \rightarrow H^* \rightarrow ZZ \rightarrow 4\ell$ process ($m_H = 125.5$ GeV).

The kinematic discriminant is defined as in Ref. [9]:

$$\text{ME} = \log_{10} \left(\frac{P_H}{P_{gg} + c \cdot P_{q\bar{q}}} \right), \tag{7}$$

where $c = 0.1$ is an empirical constant, to approximately balance the overall cross-sections of the $q\bar{q} \rightarrow ZZ$ and $gg \rightarrow (H^* \rightarrow)ZZ$ processes. The value of c has a very small effect on the analysis sensitivity. Figure 3b shows the observed and expected distributions of the ME-based discriminant combining all lepton final states. Events with the ME-based discriminant value between -4.5 and 0.5 are selected with a signal efficiency of $>99\%$.

In addition, an alternative multivariate discriminant based on a boosted decision tree (BDT) algorithm was studied to further separate the $gg \rightarrow H^* \rightarrow ZZ$ signal and the main $q\bar{q} \rightarrow ZZ$ background, by exploiting additional kinematic information (p_T and η) of the ZZ system. The analysis sensitivity improves very little ($\sim 2\%$) compared to the ME-based discriminant alone. Due to the dependence on the p_T of the ZZ system, the BDT-based discriminant introduces additional systematic uncertainties from the higher-order QCD corrections. For these reasons, the BDT-based discriminant is not used for the final result.

4 Analysis of the $ZZ \rightarrow 2\ell\,2\nu$ final state

The analysis of the $ZZ \rightarrow 2\ell2\nu$ channel follows strategies similar to those used in the invisible Higgs boson search in the ZH channel [20]. The definitions of the reconstructed physics objects (electrons, muons, jets, and missing transverse momentum) are identical, but some of the kinematic cuts were optimised for the current analysis.

4.1 Event selection

As the neutrinos in the final state do not allow for a kinematic reconstruction of m_{ZZ}, the transverse mass (m_T^{ZZ}) reconstructed from the transverse momentum of the dilepton system ($p_T^{\ell\ell}$) and the magnitude of the missing transverse momentum (E_T^{miss}):

$$m_T^{ZZ} \equiv \sqrt{\left(\sqrt{m_Z^2 + \left| \boldsymbol{p}_T^{\ell\ell} \right|^2} + \sqrt{m_Z^2 + \left| \boldsymbol{E}_T^{\text{miss}} \right|^2} \right)^2 - \left| \boldsymbol{p}_T^{\ell\ell} + \boldsymbol{E}_T^{\text{miss}} \right|^2}, \tag{8}$$

is chosen as the discriminating variable to enhance sensitivity to the $gg \rightarrow H^* \rightarrow ZZ$ signal.

The selection criteria are optimised to maximise the signal significance with respect to the main backgrounds, which

are ZZ, WZ, WW, top-quark, and W/Z+jets events, as described in Sect. 4.2. The impact of the background uncertainty is considered in the significance calculation.

First, events with two oppositely charged electron or muon candidates in the Z mass window 76 GeV $< m_{\ell\ell} < 106$ GeV are selected. Events with a third lepton (e or μ) identified using looser identification criteria for the electrons and a lower p_T threshold of 7 GeV are rejected. A series of selection requirements are necessary to suppress the Drell–Yan background, including: $E_T^{\text{miss}} > 180$ GeV; 380 GeV $< m_T^{ZZ} < 1000$ GeV; the azimuthal angle between the transverse momentum of the dilepton system and the missing transverse momentum $\Delta\phi(p_T^{\ell\ell}, E_T^{\text{miss}}) > 2.5$; and $\left| \left| \boldsymbol{E}_T^{\text{miss}} + \sum_{\text{jet}} \boldsymbol{p}_T^{\text{jet}} \right| - p_T^{\ell\ell} \right| / p_T^{\ell\ell} < 0.3$ Events with a b-jet with $p_T > 20$ GeV and $|\eta| < 2.5$, identified by the MV1 algorithm [56,57] with 70 % tagging efficiency, are rejected to suppress the top-quark background. Finally, the selection on the azimuthal angle between the two leptons $\Delta\phi_{\ell\ell} < 1.4$ is applied to select events with boosted Z bosons to further discriminate the signal from the background.

4.2 Background estimation

The dominant background is $q\bar{q} \rightarrow ZZ$ production, followed by $q\bar{q} \rightarrow WZ$ production. Background contributions from events with a genuine isolated lepton pair, not originating from a $Z \rightarrow ee$ or $Z \rightarrow \mu\mu$ decay, arise from the WW, $t\bar{t}$, Wt, and $Z \rightarrow \tau\tau$ processes. The remaining backgrounds are from $Z \rightarrow ee$ or $Z \rightarrow \mu\mu$ decays with poorly reconstructed E_T^{miss}, and from events with at least one misidentified electron or muon coming from W+jets, semileptonic top decays ($t\bar{t}$ and single top), and multi-jet events.

The $q\bar{q} \rightarrow ZZ$ background is estimated in the same way as for the $ZZ \rightarrow 4\ell$ analysis using the POWHEG-BOX simulation as described in Sect. 2.3. The WZ background is also estimated with the simulation (described in Sect. 2.3) and validated with data in a three-lepton control region. The observed number of events in the control region for $E_T^{\text{miss}} > 180$ GeV (300 GeV) is 30 (3), whereas the predicted event yield is 22.9 ± 0.8 (3.4 ± 0.3). No significant difference is observed between the data and simulation.

The WW, $t\bar{t}$, Wt, and $Z \rightarrow \tau\tau$ backgrounds are inclusively estimated with data assuming lepton flavour symmetry in an $e\mu$ control region using a relaxed selection. The following equations show how these backgrounds in the signal region can be estimated with $e\mu$ events:

$$N_{ee}^{\text{bkg}} = \frac{1}{2} \times N_{e\mu}^{\text{data,sub}} \times \alpha,$$

$$N_{\mu\mu}^{\text{bkg}} = \frac{1}{2} \times N_{e\mu}^{\text{data,sub}} \times \frac{1}{\alpha}, \tag{9}$$

where N_{ee}^{bkg} and $N_{\mu\mu}^{\text{bkg}}$ are the number of dielectron and dimuon events in the signal region. $N_{e\mu}^{\text{data,sub}}$ is the num-

ber of events in the $e\mu$ control region with WZ, ZZ, and other small backgrounds (W+jets, $t\bar{t}V$, and triboson) subtracted using simulation. The different e and μ efficiencies are taken into account using the α variable, which is an efficiency correction factor determined from the ratio of dielectron to dimuon event yields after the inclusive Z mass requirement (76 GeV $< m_{\ell\ell} <$ 106 GeV). The measured value of α is 0.942 with a systematic uncertainty of 0.004 and a negligible statistical uncertainty. This scale factor is applied to the MC predictions. The other source of systematic uncertainty comes from the subtraction of WZ, ZZ, and other small backgrounds in the $e\mu$ control region using the simulation. As no data event remains after applying the full selection, a scale factor of 1.4 ± 0.3 is derived by comparing the event yields from the data-driven and MC predictions with a relaxed selection applying the $E_{\mathrm{T}}^{\mathrm{miss}}$ and m_{T}^{ZZ} requirements but no further cuts. Experimental systematic uncertainties are considered for the MC predictions.

Imperfect modelling of detector non-uniformities and $E_{\mathrm{T}}^{\mathrm{miss}}$ response could lead to an incorrect estimate of the Z boson background in the signal region. The Z boson background is estimated with data using the two-dimensional sideband regions constructed by reversing one or both of the $\Delta\phi(p_{\mathrm{T}}^{\ell\ell}, E_{\mathrm{T}}^{\mathrm{miss}})$ and $\Delta\phi_{\ell\ell}$ selections [20]. The main uncertainty on the mis-measured Z boson background arises from the differences in shape of the $E_{\mathrm{T}}^{\mathrm{miss}}$ and m_{T}^{ZZ} distributions in the signal and sideband regions and the small correlation between these two variables. Other systematic uncertainties originate from the subtraction of the non-Z boson backgrounds in the sideband regions.

The W+jets and multi-jet backgrounds are estimated from data using the fake-factor method [20]. The predicted background with a looser $E_{\mathrm{T}}^{\mathrm{miss}}$ selection applied at 100 GeV, and without the m_{T}^{ZZ} selection, is 0.04 ± 0.01 events. No event remains after applying the full event selection for both the data-driven method and MC samples, and hence this background is estimated to be negligible.

The predicted signals and backgrounds with statistical and systematic uncertainties are summarised in Table 1. The observed event yields agree with the total predicted ones from the SM within the uncertainties. Figure 4 shows the distributions of m_{T}^{ZZ} for the ee and $\mu\mu$ channels in the signal region, compared to the predicted contributions from the SM as well as to a Higgs boson with $\mu_{\mathrm{off\text{-}shell}} = 10$.

5 Analysis of the $WW \to e\nu\mu\nu$ final state

The analysis of the $WW \to e\nu\mu\nu$ channel closely follows the Higgs boson measurements in the oppositely charged electron–muon pair final state in Ref. [58]. This selection ensures orthogonality with the $ZZ \to 2\ell 2\nu$ final state. The same object identification and selection as in Ref. [58] is used
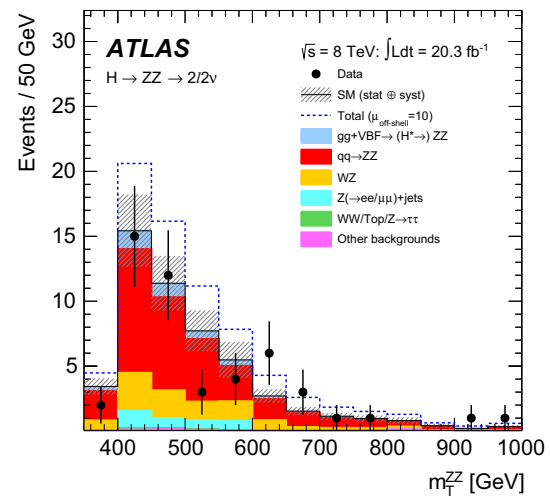

Fig. 4 Observed distribution of the ZZ transverse mass m_{T}^{ZZ} in the range 380 GeV $< m_{\mathrm{T}}^{ZZ} <$ 1000 GeV combining the $2e2\nu$ and $2\mu2\nu$ channels, compared to the expected contributions from the SM including the Higgs boson (*stack*). The first bin only contains events in the range 380 GeV $< m_{\mathrm{T}}^{ZZ} <$ 400 GeV. The *hatched area* shows the combined statistical and systematic uncertainties. The *dashed line* corresponds to the total expected event yield, including all backgrounds and the Higgs boson with $\mu_{\mathrm{off\text{-}shell}} = 10$. A relative $gg \to ZZ$ background K-factor of $\mathrm{R}_{H^*}^B = 1$ is assumed

in this analysis. Additionally, an event selection identical to that used for the gluon fusion initial states in $H \to WW \to e\nu\mu\nu$ is used, up to and including a requirement on missing transverse momentum: leading lepton $p_{\mathrm{T}} >$ 22 GeV, subleading lepton $p_{\mathrm{T}} >$ 10 GeV, $m_{\ell\ell} >$ 10 GeV, and $p_{\mathrm{T}}^{\mathrm{miss,track}} >$ 20 GeV, the magnitude of the missing transverse momentum, with a track-based soft term. The signal region (SR) and background estimations were revised for the high-mass region used in this analysis. Contrary to the base analysis [58], events are not binned by the number of jets. Top-quark events and SM WW production remain the largest expected backgrounds.

5.1 Event selection

As with the $ZZ \to 2\ell 2\nu$ channel, the neutrinos in the final state do not allow for a kinematic reconstruction of m_{VV}. Thus a transverse mass (m_{T}^{WW}) is calculated from the dilepton system transverse energy ($E_{\mathrm{T}}^{\ell\ell}$), the vector sum of lepton transverse momenta ($p_{\mathrm{T}}^{\ell\ell}$), and the vector sum of neutrino transverse momenta ($p_{\mathrm{T}}^{\nu\nu}$), measured with $p_{\mathrm{T}}^{\mathrm{miss,track}}$:

$$m_{\mathrm{T}}^{WW} = \sqrt{\left(E_{\mathrm{T}}^{\ell\ell} + p_{\mathrm{T}}^{\nu\nu}\right)^2 - \left|\boldsymbol{p}_{\mathrm{T}}^{\ell\ell} + \boldsymbol{p}_{\mathrm{T}}^{\nu\nu}\right|^2},$$
$$\text{where } E_{\mathrm{T}}^{\ell\ell} = \sqrt{\left(p_{\mathrm{T}}^{\ell\ell}\right)^2 + \left(m_{\ell\ell}\right)^2}. \tag{10}$$

The transverse mass is modified compared to the definition in Eq. (8) as the neutrinos do not come from the same parent particle, and there is no m_Z constraint.
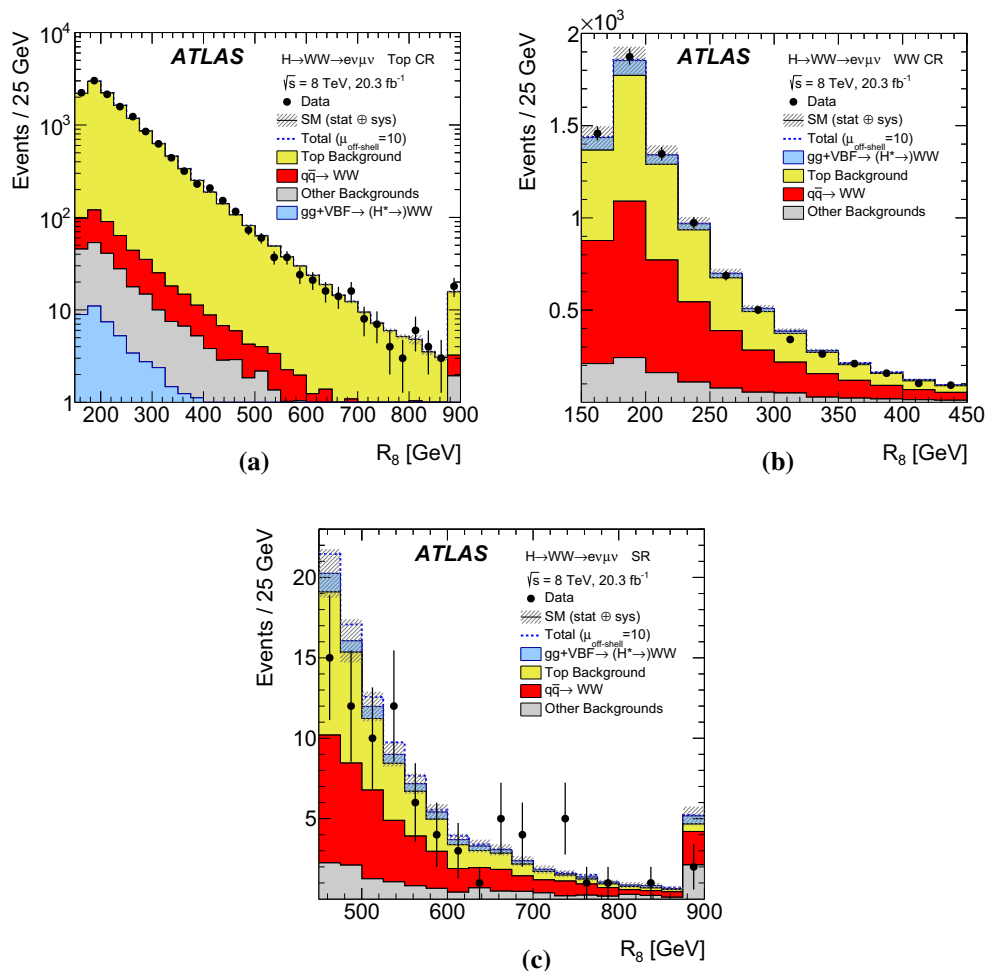
Fig. 5 Observed distributions of R_8, constructed from the dilepton invariant mass and transverse mass, Eq. (11), in the $WW \rightarrow e\nu\mu\nu$ channel for **a** the top control region, **b** WW control region (the CRs start at 160 GeV), and **c** the signal region for R_8 above 450 GeV, compared to the expected contributions from the SM including the Higgs boson (*stack*). The *dashed line* corresponds to the total expected event yield, including all backgrounds and the Higgs boson with $\mu_{\text{off-shell}} = 10$. The last bin in **a** and **c** includes the overflow. A relative $gg \rightarrow WW$ background K-factor of $R^B_{H^*} = 1$ is assumed. The top-quark and WW backgrounds are normalised to data as described in Sect. 5.1. The stacking order follows the legend in each plot

In order to isolate the off-shell Higgs boson production while minimising the impact of higher-order QCD effects on $gg \rightarrow WW$ kinematics, a new variable, R_8, is introduced:

$$R_8 = \sqrt{m_{\ell\ell}^2 + \left(a \cdot m_{\text{T}}^{WW}\right)^2}. \tag{11}$$

Both the coefficient $a = 0.8$ and the requirement $R_8 > 450$ GeV are optimised for off-shell signal sensitivity while also rejecting on-shell Higgs boson events, which have relatively low values of $m_{\ell\ell}$ and m_{T}^{WW}. The predicted on-shell signal contamination is $0.04 \pm 0.03(\text{stat.})$ events. The MV1 algorithm, at 85 % efficiency, is used to reject b-jets with $p_{\text{T}} > 20$ GeV and $|\eta| < 2.4$ in order to reject backgrounds containing top quarks. A more efficient working point for b-jet tagging is used compared to the $ZZ \rightarrow 2\ell 2\nu$ analysis because of the need to reject a substantially larger top-

quark background. A requirement on the separation between leptons, $\Delta\eta_{\ell\ell} < 1.2$, suppresses $q\bar{q}$-initiated WW production relative to gg-initiated production. The b-jet veto and $\Delta\eta_{\ell\ell}$ requirement are found to have a minimal impact on the WW-system kinematics and jet multiplicity in the $gg \rightarrow (H^* \rightarrow)WW$ processes. Table 1 contains the predicted and observed event yields in the signal region, 90 ± 4 and 82 respectively, in agreement with the SM with a small deficit in data. The distribution of the R_8 variable in the signal region is shown in Fig. 5c for the SM expectation and for a Higgs boson with $\mu_{\text{off-shell}} = 10$.

5.2 Background estimation

The dominant backgrounds arise from processes with real W bosons in the final state. The two backgrounds with the largest expected event yield are top-quark and $q\bar{q} \rightarrow WW$

production. Dedicated control regions (CRs) are constructed to normalise these two backgrounds in the signal region with a simultaneous fit. Uncertainties on the extrapolation from the CRs to the signal region are described in Sects. 6.2 and 6.3.

The top-quark background predictions in the signal and WW control region are both normalised from the same top CR. A sample of top-quark events is obtained by starting from the signal region and reversing the b-jet veto by requiring exactly one b-tagged jet. This is closer in phase space to the b-jet-vetoed signal region than requiring at least one b-tag and results in a smaller uncertainty. The statistical error on the top-quark background normalisation is reduced by expanding the top CR down to $R_8 > 160$ GeV and dropping the $\Delta\eta_{\ell\ell}$ requirement. The impact of these changes is discussed in Sect. 6.3. An event yield of 13498 events is observed in the top CR (Fig. 5a), resulting in a fit normalisation factor of 1.03 ± 0.04, where the uncertainty includes all systematic sources, including extrapolation uncertainties described in Sect. 6.3. The top CR is approximately 96 % pure in top-quark events.

The $q\bar{q} \to WW$ background is normalised to data using an additional CR. The region 160 GeV $< R_8 <$ 450 GeV without the $\Delta\eta_{\ell\ell}$ requirement is used because it has a large WW contribution with negligible on-shell Higgs boson contamination and is adjacent to the signal region. A b-jet veto is applied to reject part of the substantial top-quark contamination. An event yield of 8007 events is observed in the WW CR (Fig. 5b), resulting in a fit normalisation factor of 1.03 ± 0.11, including all of the uncertainties as above. This CR is approximately 46 % pure in $q\bar{q} \to WW$, while the leading background of top-quark events contributes 39 %. The gg-initiated WW background is estimated from MC simulation, as discussed in Sect. 2.1.

The remaining background predictions, except for W+jets and multi-jet production, are taken from MC simulation, as described in Ref. [58]. The predicted fraction of the total background in the signal region arising from $gg \to WW$, W+jets, and $W\gamma/W\gamma^*/WZ/ZZ$ events is approximately 4 % each, while for Z+jets it is 2 %. The W+jets and multi-jet backgrounds are estimated by applying a data-driven extrapolation factor to CRs with lepton candidates failing the nominal lepton identification and isolation, while passing a loosened requirement [58].

6 Systematic uncertainties

The largest systematic uncertainties for this analysis arise from theoretical uncertainties on the $gg \to H^* \to VV$ signal process, the $gg/q\bar{q} \to VV$ background processes and the interference between the $gg \to VV$ signal and background processes. The electroweak ($H^* \to VV$) processes in association with two jets contribute about 10–30 % of the total signal. The associated theoretical uncertainties due to the missing higher-order corrections and PDF variations are small for VH-like and VBF-like processes $pp \to ZZ + 2j$, and are therefore not included in the analysis. Compared to the theoretical uncertainties, the experimental uncertainties are small in the $ZZ \to 2\ell 2\nu$ and $WW \to e\nu\mu\nu$ analyses and close to negligible in the $ZZ \to 4\ell$ analysis. In the $ZZ \to 2\ell 2\nu$ and $WW \to e\nu\mu\nu$ analyses, uncertainties on the extrapolations from the control regions to the signal regions are included.

6.1 Systematic uncertainties on $gg \to (H^* \to)VV$

The uncertainty from missing higher-order QCD and EW corrections to the off-shell $gg \to H^* \to VV$ signal is estimated in Ref. [25] as a function of the Higgs boson virtuality, m_{VV}, and adopted for this analysis. The uncertainty is 20–30 % for the high-mass region used in this analysis. The PDF uncertainty for the $gg \to (H^* \to)VV$ process as a function of m_{VV} is found to be 10–20 % in the high-mass region used in this analysis. This is consistent with an earlier study at $\sqrt{s} = 7$ TeV [39].

For the $gg \to VV$ background, higher-order QCD calculations are not available. As discussed in Sect. 2.1, the gluon-induced part of the signal K-factor $K_{gg}^{H^*}(m_{VV})$ is applied to the background and results are then given as a function of the unknown K-factor ratio $R_{H^*}^B$ between background and signal. The uncertainty on $K_{gg}^{H^*}(m_{VV})$ is larger than the uncertainty on $K^{H^*}(m_{VV})$ because some contributions to the full signal NNLO QCD K-factor are not present in $K_{gg}^{H^*}(m_{VV})$. Therefore, the following correlation treatment of uncertainties is applied: the uncertainty on the signal K-factor $K^{H^*}(m_{VV})$ is applied as a correlated uncertainty to $K_{gg}^{H^*}(m_{VV})$. The difference in quadrature between the uncertainty on $K_{gg}^{H^*}(m_{VV})$ and $K^{H^*}(m_{VV})$ is added as an uncorrelated uncertainty component only to $K_{gg}^{H^*}(m_{VV})$.

The interference between $gg \to H^* \to VV$ and $gg \to VV$ is calculated at LO only. In Ref. [36], a soft-collinear approximation is used to calculate the cross-section for the sum of a heavy Higgs boson ($gg \to H \to WW$) and its interference with the background. The uncertainty on this calculation is estimated to be about 10 %, which leads to about 30 % uncertainty on the interference alone. Within the ansatz of using an unknown K-factor ratio between background and signal (see Eq. (5)), this additional uncertainty of roughly 30 % on the interference term can be represented by an approximately 60 % variation of the K-factor ratio $R_{H^*}^B$ for the background around the nominal value of 1.0. Therefore the variation of $R_{H^*}^B$ from 0.5 to 2.0 should cover both the leading corrections and uncertainties for the interference and the background component taken individually.

However, there is a large cancellation between the background and the negative interference at the expected 95 % confidence level upper limit value of $\mu_{\text{off-shell}}$, shown in Tables 3 and 4. This leads to a large artificial cancellation in the uncertainties of the $gg \to ZZ$ background and the interference, when treated as correlated. To account for additional uncertainties on the interference component that are not covered by the soft-collinear approximation, the 30 % uncertainty on the interference derived in Ref. [36] is applied to the interference component in addition to, and uncorrelated with, other uncertainties.

The systematic uncertainties associated with SHERPA-based re-weighting in p_T of the VV system are assessed by varying the renormalisation, factorisation and resummation scales in SHERPA. The larger in value between the scale variations in SHERPA and 50 % of the difference between SHERPA and gg2VV+ PYTHIA8 is assigned as the systematic uncertainty. This conservative approach is chosen to consider potential uncertainties not accounted for by the scale variations. The impact of the PDF uncertainties is found to be negligible.

6.2 Systematic uncertainties on $q\bar{q} \to VV$

The missing-higher-order and PDF uncertainties for the $q\bar{q} \to ZZ$ background, as a function of m_{ZZ}, are taken from Ref. [39], based on NLO 7 TeV calculations using a fixed scale of m_Z. Slightly smaller systematic uncertainties are found for 8 TeV using a dynamic scale of $m_{ZZ}/2$, hence applying the uncertainties from Ref. [39] can be considered a conservative choice. Both the QCD scale uncertainty and the PDF uncertainty are 5–10 % for the high-mass region used in this analysis. The NNLO calculation in Ref. [43] does not yield a significantly reduced QCD scale systematic uncertainty. An evaluation of the PDF uncertainty correlations shows that the $q\bar{q} \to ZZ$ background PDF uncertainties are anti-correlated with the PDF uncertainties for the $gg \to (H^* \to)ZZ$ process, and this is taken into account in the analysis. Acceptance uncertainties on the $q\bar{q} \to ZZ$ background are evaluated by comparing PYTHIA8 and HERWIG6 [59] samples and found to be negligible. The PDF, QCD scale, and EW correction uncertainties for the $q\bar{q} \to WZ$ process are considered in the same way as for the $q\bar{q} \to ZZ$ process. Both the QCD scale uncertainty and the PDF uncertainty are estimated to be ∼5–10 % for the high-mass region used in this analysis.

Extrapolation uncertainties on the $q\bar{q} \to WW$ process in the $WW \to e\nu\mu\nu$ channel are evaluated using the method described in Ref. [58]. Uncertainties due to missing higher-order corrections are estimated by varying the renormalisation and factorisation scales independently by factors of one-half and two, keeping the ratio of the scales between one-half and two. Parton shower

Table 2 Uncertainties on the extrapolation of top-quark processes and $q\bar{q} \to WW$ from their respective CRs to the SR, and from the top CR to the WW CR, from the parton shower and underlying event (UE/PS), from matching the matrix element to the UE/PS model (Gen), from the QCD renormalisation and factorisation scale (scale), and from the PDFs. These uncertainties are used in the WW analysis and derived with the same methods as used in Ref. [58]

	UE/PS (%)	Gen. (%)	Scale (%)	PDF (%)
Top CR	6.4	2.4	2.4	2.4
WW CR	2.5	2.8	2.3	1.5

and matrix-element uncertainties are estimated by comparing POWHEG-BOX+PYTHIA8 with POWHEG-BOX+HERWIG6 and POWHEG-BOX+HERWIG6 with aMC@NLO [37]+HERWIG6, respectively. PDF uncertainties are estimated by taking the largest difference between the nominal CT10 [60] and either the MSTW2008 [35] or the NNPDF2.1 [61] PDF set and adding this in quadrature with the CT10 error eigenvectors (following the procedure described in Ref. [62]). The extrapolation uncertainties from the WW control region to the signal region are summarised in Table 2.

The EW corrections for the $q\bar{q} \to VV$ process described in Sect. 2.3 are strictly valid only for the LO QCD $q\bar{q} \to VV$ process above the diboson production threshold when both vector bosons are on shell. This is the case for all three analyses after final selections. The EW corrections are computed at LO QCD because the mixed QCD–EW corrections have not yet been calculated. In events with high QCD activity, an additional systematic uncertainty is considered by studying the variable $\rho = |\sum_i \vec{\ell}_{i,T} + \vec{E}_T^{\text{miss}}|/(\sum_i |\vec{\ell}_{i,T}| + |\vec{E}_T^{\text{miss}}|)$ introduced in Eq. (4.4) of Ref. [47] (here ℓ_T represents the transverse momentum of the lepton i from vector boson decays). A phase space region with $\rho < 0.3$ is selected, where the NLO QCD event kinematics resembles the LO event kinematics in being dominated by recoiling vector bosons and therefore the corrections are applicable without additional uncertainty. For events with $\rho > 0.3$ the correction is applied with a 100 % systematic uncertainty to account for the missing mixed QCD–EW corrections which are expected to be of the same order of magnitude. The applied corrections are partial in that they include only virtual corrections, and do not include polarisation effects. The sum of both of these effects is estimated to be $\mathcal{O}(1\%)$ [47] and is neglected in this analysis.

While the EW corrections and uncertainties directly affect the predicted size of the $q\bar{q} \to ZZ$ and $q\bar{q} \to WZ$ backgrounds in the $ZZ \to 4\ell$ and $ZZ \to 2\ell 2\nu$ analyses, only the extrapolation of the $q\bar{q} \to WW$ background from the control region to the signal region is affected in the $WW \to e\nu\mu\nu$ analysis.

6.3 Systematic uncertainties on top-quark events

Theory uncertainties on extrapolating top-quark processes from the control region to the signal region in the $WW \rightarrow e\nu\mu\nu$ channel are also evaluated using methods similar to those of Ref. [58]. For the evaluation of the extrapolation uncertainties, the signal region requirements are relaxed to increase the sample size; the region is extended down to $R_8 > 160$ GeV and the $\Delta\eta_{\ell\ell}$ requirement is dropped. The extra uncertainty from this extension is checked in a separate sample with at least one b-tagged jet, again defined so as to reduce the statistical uncertainties, which is simultaneously re-weighted in $\Delta\eta_{\ell\ell}$ and R_8 to match the b-vetoed region. With this b-tagged sample, the extra uncertainty from the removal of the $\Delta\eta_{\ell\ell}$ requirement, and from extending the range in R_8, is found to be 3.5 %.

The method described in Sect. 6.2 is used to evaluate the systematic uncertainties on top-quark processes. Since the extended signal region covers the WW CR, the same systematic uncertainties are valid for the extrapolation from the top CR to the WW CR. These uncertainties, summarised in Table 2, are applied to both $t\bar{t}$ and single-top processes, which make up approximately 22 % of the top background in the signal region. A 20 % uncertainty is assigned to the single-top processes in order to take into account the uncertainty on the single-top fraction; the impact on the result is negligible.

6.4 Experimental systematic uncertainties

For the $ZZ \rightarrow 4\ell$ analysis, the same sources of experimental uncertainty as in Ref. [55] are evaluated. In the off-shell Higgs boson region, the leptons come from the decay of on-shell Z bosons; hence the lepton-related systematic uncertainties are small compared to those for the leptons from on-shell Higgs boson production. The leading, but still very small, experimental systematic uncertainties are due to the electron and muon reconstruction efficiency uncertainties.

Similarly, for the $2\ell2\nu$ channel, the same sources of experimental uncertainty as in Ref. [20] are evaluated. The electron energy scale, electron identification efficiency, muon reconstruction efficiency, jet energy scale, and systematic uncertainties from the data-driven Z background estimates are the main sources of the experimental systematic uncertainties. These experimental uncertainties affect the expected sensitivity of the $\mu_{\text{off-shell}}$ measurement only at the percent level.

Finally, for the $WW \rightarrow e\nu\mu\nu$ channel, the same sources of experimental uncertainty as in Ref. [58] are evaluated. The uncertainty on the electron energy scale, followed by the uncertainty on the rate for mis-tagged light-flavour jets as b-jets, and the uncertainty on the jet energy scale and resolution, are the dominant experimental sources of uncertainty.

The remaining experimental sources are significantly smaller than the theoretical uncertainties.

The uncertainty on the integrated luminosity is 2.8 %. It is derived, following the same methodology as that detailed in Ref. [63], from a preliminary calibration of the luminosity scale derived from beam-separation scans performed in November 2012.

7 Results

In this section the results for the $ZZ \rightarrow 4\ell$, $ZZ \rightarrow 2\ell2\nu$ and $WW \rightarrow e\nu\mu\nu$ analyses are presented and translated into limits on the off-shell signal strength $\mu_{\text{off-shell}}$ for the individual analyses and for the combination of all three channels. In a second step, the off-shell analyses are combined with the on-shell $ZZ^* \rightarrow 4\ell$ [55] and $WW^* \rightarrow \ell\nu\ell\nu$ [58] analyses based on the 8 TeV data taken in 2012. In combining the ZZ and WW channels it is assumed that the ratio of the ZZ cross-section $\sigma^{gg \rightarrow H^{(*)} \rightarrow ZZ}(\hat{s})$ to the WW cross-section $\sigma^{gg \rightarrow H^{(*)} \rightarrow WW}(\hat{s})$ (and similarly for VBF) is as predicted in the SM for both the on- and off-shell processes.

Two different off-shell combinations are presented based on different assumptions. First, a single off-shell signal strength parameter is applied for all production modes. This is equivalent to assuming that the ratio of the off-shell production rates via the process $gg \rightarrow H$ to those via the VBF process are as predicted in the SM. In a second combination, only the off-shell signal strength of the $gg \rightarrow H^* \rightarrow VV$ production process is considered while the VBF production process is fixed to the SM prediction. In this case the combined signal strength $\mu_{\text{off-shell}}^{gg \rightarrow H^* \rightarrow VV}$ can be interpreted as a constraint on the off-shell coupling strength $\kappa_{g,\text{off-shell}}$ associated with the $gg \rightarrow H^*$ production mode.

The combination with the on-shell analyses is also performed under two assumptions that correspond to different interpretations of the results. The first is performed using different signal strengths for the $gg \rightarrow H^{(*)}$ and the VBF production modes.[6] The parameter of interest is described by the ratio of the off-shell to the on-shell signal strengths, which can be interpreted as the Higgs boson total width normalised to its SM prediction: $\mu_{\text{off-shell}}/\mu_{\text{on-shell}} = \Gamma_H/\Gamma_H^{\text{SM}}$. This interpretation requires that the off- and on-shell couplings are the same for both $gg \rightarrow H^{(*)}$ and VBF production modes (i.e., $\kappa_{g,\text{on-shell}} = \kappa_{g,\text{off-shell}}$ and $\kappa_{V,\text{on-shell}} = \kappa_{V,\text{off-shell}}$[7]). In a second combination, the coupling scale factors $\kappa_V =$

---

[6] In all results the signal strength for VH associated production is assumed to scale with VBF production while the $b\bar{b}H$ and $t\bar{t}H$ processes scale with the $gg \rightarrow H$ process. These additional production modes are expected to give negligible contributions to the off-shell measurements, but have small contributions to the on-shell signal yields.

[7] To set an upper limit, the assumption in Eq. (3), and the equivalent assumption for the VBF production mode, is sufficient.

$\kappa_{V,\text{on-shell}} = \kappa_{V,\text{off-shell}}$ associated with the on- and off-shell VBF production and the $H^{(*)} \to VV$ decay, are assumed to be the same and fitted to the data (profiled). In this case the parameter of interest, $R_{gg} = \mu_{\text{off-shell}}^{gg \to H^*} / \mu_{\text{on-shell}}^{gg \to H}$, can be interpreted as the ratio of the off-shell to the on-shell gluon couplings: $R_{gg} = \kappa_{g,\text{off-shell}}^2 / \kappa_{g,\text{on-shell}}^2$. This also assumes that the total width is equal to the SM prediction.

In the $ZZ \to 4\ell$ channel, a binned maximum-likelihood fit to the ME-based discriminant distribution is performed to extract the limits on the off-shell Higgs boson signal strength. The fit model accounts for signal and background processes, including $gg \to (H^* \to)ZZ$, VBF$(H^* \to)ZZ$ and $q\bar{q} \to ZZ$. The probability density functions (pdf) of the signal-related processes $gg \to (H^* \to)ZZ$ and VBF $(H^* \to)ZZ$ are parameterised as a function of both the off-shell Higgs boson signal strength $\mu_{\text{off-shell}}$ and the unknown background K-factor ratio $R_{H^*}^B$ as given in Eqs. (15) and (19). Normalisation and shape systematic uncertainties on the signal and background processes are taken into account as described in Sect. 6.1, with correlations between different components and processes as indicated therein.

In the $ZZ \to 2\ell2\nu$ channel, a similar maximum-likelihood fit to the transverse mass (m_T^{ZZ}) is performed, comparing the event yield in the signal-enriched region in data with the predictions. The fit model accounts for the signal and all background processes mentioned in Table 1. The modelling of the dominant signal and background processes is the same as in the $ZZ \to 4\ell$ channel.

In the $WW \to e\nu\mu\nu$ channel, a maximum-likelihood fit is performed using the event yields in the signal region and the two control regions. As in the ZZ channels, the fit model accounts for the parameterised signal and all background processes mentioned in Sect. 5.2. Unconstrained strength parameters common among fit regions for the $q\bar{q} \to WW$ and top-quark processes allow the control regions to constrain the predicted event yields in the signal region.

The likelihood is a function of a parameter of interest μ and nuisance parameters $\vec{\theta}$. Hypothesis testing and confidence intervals are based on the profile likelihood ratio [64]. The parameters of interest are different in the various tests, while the remaining parameters are profiled. Hypothesised values for a parameter of interest μ are tested with a statistic

$$\Lambda(\mu) = \frac{L\left(\mu, \hat{\hat{\vec{\theta}}}(\mu)\right)}{L(\hat{\mu}, \hat{\vec{\theta}})},\tag{12}$$

where the single circumflex denotes the unconditional maximum-likelihood estimate of a parameter and the double circumflex [e.g. $\hat{\hat{\vec{\theta}}}(\mu)$] denotes the conditional maximum-likelihood estimate (e.g. of $\vec{\theta}$) for given fixed values of μ. This test statistic extracts the information on the parameters of interest from the full likelihood function.

All 95 % confidence level (CL) upper limits are derived using the CL_s method [65], based on the following ratio of one-sided p-values: $CL_s(\mu) = p_\mu/(1 - p_1)$ where p_μ is the p-value for testing a given $\mu = \mu_{\text{off-shell}}$ or $\mu = \Gamma_H/\Gamma_H^{\text{SM}}$ (the non-SM hypothesis) and p_1 is the p-value derived from the same test statistic under the SM hypothesis of $\mu_{\text{off-shell}} = 1$ in the first case and $\Gamma_H/\Gamma_H^{\text{SM}} = \mu_{\text{on-shell}} = 1$ in the second case.[8] The 95 % CL_s upper limit is found by solving for $CL_s(\mu^{95\%}) = 5\%$. Values $\mu > \mu^{95\%}$ are regarded as excluded at 95 % CL. A detailed description of the implementation of the CL_s procedure can be found in Ref. [66].

The results presented in this paper rely on the asymptotic approximation [64] for the test statistic $\Lambda(\mu)$. This approximation was cross-checked with Monte Carlo ensemble tests that confirm its validity in the range of the parameters for which the 95 % CL limits are derived. Deviations appear close to the boundary of $\mu_{\text{off-shell}} \geq 0$ imposed by Eq. (5) and hence the 1σ uncertainties can only be seen as approximate.

While the final 95 % CL limits are given as a function of the unknown background K-factor ratio $R_{H^*}^B$, comparisons between the data and the MC predictions, and values in other figures and tables, are given assuming $R_{H^*}^B = 1$.

7.1 Results of the individual off-shell analyses

The scan of the negative log-likelihood, $-2 \ln \Lambda$, as a function of $\mu_{\text{off-shell}}$ for data and the expected curve for an SM Higgs boson for the three individual off-shell analyses is illustrated in Fig. 6. The observed and expected 95 % CL upper limits on $\mu_{\text{off-shell}}$ as a function of $R_{H^*}^B$ are shown in Fig. 7 and are summarised in Table 3. The $ZZ \to 4\ell$ and $ZZ \to 2\ell2\nu$ analysis have a very similar expected sensitivity. The $ZZ \to 4\ell$ analysis is statistics limited, while the sensitivity in the $ZZ \to 2\ell2\nu$ analysis is significantly reduced by the theoretical systematic uncertainties as can be seen in Fig. 6. The similar expected CL_s limits for the two channels for $R_{H^*}^B = 0.5$ and 1.0 in Table 3 is a coincidence, caused by the different statistical and systematic uncertainty components.

The typical off-shell mass scales tested by the analyses are in the range 400 GeV $< m_{VV} < 1000$ GeV, with a small fraction of the expected $H^* \to WW$ signal extending to substantially higher mass scales.[9] This is illustrated in Fig. 8, which shows the generated m_{VV} mass for the $gg \to H^* \to VV$ and the VBF $H^* \to VV$ signal processes weighted by the expected S/B ratio in each bin of the final discriminant

---

[8] In the context of this analysis the alternative hypothesis is given by the SM value(s) for all relevant parameters of the fit model.

[9] While the $H^* \to ZZ$ analysis includes a selection cut to limit the mass range to $m_{ZZ} \lesssim 1000$ GeV, no such cut can be efficiently implemented for the $H^* \to WW$ analysis due to the poor mass resolution.

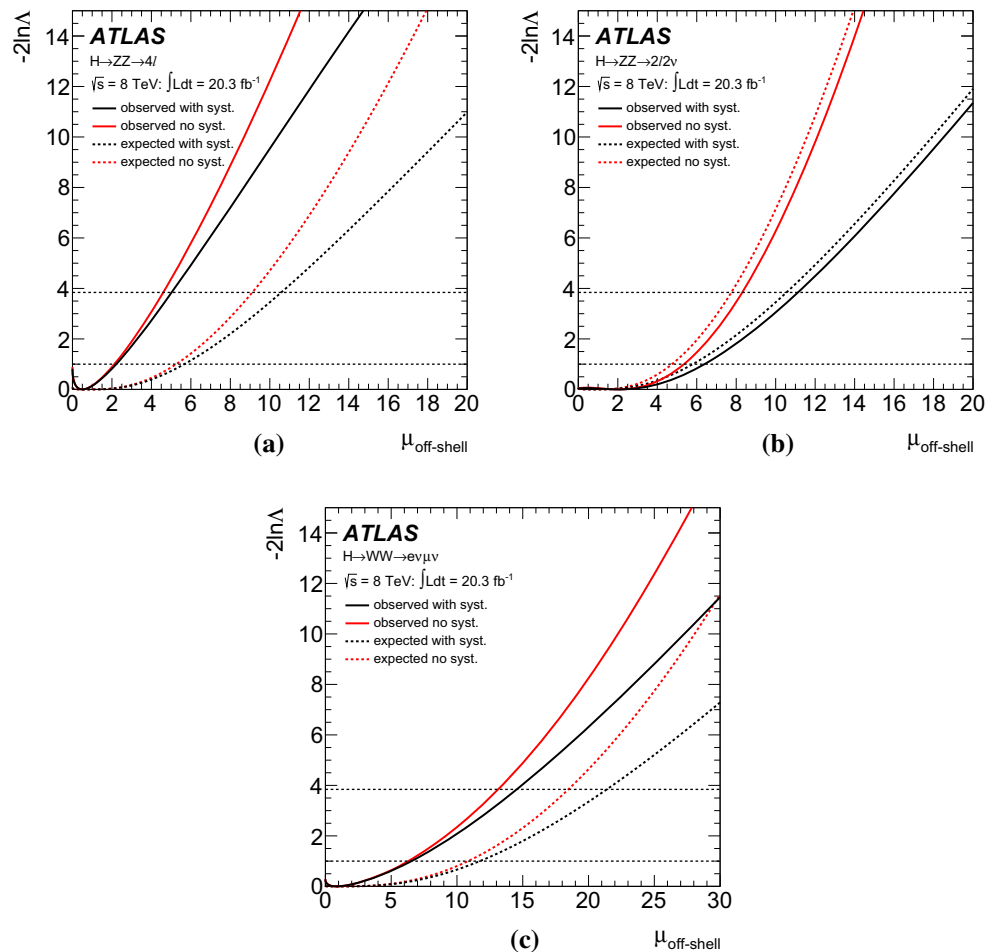**Fig. 6** Scan of the negative log-likelihood, $-2\ln\Lambda$, as a function of $\mu_{\text{off-shell}}$, in the $ZZ \rightarrow 4\ell$ (**a**), $ZZ \rightarrow 2\ell\,2\nu$ (**b**) and $WW \rightarrow e\nu\,\mu\nu$ (**c**) channels. The *black solid* (*dashed*) *line* represents the observed (expected) value including all systematic uncertainties, while the *red* *solid* (*dashed*) *line* is for the observed (expected) value without systematic uncertainties. A relative $gg \rightarrow VV$ background K-factor of $R^B_{H^*} = 1$ is assumed in these figures

for the $ZZ \rightarrow 4\ell$ and $ZZ \rightarrow 2\ell2\nu$ analyses and for all signal events in the signal region for the $WW \rightarrow e\nu\,\mu\nu$ analysis.

7.2 Combination of the off-shell ZZ and WW analyses

The analyses described in the previous sections are combined to obtain a limit on $\mu_{\text{off-shell}}$. In combining the off-shell results the main systematic uncertainties related to the theory uncertainties on the $gg \rightarrow (H^* \rightarrow)VV$ (including signal and interference contributions) and $q\bar{q} \rightarrow VV$ processes are treated as correlated between the different channels. The same K-factor ratio $R^B_{H^*}$ is assumed for the $gg \rightarrow ZZ$ and $gg \rightarrow WW$ backgrounds. Where appropriate, the experimental systematic uncertainties are also treated as correlated. However, they are found to have a very small impact on the final combined limit.

The limits on $\mu_{\text{off-shell}}$ are obtained under two different assumptions:

- Determination of the signal strength $\mu_{\text{off-shell}}$ when fixing the ratio of the signal strength in $gg \rightarrow H^*$ and VBF to the SM prediction, namely $\mu^{gg \rightarrow H^*}_{\text{off-shell}} / \mu^{VBF}_{\text{off-shell}} = 1$.
- Determination of the signal strength $\mu^{gg \rightarrow H^* \rightarrow VV}_{\text{off-shell}}$ when fixing the VBF off-shell signal strength to the SM prediction, i.e. $\mu^{\text{VBF } H^* \rightarrow VV}_{\text{off-shell}} = 1$.

The scan of the negative log-likelihood, $-2\ln\Lambda$, as a function of $\mu_{\text{off-shell}}$ for data and the expected curve for an SM Higgs boson for the two cases above are shown in Fig. 9.

The limits on $\mu_{\text{off-shell}}$ and $\mu^{gg \rightarrow H^*}_{\text{off-shell}}$ are computed with the CL_s method, assuming for the alternative hypothesis that all the off-shell rates are at their SM predictions. They are derived as a function of the $gg \rightarrow VV$ background K-factor ratio $R^B_{H^*}$. These results are reported in Table 4 and shown in Fig. 10, assuming either one common scale factor for both the $gg \rightarrow H^*$ and VBF processes or using a scale factor for the $gg \rightarrow H^*$ process and fixing the VBF production to the SM prediction.
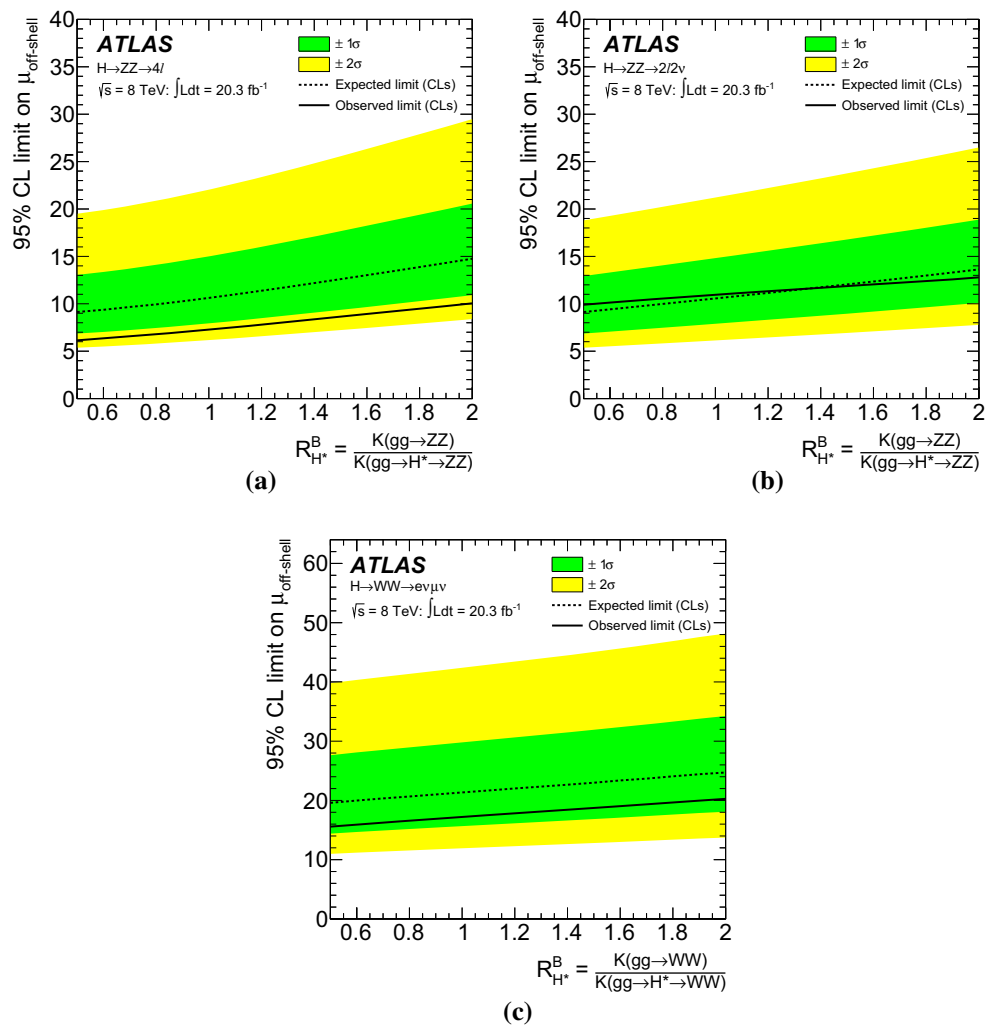
Fig. 7 The observed and expected 95 % CL upper limit on $\mu_{\text{off-shell}}$ as a function of R^B_{H*}, for the $ZZ \to 4\ell$ (**a**), $ZZ \to 2\ell 2\nu$ (**b**) and $WW \to e\nu\mu\nu$ (**c**) channels. The upper limits are evaluated using the CL_s method, with the alternative hypothesis $\mu_{\text{off-shell}} = 1$. The *green* (*yellow*) *bands* represent the 68 % (95 %) confidence intervals for the CL_s expected limit

Table 3 The observed and expected 95 % CL upper limits on $\mu_{\text{off-shell}}$ within the range of $0.5 < R^B_{H*} < 2.0$. The bold numbers correspond to the limit assuming $R^B_{H*} = 1$. The upper limits are evaluated using the CL_s method, with the alternative hypothesis $\mu_{\text{off-shell}} = 1$

R^B_{H*}	Observed			Median expected		
	0.5	**1.0**	2.0	0.5	**1.0**	2.0
$ZZ \to 4\ell$ analysis	6.1	**7.3**	10.0	9.1	**10.6**	14.8
$ZZ \to 2\ell 2\nu$ analysis	9.9	**11.0**	12.8	9.1	**10.6**	13.6
$WW \to e\nu\mu\nu$ analysis	15.6	**17.2**	20.3	19.6	**21.3**	24.7

The impact of the various systematic uncertainties on the combined expected limit in the off-shell fit are listed in Table 5 when fixing the ratio of the signal strength in $gg \to H^*$ and VBF to the SM prediction. The values in this table were derived by fixing all the nuisance parameters associated with the systematic uncertainties to the values derived from the SM-conditional fit to the data, with the exception of the one under study.

7.3 Combination of the off-shell and on-shell ZZ and WW analyses

In this section, the off-shell results reported above are combined with the on-shell $H \to ZZ^* \to 4\ell$ [55] and $H \to WW^* \to \ell\nu\ell\nu$ [58] analyses based on the 8 TeV data taken in 2012. In these analyses a Higgs boson mass value of 125.36 GeV [11] is assumed. For the on-shell ZZ and WW

combination the main common sources of theoretical and experimental systematic uncertainties are treated as correlated [3].
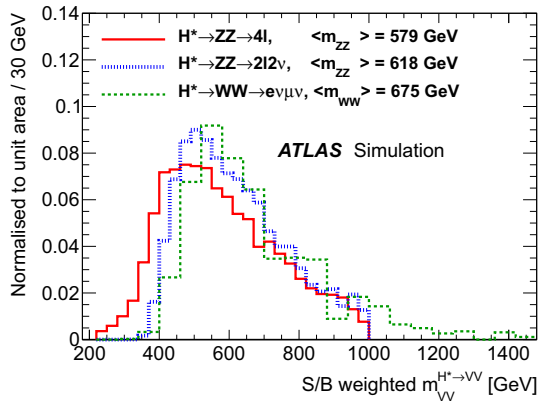

Fig. 8 Normalised distribution of the generated mass m_{VV} for the $gg \to H^* \to VV$ and the VBF $H^* \to VV$ signal processes weighted by the expected S/B ratio in each bin of the final discriminant for the $ZZ \to 4\ell$ and $ZZ \to 2\ell 2\nu$ analyses and for all events in the signal region for the $WW \to e\nu\mu\nu$ analysis

The uncertainties from the impact of higher-order QCD corrections on the $gg \to H^{(*)}$ and $qq \to VV$ processes are considered correlated between the on-shell and off-shell measurements. The PDF uncertainties are treated as uncorrelated between on-shell and off-shell analyses. The correlations between the PDF uncertainties for the on-shell and off-shell analyses are expected to be small with the exception of the ones for the $q\bar{q} \to VV$ process, which have negligible impact on the on-shell results.

In addition to the main theoretical uncertainties, the common experimental systematic uncertainties are treated as correlated.

The results reported in the following are based on two different assumptions:

- Determination of Γ_H / Γ_H^{SM} when profiling the coupling scale factors κ_g and κ_V associated with the on- and off-shell $gg \to H^{(*)}$ and VBF production and the $H^{(*)} \to VV$ decay, assuming $\kappa_g = \kappa_{g,\text{on-shell}} = \kappa_{g,\text{off-shell}}$ and $\kappa_V = \kappa_{V,\text{on-shell}} = \kappa_{V,\text{off-shell}}$.
- Determination of $R_{gg} = \kappa_{g,\text{off-shell}}^2 / \kappa_{g,\text{on-shell}}^2$ when profiling the coupling scale factor $\kappa_V = \kappa_{V,\text{on-shell}} =$
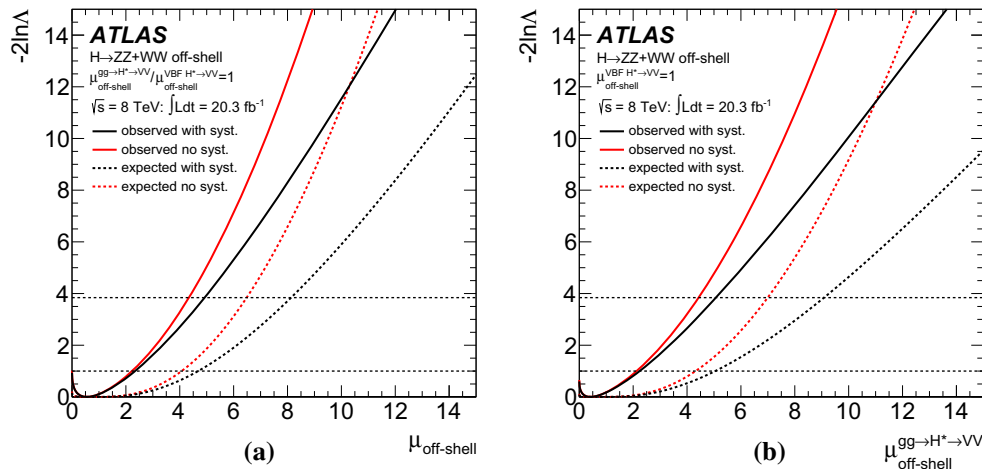

Fig. 9 Scan of the negative log-likelihood, $-2 \ln \Lambda$, as a function of $\mu_{\text{off-shell}}$, for the combined ZZ and WW analyses. **a** Common signal strength $\mu_{\text{off-shell}}$ applied to both the $gg \to H^*$ and VBF processes. The ratio of the $gg \to H^*$ and VBF processes is assumed to be as in the SM. **b** Signal strength $\mu_{\text{off-shell}}^{gg \to H^* \to VV}$ for the $gg \to H^* \to VV$ process. The production rate for the VBF

off-shell process is fixed to the SM prediction. The *black solid (dashed) line* represents the observed (expected) value including all systematic uncertainties, while the *red solid (dashed) line* is for the observed (expected) value without systematic uncertainties. A relative $gg \to VV$ background K-factor of $R_{H^*}^B = 1$ is assumed in these figures

Table 4 The observed and expected 95 % CL upper limits on $\mu_{\text{off-shell}}$ and $\mu_{\text{off-shell}}^{gg \to H^* \to VV}$ within the range of $0.5 < R_{H^*}^B < 2$ for the combined ZZ and WW analyses. Results are shown for two hypotheses, which

are defined in the assumption column. The bold numbers correspond to the limit assuming $R_{H^*}^B = 1$. The upper limits are evaluated using the CL_s method, with the alternative hypothesis $\mu_{\text{off-shell}} = 1$

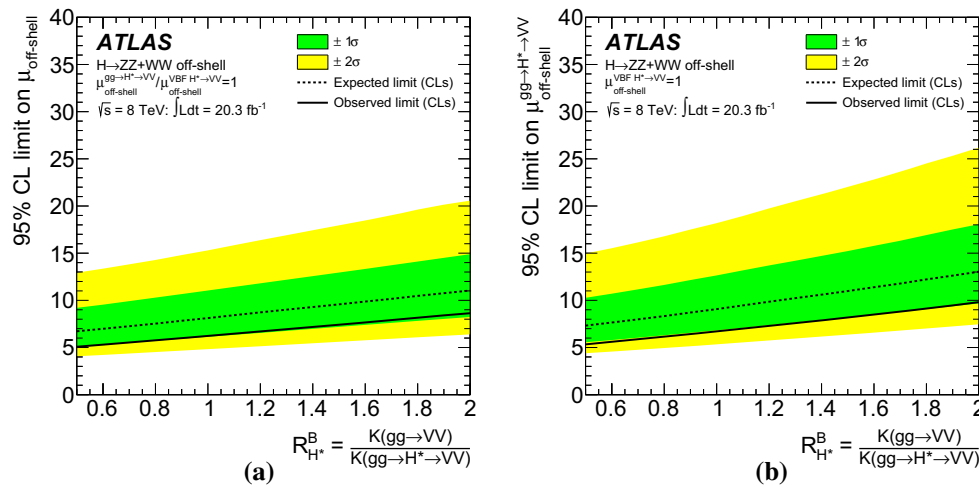| $R_{H^*}^B$	Observed			Median expected			Assumption
	0.5	**1.0**	2.0	0.5	**1.0**	2.0	
$\mu_{\text{off-shell}}$	5.1	**6.2**	8.6	6.7	**8.1**	11.0	$\mu_{\text{off-shell}}^{gg \to H^*} / \mu_{\text{off-shell}}^{VBF} = 1$
$\mu_{\text{off-shell}}^{gg \to H^* \to VV}$	5.3	**6.7**	9.8	7.3	**9.1**	13.0	$\mu_{\text{off-shell}}^{VBF\ H^* \to VV} = 1$

Fig. 10 The observed and expected combined 95 % CL upper limit on $\mu_{\text{off-shell}}$ as a function of $R_{H^*}^B$ for the combined ZZ and WW analyses. The upper limits are calculated using the CL_s method, with the SM as the alternative hypothesis. **a** Limit on the common signal strength $\mu_{\text{off-shell}}$ applied to both the $gg \to H^*$ and VBF processes. The ratio

of the $gg \to H^*$ and VBF processes is assumed to be as in the SM. **b** Limit on the signal strength $\mu_{\text{off-shell}}^{gg \to H^* \to VV}$ for the $gg \to H^* \to VV$ process. The production rate for the VBF off-shell process is fixed to the SM prediction. The *green (yellow) bands* represent the 68 % (95 %) confidence intervals for the CL_s expected limit

Table 5 The expected 95 % CL upper limit on $\mu_{\text{off-shell}}$ for the combined ZZ and WW analyses, with a ranked listing of each systematic uncertainty individually, comparing with no systematic uncertainty or all systematic uncertainties. The upper limits are evaluated using the CL_s method, assuming $R_{H^*}^B = 1$. The ratio of the $gg \to H^*$ and VBF processes is assumed to be as expected in the SM

Systematic uncertainty	95 % CL lim. (CL_s) on $\mu_{\text{off-shell}}$
Interference $gg \to (H^* \to)VV$	7.2
QCD scale $K^{H^*}(m_{VV})$ (correlated component)	7.1
PDF $q\bar{q} \to VV$ and $gg \to (H^* \to)VV$	6.7
QCD scale $q\bar{q} \to VV$	6.7
Luminosity	6.6
Drell–Yan background	6.6
QCD scale $K_{gg}^{H^*}(m_{VV})$ (uncorrelated component)	6.5
Remaining systematic uncertainties	6.5
All systematic uncertainties	8.1
No systematic uncertainties	6.5

$\kappa_{V,\text{off-shell}}$ associated with the VBF production and the $H^{(*)} \to VV$ decay. The ratio $\Gamma_H / \Gamma_H^{\text{SM}} = 1$ is fixed to the SM prediction. The parameter R_{gg} is sensitive to possible modifications of the gluon couplings in the high-mass range with respect to the on-shell value.

The negative log-likelihood scans for the above-defined fitting configurations as well as the combined upper limit at 95 % CL on $\Gamma_H / \Gamma_H^{\text{SM}}$ and R_{gg} are illustrated in Figs. 11 and

12 and the corresponding limits are listed in Table 6. The limits are all computed with the CL_s method, taking the SM values as the alternative hypothesis.

The limit on $\Gamma_H / \Gamma_H^{\text{SM}}$ can be translated into a limit on the total width of the Higgs boson under the assumptions reported above, out of which the most important is that the relevant Higgs boson coupling scale factors are independent of the energy scale of the Higgs boson production. Assuming a value of $R_{H^*}^B = 1$, this translates into an observed (expected) 95 % CL upper limit on the Higgs boson total width of 22.7 (33.0) MeV.[10]

8 Conclusion

The measurement of the ZZ and WW final states in the mass range above the $2m_Z$ and $2m_W$ thresholds provides a unique opportunity to measure the off-shell coupling strengths of the observed Higgs boson. In this paper constraints on the off-shell Higgs boson signal strengths in the $ZZ \to 4\ell$, $ZZ \to 2\ell 2\nu$ and $WW \to e\nu\mu\nu$ final states and their combination are presented. The result is based on pp collision data collected by the ATLAS experiment at the LHC, corresponding to an integrated luminosity of 20.3 fb^{-1} at a collision energy of $\sqrt{s} = 8$ TeV.

Using the CL_s method, the observed 95 % confidence level (CL) upper limit on the off-shell signal strength is in the range 5.1–8.6, with an expected range of 6.7–11.0. In each

---

[10] The value of the SM Higgs boson width of 4.12 MeV at a mass of 125.4 GeV [23] is used to convert the limit $\Gamma_H / \Gamma_H^{\text{SM}}$ into the total width limit.
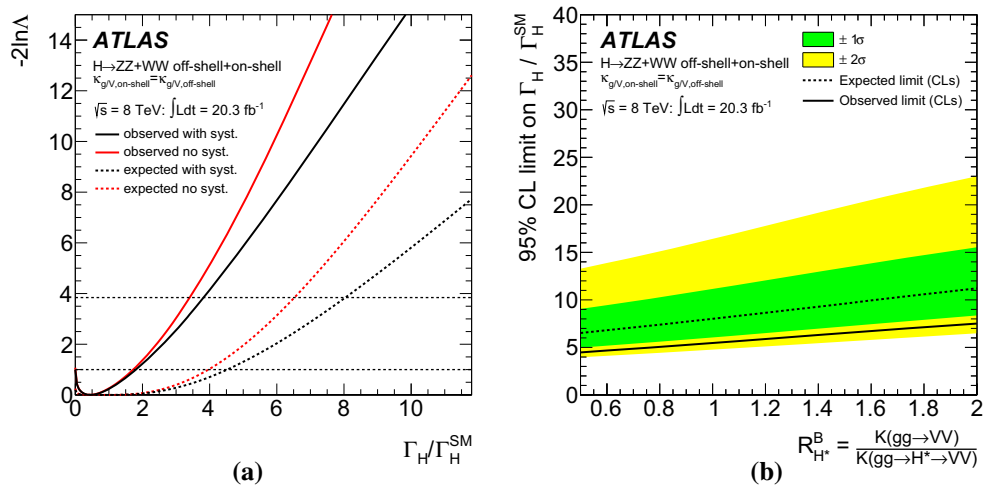
(a)

(b)

Fig. 11 **a** Scan of the negative log-likelihood as a function of Γ_H / Γ_H^{SM} when profiling the coupling scale factors κ_g and κ_V associated with the on- and off-shell $gg \to H^{(*)}$ and VBF production and the $H^{(*)} \to VV$ decay. The *black solid (dashed) line* represents the observed (expected) value including all systematic uncertainties, while the *red solid (dashed) line* is for the observed (expected) value without systematic

uncertainties. **b** Observed and expected combined 95 % CL upper limit on Γ_H / Γ_H^{SM} as a function of R_{H*}^B under the same assumption as **a**. The upper limits are calculated from the CL_s method, with the SM values as the alternative hypothesis. The *green (yellow) bands* represent the 68 % (95 %) confidence intervals for the CL_s expected limit

(a)

(b)

Fig. 12 **a** Scan of $R_{gg} = \kappa_{g,\text{off-shell}}^2 / \kappa_{g,\text{on-shell}}^2$ when profiling the coupling scale factor κ_V associated with the on- and off-shell VBF production and the $H^{(*)} \to VV$ decay. The ratio Γ_H / Γ_H^{SM} is set to 1.0. The *black solid (dashed) line* represents the observed (expected) value including all systematic uncertainties, while the *red solid (dashed) line* is for the observed (expected) value without systematic uncertainties.

b Observed and expected combined 95 % CL upper limit on R_{gg} as a function of R_{H*}^B under the same assumption as **a**. The upper limits are calculated from the CL_s method, with the SM values as the alternative hypothesis. The *green (yellow) bands* represent the 68 % (95 %) confidence intervals for the CL_s expected limit
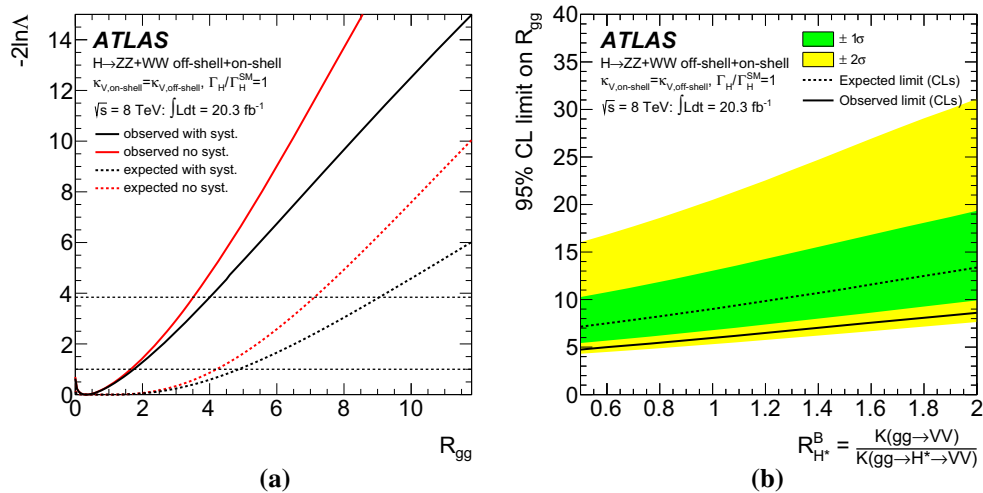
Table 6 Observed and expected 95 % CL upper limits on Γ_H / Γ_H^{SM} and R_{gg} for the combined on- and off-shell ZZ and WW analyses. Results are shown for two hypotheses, which are defined in the assumption column. R_{H*}^B is within the range $0.5 < R_{H*}^B < 2$

R_{H*}^B	Observed			Median expected			Assumption
	0.5	**1.0**	2.0	0.5	**1.0**	2.0	
Γ_H / Γ_H^{SM}	4.5	**5.5**	7.5	6.5	**8.0**	11.2	$\kappa_{i,\text{on-shell}} = \kappa_{i,\text{off-shell}}$
$R_{gg} = \kappa_{g,\text{off-shell}}^2 / \kappa_{g,\text{on-shell}}^2$	4.7	**6.0**	8.6	7.1	**9.0**	13.4	$\kappa_{V,\text{on-shell}} = \kappa_{V,\text{off-shell}}, \Gamma_H / \Gamma_H^{SM} = 1$

case the range is determined by varying the unknown $gg \to ZZ$ and $gg \to WW$ background K-factor from higher-order QCD corrections between half and twice the value of the known signal K-factor.

Assuming the relevant Higgs boson couplings are independent of the energy scale of the Higgs boson production, a combination with the on-shell measurements of ZZ and WW in the same dataset yields an observed (expected) 95 % CL upper limit on Γ_H / Γ_H^{SM} in the range 4.5–7.5 (6.5–11.2) under the same variations of the background K-factor. Assuming the value of $R_{H^*}^B = 1$ and under the assumptions reported above, this translates into an observed (expected) 95 % CL upper limit on the Higgs boson total width of 22.7 (33.0) MeV.

Assuming that the total width of the Higgs boson is as expected in the SM, the same combination can be interpreted as a limit on the ratio of the off-shell to the on-shell couplings to gluons $R_{gg} = \kappa_{g,\text{off-shell}}^2 / \kappa_{g,\text{on-shell}}^2$. An observed (expected) 95 % CL upper limit on R_{gg} in the range 4.7–8.6 (7.1–13.4) under the same variations of the background K-factor is found.

Appendix A: Monte Carlo and PDF scaling to arbitrary $\mu_{\text{off-shell}}$

The known dependence of the off-shell Higgs boson signal process, the background process and the interference term on the off-shell signal strength $\mu_{\text{off-shell}}$ can be used to construct MC samples for arbitrary values of $\mu_{\text{off-shell}}$ from three basic samples generated at different fixed values of $\mu_{\text{off-shell}}$.

A.1: Dependence of the $gg \to (H^* \to) VV$ off-shell cross-sections on the signal strength

An event sample $\sigma_{gg \to (H^* \to) VV}(\mu_{\text{off-shell}})$ for the $gg \to (H^* \to) VV$ process with an arbitrary value of the off-shell Higgs boson signal strength $\mu_{\text{off-shell}}$ can be constructed from the MC sample for the SM Higgs boson signal $gg \to H^* \to VV$ ($\sigma_{gg \to H^* \to VV}^{SM}$), the $gg \to VV$ continuum background MC sample ($\sigma_{gg \to VV, \text{cont}}$) and a full SM Higgs boson signal plus background $gg \to (H^* \to) VV$ MC sample ($\sigma_{gg \to (H^* \to) VV}^{SM}$) using the following weighting function:

$$
\begin{aligned}
&\sigma_{gg \to (H^* \to) VV}(\mu_{\text{off-shell}}, m_{VV}) \\
&= K^{H^*}(m_{VV}) \cdot \mu_{\text{off-shell}} \cdot \sigma_{gg \to H^* \to VV}^{SM}(m_{VV}) \\
&\quad + \sqrt{K_{gg}^{H^*}(m_{VV}) \cdot K^B(m_{VV}) \cdot \mu_{\text{off-shell}}} \\
&\qquad \cdot \sigma_{gg \to VV, \text{Interference}}^{SM}(m_{VV}) \\
&\quad + K^B(m_{VV}) \cdot \sigma_{gg \to VV, \text{cont}}(m_{VV}),
\end{aligned} \tag{13}
$$

$$
\begin{aligned}
&\sigma_{gg \to VV, \text{Interference}}^{SM}(m_{VV}) \\
&= \sigma_{gg \to (H^* \to) VV}^{SM}(m_{VV}) - \sigma_{gg \to H^* \to VV}^{SM}(m_{VV}) \\
&\quad - \sigma_{gg \to VV, \text{cont}}^{SM}(m_{VV}),
\end{aligned} \tag{14}
$$

where the K-factors are calculated inclusively without any selections.

As a direct simulation of an interference MC sample is not possible, Eq. (13) and $R_{H^*}^B$ are used to obtain:

$$
\begin{aligned}
&\sigma_{gg \to (H^* \to) VV}(\mu_{\text{off-shell}}, m_{VV}) \\
&= \left(K^{H^*}(m_{VV}) \cdot \mu_{\text{off-shell}} - K_{gg}^{H^*}(m_{VV}) \right. \\
&\qquad \left. \cdot \sqrt{R_{H^*}^B \cdot \mu_{\text{off-shell}}} \right) \cdot \sigma_{gg \to H^* \to VV}^{SM}(m_{VV}) \\
&\quad + K_{gg}^{H^*}(m_{VV}) \cdot \sqrt{R_{H^*}^B \cdot \mu_{\text{off-shell}}} \\
&\qquad \cdot \sigma_{gg \to (H^* \to) VV}^{SM}(m_{VV}) \\
&\quad + K_{gg}^{H^*}(m_{VV}) \cdot \left(R_{H^*}^B - \sqrt{R_{H^*}^B \cdot \mu_{\text{off-shell}}} \right) \cdot \\
&\qquad \cdot \sigma_{gg \to VV, \text{cont}}(m_{VV}).
\end{aligned} \tag{15}
$$

A.2: Dependence of the $VV + 2j$ off-shell signal and background interference on the signal strength

An MC event sample for the EW $pp \rightarrow (H^* + 2j \rightarrow)VV + 2j$ process with an arbitrary value of the off-shell Higgs boson signal strength $\mu_{\text{off-shell}}$ can be constructed from a pure $pp \rightarrow VV + 2j$ continuum background MC sample, a full SM Higgs boson signal plus background $pp \rightarrow (H^* + 2j \rightarrow)VV + 2j$ MC sample and a third Higgs boson signal plus background $pp \rightarrow (H^* + 2j \rightarrow) VV + 2j$ MC sample with $\mu_{\text{off-shell}} = \kappa_V^4 = \Gamma_H / \Gamma_H^{\text{SM}} = 10$. Using $\Gamma_H / \Gamma_H^{\text{SM}} = 10$ for the last sample ensures that the on-shell VH events are generated with SM-like signal strength.

The following weighting function is used:

$$\sigma_{pp \rightarrow (H^*+2j \rightarrow)VV+2j}(\mu_{\text{off-shell}})$$
$$= \mu_{\text{off-shell}} \cdot \sigma_{pp \rightarrow H^*+2j \rightarrow VV+2j}^{\text{SM}}$$
$$+ \sqrt{\mu_{\text{off-shell}}} \cdot \sigma_{pp \rightarrow VV+2j, \text{ Interference}} + \sigma_{pp \rightarrow VV+2j, \text{ cont}},$$
$$(16)$$

where the signal and interference samples are implicitly defined through the SM $pp \rightarrow (H^* + 2j \rightarrow)VV + 2j$ MC sample

$$\sigma_{pp \rightarrow (H^*+2j \rightarrow)VV+2j}^{\text{SM}} = \sigma_{pp \rightarrow H^*+2j \rightarrow VV+2j}^{\text{SM}}$$
$$+ \sigma_{pp \rightarrow VV+2j, \text{ Interference}}$$
$$+ \sigma_{pp \rightarrow VV+2j, \text{ cont}} \qquad (17)$$

and a $\mu_{\text{off-shell}} = 10$ MC sample:

$$\sigma_{pp \rightarrow (H^*+2j \rightarrow)VV+2j}^{\kappa_V^4=10} = 10 \cdot \sigma_{pp \rightarrow H^*+2j \rightarrow VV+2j}^{\text{SM}}$$
$$+ \sqrt{10} \cdot \sigma_{pp \rightarrow VV+2j, \text{ Interference}}$$
$$+ \sigma_{pp \rightarrow VV+2j, \text{ cont}} \cdot \qquad (18)$$

Solving for the generated MC samples yields:

$$\sigma_{pp \rightarrow (H^*+2j \rightarrow)VV+2j}(\mu_{\text{off-shell}})$$
$$= \frac{\mu_{\text{off-shell}} - \sqrt{\mu_{\text{off-shell}}}}{10 - \sqrt{10}} \sigma_{pp \rightarrow (H^*+2j \rightarrow)VV+2j}^{\kappa_V^4=10}$$
$$+ \frac{10\sqrt{\mu_{\text{off-shell}}} - \sqrt{10}\mu_{\text{off-shell}}}{10 - \sqrt{10}} \sigma_{pp \rightarrow (H^*+2j \rightarrow)VV+2j}^{\text{SM}}$$
$$+ \frac{(\sqrt{\mu_{\text{off-shell}}} - 1) \cdot (\sqrt{\mu_{\text{off-shell}}} - \sqrt{10})}{\sqrt{10}} \sigma_{pp \rightarrow VV+2j, \text{ cont}} \cdot \qquad (19)$$

References

1. ATLAS Collaboration, Observation of a new particle in the search for the Standard Model Higgs boson with the ATLAS detector at the LHC. Phys. Lett. B **716**, 1 (2012). arXiv:1207.7214 [hep-ex]
2. CMS Collaboration, Observation of a new boson at a mass of 125 GeV with the CMS experiment at the LHC. Phys. Lett. B **716**, 30 (2012). arXiv:1207.7235 [hep-ex]
3. ATLAS Collaboration, Measurements of Higgs boson production and couplings in diboson final states with the ATLAS detector at the LHC. Phys. Lett. B **726**, 88 (2013). arXiv:1307.1427 [hep-ex]
4. CMS Collaboration, Precise determination of the mass of the Higgs boson and tests of compatibility of its couplings with the standard model predictions using proton collisions at 7 and 8 TeV. Eur. Phys. J. C **75**(5), 212 (2015). arXiv:1412.8662 [hep-ex]
5. ATLAS Collaboration, Evidence for the spin-0 nature of the Higgs boson using ATLAS data. Phys. Lett. B **726**, 120 (2013). arXiv:1307.1432 [hep-ex]
6. CMS Collaboration, Constraints on the spin-parity and anomalous HVV couplings of the Higgs boson in proton collisions at 7 and 8 TeV. arXiv:1411.3441 [hep-ex]
7. N. Kauer, G. Passarino, Inadequacy of zero-width approximation for a light Higgs boson signal. JHEP **08**, 116 (2012). arXiv:1206.4803 [hep-ph]
8. F. Caola, K. Melnikov, Constraining the Higgs boson width with ZZ production at the LHC. Phys. Rev. D **88**, 054024 (2013). arXiv:1307.4935 [hep-ph]
9. J.M. Campbell, R.K. Ellis, C. Williams, Bounding the Higgs width at the LHC using full analytic results for $gg \rightarrow e^- e^+ \mu^- \mu^+$. JHEP **04**, 060 (2014). arXiv:1311.3589 [hep-ph]
10. J.M. Campbell, R.K. Ellis, C. Williams, Bounding the Higgs width at the LHC: complementary results from $H \rightarrow WW$. Phys. Rev. D **89**, 053011 (2014). arXiv:1312.1628 [hep-ph]
11. ATLAS Collaboration, Measurement of the Higgs boson mass from the $H \rightarrow \gamma\gamma$ collision data. Phys. Rev. D **90**, 052004 (2014). arXiv:1406.3827 [hep-ex]
12. C. Englert, M. Spannowsky, Limitations and opportunities of off-shell coupling measurements. Phys. Rev. D **90**, 053003 (2014). arXiv:1405.0285 [hep-ph]
13. G. Cacciapaglia, A. Deandrea, G.D. La Rochelle, J.-B. Flament, Higgs couplings: disentangling new physics with off-shell measurements. Phys. Rev. Lett. **113**, 201802 (2014). arXiv:1406.1757 [hep-ph]
14. A. Azatov, C. Grojean, A. Paul, E. Salvioni, Taming the off-shell Higgs boson. JETP **147**(3) (2015). arXiv:1406.6338 [hep-ph]
15. M. Ghezzi, G. Passarino, S. Uccirati, Bounding the Higgs width using effective field theory. PoS **LL2014**, 072 (2014). arXiv:1405.1925 [hep-ph]
16. M. Buschmann, D. Goncalves, S. Kuttimalai, M. Schonherr, F. Krauss et al., Mass effects in the Higgs-gluon coupling: boosted vs off-shell production. JHEP **2**, 38 (2015). doi:10.1007/JHEP02(2015)038. arXiv:1410.5806 [hep-ph]
17. J.S. Gainer, J. Lykken, K.T. Matchev, S. Mrenna, M. Park, Beyond geolocating: constraining higher dimensional operators in $H \rightarrow 4\ell$ with off-shell production and more. Phys. Rev. D **91**(3), 035011 (2015). arXiv:1403.4951 [hep-ph]
18. C. Englert, Y. Soreq, M. Spannowsky, Off-shell Higgs coupling measurements in BSM scenarios. JHEP **5**, 145 (2015). doi:10.1007/JHEP05(2015)145. arXiv:1410.5440 [hep-ph]
19. CMS Collaboration, Constraints on the Higgs boson width from off-shell production and decay to Z-boson pairs. Phys. Lett. B **736**, 64 (2014). arXiv:1405.3455 [hep-ex]
20. ATLAS Collaboration, Search for invisible decays of a Higgs boson produced in association with a Z boson in ATLAS. Phys. Rev. Lett. **112**, 201802 (2014). arXiv:1402.3244 [hep-ex]
21. CMS collaboration, Search for invisible decays of Higgs bosons in the vector boson fusion and associated ZH production modes. Eur. Phys. J. C **74**, 2980 (2014). arXiv:1404.1344 [hep-ex]
22. ATLAS Collaboration, The ATLAS experiment at the CERN Large Hadron Collider. JINST **3**, S08003 (2008)
23. LHC Higgs Cross Section Working Group, S. Heinemeyer, C. Mariotti, G. Passarino, R. Tanaka (eds.), *Handbook of LHC Higgs Cross Sections: 3. Higgs Properties*. arXiv:1307.1347 [hep-ph]

24. H.E. Logan, Hiding a Higgs width enhancement from off-shell gg ($\rightarrow h^*$) $\rightarrow ZZ$ measurements. arXiv:1412.7577 [hep-ph]
25. G. Passarino, Higgs CAT. Eur. Phys. J. C **74**, 2866 (2014). arXiv:1312.2397 [hep-ph]
26. S. Agostinelli et al., Geant4, a simulation toolkit. Nucl. Instrum. Methods A **506**, 250 (2003)
27. ATLAS Collaboration, The ATLAS simulation infrastructure. Eur. Phys. J. C **70**, 823 (2010). arXiv:1005.4568 [hep-ph]
28. N. Kauer, Interference effects for $H \rightarrow WW/ZZ \rightarrow \ell\bar{\nu}_\ell\bar{\ell}\nu_\ell$ searches in gluon fusion at the LHC. JHEP **12**, 082 (2013). arXiv:1310.7011 [hep-ph]
29. T. Sjostrand, S. Mrenna, P.Z. Skands, A. Brief, Introduction to PYTHIA 8.1. Comput. Phys. Commun. **178**, 852–867 (2008). arXiv:0710.3820 [hep-ph]
30. F. Cascioli et al., Precise Higgs-background predictions: merging NLO QCD and squared quark-loop corrections to four-lepton + 0,1 jet production. JHEP **01**, 046 (2014). arXiv:1309.0500 [hep-ph]
31. T. Gleisberg et al., Event generation with SHERPA 1.1. JHEP **02**, 007 (2009). arXiv:0811.4622 [hep-ph]
32. F. Cascioli, P. Maierhöfer, S. Pozzorini, Scattering amplitudes with open loops. Phys. Rev. Lett. **108**, 111601 (2012). arXiv:1111.5206 [hep-ph]
33. A. Denner, S. Dittmaier, L. Hofer, COLLIER – a fortran-library for one-loop integrals. PoS **LL2014**, 071 (2014). arXiv:1407.0087 [hep-ph]
34. J. Gao et al., The CT10 NNLO global analysis of QCD. Phys. Rev. D **89**, 033009 (2014). arXiv:1302.6246 [hep-ph]
35. A. Martin, W. Stirling, R. Thorne, G. Watt, Parton distributions for the LHC. Eur. Phys. J. C **63**, 189–285 (2009). arXiv:0901.0002 [hep-ph]
36. M. Bonvini, F. Caola, S. Forte, K. Melnikov, G. Ridolfi, Signal-background interference effects for $gg \rightarrow H \rightarrow W^+W^-$ beyond leading order. Phys. Rev. D **88**, 034032 (2013). arXiv:1304.3053 [hep-ph]
37. J. Alwall et al., The automated computation of tree-level and next-to-leading order differential cross sections, and their matching to parton shower simulations. JHEP **07**, 079 (2014). arXiv:1405.0301 [hep-ph]. (optimised by the authors for the production of VBF ($H^* \rightarrow)VV$)
38. A. Ballestrero, A. Belhouari, G. Bevilacqua, V. Kashkan, E. Maina, PHANTOM: a Monte Carlo event generator for six parton final states at high energy colliders. Comput. Phys. Commun. **180**, 401–417 (2009). arXiv:0801.3359 [hep-ph]. (extended by the authors to include the production of the VBF $H^*) \rightarrow VV$ signal process
39. LHC Higgs Cross Section Working Group, S. Dittmaier, C. Mariotti, G. Passarino, R. Tanaka (eds.), *Handbook of LHC Higgs Cross Sections: 2. Differential Distributions, CERN-2012-002* (CERN, Geneva, 2012). arXiv:1201.3084 [hep-ph]
40. J. Pumplin et al., New generation of parton distributions with uncertainties from global QCD analysis. JHEP **07**, 012 (2002). arXiv:hep-ph/0201195
41. T. Sjostrand et al., PYTHIA 6.4 physics and manual. JHEP **05**, 026 (2006)
42. T. Melia, P. Nason, R. Röntsch, G. Zanderighi, W^+W^-, WZ and ZZ production in the POWHEG BOX. JHEP **11**, 078 (2011). arXiv:1107.5051 [hep-ph]
43. F. Cascioli et al., ZZ production at hadron colliders in NNLO QCD. Phys. Lett. B **735**, 311 (2014). arXiv:1405.2219 [hep-ph]. (extended by the authors to provide NNLO/NLO K-factors as a function of m_{ZZ})
44. T. Gehrmann et al., W^+W^- production at hadron colliders in NNLO QCD. Phys. Rev. Lett. **113**, 212001 (2014). arXiv:1408.5243 [hep-ph]. (extended by the authors to provide NNLO/NLO K-factors as a function of m_{WW})
45. A. Bierweiler, T. Kasprzik, J.H. Kühn, Vector-boson pair production at the LHC to $\mathcal{O}(\alpha^3)$ accuracy. JHEP **12**, 071 (2013). arXiv:1305.5402 [hep-ph]
46. J. Baglio, L.D. Ninh, M.M. Weber, Massive gauge boson pair production at the LHC: a next-to-leading order story. Phys. Rev. D **88**, 113005 (2013). arXiv:1307.4331
47. S. Gieseke, T. Kasprzik, J.H. Kühn, Vector-boson pair production and electroweak corrections in HERWIG++. Eur. Phys. J. C **74**, 2988 (2014)
48. S. Alioli, S.-O. Moch, P. Uwer, Hadronic top-quark pair-production with one jet and parton showering. JHEP **1201**, 137 (2012). arXiv:1110.5251 [hep-ph]
49. S. Alioli, P. Nason, C. Oleari, E. Re, NLO single-top production matched with shower in POWHEG: s- and t-channel contributions. JHEP **0909**, 111 (2009). arXiv:0907.4076 [hep-ph]
50. B.P. Kersevan, E. Richter-Was, The Monte Carlo event generator AcerMC version 2.0 with interfaces to PYTHIA 6.2 and HERWIG 6.5. arXiv:hep-ph/0405247
51. M. Czakon, A. Mitov, Top++: a program for the calculation of the top-pair cross-section at hadron colliders. Comput. Phys. Commun. **185**(11), 2930–2938 (2014). http://www.sciencedirect.com/science/article/pii/S0010465514002264
52. N. Kidonakis, Next-to-next-to-leading logarithm resummation for s-channel single top quark production. Phys. Rev. D **81**, 054028 (2010). doi:10.1103/PhysRevD.81.054028
53. N. Kidonakis, Next-to-next-to-leading-order collinear and soft gluon corrections for t-channel single top quark production. Phys. Rev. D **83**, 091503 (2011). doi:10.1103/PhysRevD.83.091503
54. N. Kidonakis, Two-loop soft anomalous dimensions for single top quark associated production with a W^-. Phys. Rev. D **82**, 054018 (2010). doi:10.1103/PhysRevD.82.054018
55. ATLAS Collaboration, Measurements of Higgs boson production and couplings in the four-lepton channel in pp collisions at center-of-mass energies of 7 and 8 TeV with the ATLAS detector. Phys. Rev. D **91**, 012006 (2015). arXiv:1408.5191 [hep-ex]
56. ATLAS Collaboration, Calibration of b-tagging using dileptonic top pair events in a combinatorial likelihood approach with the ATLAS experiment, ATLAS-CONF-2014-004 (2014). https://cds.cern.ch/record/1664335
57. ATLAS Collaboration, Calibration of the performance of b and light-flavour jets in the 2012 ATLAS data, ATLAS-CONF-2014-046 (2014). https://cds.cern.ch/record/1741020
58. ATLAS Collaboration, Observation and measurement of Higgs boson decays to WW^* with the ATLAS detector. arXiv:1412.2641 [hep-ex]
59. G. Corcella et al., HERWIG 6: an event generator for hadron emission reactions with interfering gluons (including supersymmetric processes). JHEP **01**, 010 (2001)
60. H.-L. Lai et al., New parton distributions for collider physics. Phys. Rev. D **82**, 074024 (2010)
61. R.D. Ball et al., Impact of heavy quark masses on parton distributions and LHC phenomenology. Nucl. Phys. B **849**, 296 (2011). arXiv:1101.1300 [hep-ph]

62. M. Botje et al., The PDF4LHC working group interim recommendations. arXiv:1101.0538 [hep-ph]
63. ATLAS Collaboration, Improved luminosity determination in $pp = 7$ TeV using the ATLAS detector at the LHC. Eur. Phys. J. C **73**, 2518 (2013). arXiv:1302.4393 [hep-ex]
64. G. Cowan, K. Cranmer, E. Gross, O. Vitells, Asymptotic formulae for likelihood-based tests of new physics. Eur. Phys. J. C **71**, 1554 (2011). arXiv:1007.1727 [physics.data-an]

65. A.L. Read, Presentation of search results: the CL_s technique. J. Phys. **G28**, 2693 (2002)
66. ATLAS Collaboration, Combined search for the Standard Model Higgs boson in $pp = 7$ TeV with the ATLAS detector. Phys. Rev. D **86**, 032003 (2012). arXiv:1207.0319 [hep-ex]

ATLAS Collaboration

G. Aad[85], B. Abbott[113], J. Abdallah[152], O. Abdinov[11], R. Aben[107], M. Abolins[90], O. S. AbouZeid[159], H. Abramowicz[154], H. Abreu[153], R. Abreu[30], Y. Abulaiti[147a,147b], B. S. Acharya[165a,165b,a], L. Adamczyk[38a], D. L. Adams[25], J. Adelman[108], S. Adomeit[100], T. Adye[131], A. A. Affolder[74], T. Agatonovic-Jovin[13], J. A. Aguilar-Saavedra[126a,126f], M. Agustoni[17], S. P. Ahlen[22], F. Ahmadov[65,b], G. Aielli[134a,134b], H. Akerstedt[147a,147b], T. P. A. Åkesson[81], G. Akimoto[156], A. V. Akimov[96], G. L. Alberghi[20a,20b], J. Albert[170], S. Albrand[55], M. J. Alconada Verzini[71], M. Aleksa[30], I. N. Aleksandrov[65], C. Alexa[26a], G. Alexander[154], T. Alexopoulos[10], M. Alhroob[113], G. Alimonti[91a], L. Alio[85], J. Alison[31], S. P. Alkire[35], B. M. M. Allbrooke[18], P. P. Allport[74], A. Aloisio[104a,104b], A. Alonso[36], F. Alonso[71], C. Alpigiani[76], A. Altheimer[35], B. Alvarez Gonzalez[90], D. Álvarez Piqueras[168], M. G. Alviggi[104a,104b], K. Amako[66], Y. Amaral Coutinho[24a], C. Amelung[23], D. Amidei[89], S. P. Amor Dos Santos[126a,126c], A. Amorim[126a,126b], S. Amoroso[48], N. Amram[154], G. Amundsen[23], C. Anastopoulos[140], L. S. Ancu[49], N. Andari[30], T. Andeen[35], C. F. Anders[58b], G. Anders[30], K. J. Anderson[31], A. Andreazza[91a,91b], V. Andrei[58a], S. Angelidakis[9], I. Angelozzi[107], P. Anger[44], A. Angerami[35], F. Anghinolfi[30], A. V. Anisenkov[109,c], N. Anjos[12], A. Annovi[124a,124b], M. Antonelli[47], A. Antonov[98], J. Antos[145b], F. Anulli[133a], M. Aoki[66], L. Aperio Bella[18], G. Arabidze[90], Y. Arai[66], J. P. Araque[126a], A. T. H. Arce[45], F. A. Arduh[71], J-F. Arguin[95], S. Argyropoulos[42], M. Arik[19a], A. J. Armbruster[30], O. Arnaez[30], V. Arnal[82], H. Arnold[48], M. Arratia[28], O. Arslan[21], A. Artamonov[97], G. Artoni[23], S. Asai[156], N. Asbah[42], A. Ashkenazi[154], B. Åsman[147a,147b], L. Asquith[150], K. Assamagan[25], R. Astalos[145a], M. Atkinson[166], N. B. Atlay[142], B. Auerbach[6], K. Augsten[128], M. Aurousseau[146b], G. Avolio[30], B. Axen[15], M. K. Ayoub[117], G. Azuelos[95,d], M. A. Baak[30], A. E. Baas[58a], C. Bacci[135a,135b], H. Bachacou[137], K. Bachas[155], M. Backes[30], M. Backhaus[30], E. Badescu[26a], P. Bagiacchi[133a,133b], P. Bagnaia[133a,133b], Y. Bai[33a], T. Bain[35], J. T. Baines[131], O. K. Baker[177], P. Balek[129], T. Balestri[149], F. Balli[84], E. Banas[39], Sw. Banerjee[174], A. A. E. Bannoura[176], H. S. Bansil[18], L. Barak[30], S. P. Baranov[96], E. L. Barberio[88], D. Barberis[50a,50b], M. Barbero[85], T. Barillari[101], M. Barisonzi[165a,165b], T. Barklow[144], N. Barlow[28], S. L. Barnes[84], B. M. Barnett[131], R. M. Barnett[15], Z. Barnovska[5], A. Baroncelli[135a], G. Barone[49], A. J. Barr[120], F. Barreiro[82], J. Barreiro Guimarães da Costa[57], R. Bartoldus[144], A. E. Barton[72], P. Bartos[145a], A. Bassalat[117], A. Basye[166], R. L. Bates[53], S. J. Batista[159], J. R. Batley[28], M. Battaglia[138], M. Bauce[133a,133b], F. Bauer[137], H. S. Bawa[144,e], J. B. Beacham[111], M. D. Beattie[72], T. Beau[80], P. H. Beauchemin[162], R. Beccherle[124a,124b], P. Bechtle[21], H. P. Beck[17,f], K. Becker[120], M. Becker[83], S. Becker[100], M. Beckingham[171], C. Becot[117], A. J. Beddall[19c], A. Beddall[19c], V. A. Bednyakov[65], C. P. Bee[149], L. J. Beemster[107], T. A. Beermann[176], M. Begel[25], J. K. Behr[120], C. Belanger-Champagne[87], W. H. Bell[49], G. Bella[154], L. Bellagamba[20a], A. Bellerive[29], M. Bellomo[86], K. Belotskiy[98], O. Beltramello[30], O. Benary[154], D. Benchekroun[136a], M. Bender[100], K. Bendtz[147a,147b], N. Benekos[10], Y. Benhammou[154], E. Benhar Noccioli[49], J. A. Benitez Garcia[160b], D. P. Benjamin[45], J. R. Bensinger[23], S. Bentvelsen[107], L. Beresford[120], M. Beretta[47], D. Berge[107], E. Bergeaas Kuutmann[167], N. Berger[5], F. Berghaus[170], J. Beringer[15], C. Bernard[22], N. R. Bernard[86], C. Bernius[110], F. U. Bernlochner[21], T. Berry[77], P. Berta[129], C. Bertella[83], G. Bertoli[147a,147b], F. Bertolucci[124a,124b], C. Bertsche[113], D. Bertsche[113], M. I. Besana[91a], G. J. Besjes[106], O. Bessidskaia Bylund[147a,147b], M. Bessner[42], N. Besson[137], C. Betancourt[48], S. Bethke[101], A. J. Bevan[76], W. Bhimji[46], R. M. Bianchi[125], L. Bianchini[23], M. Bianco[30], O. Biebel[100], S. P. Bieniek[78], M. Biglietti[135a], J. Bilbao De Mendizabal[49], H. Bilokon[47], M. Bindi[54], S. Binet[117], A. Bingul[19c], C. Bini[133a,133b], C. W. Black[151], J. E. Black[144], K. M. Black[22], D. Blackburn[139], R. E. Blair[6], J.-B. Blanchard[137], J. E. Blanco[77], T. Blazek[145a], I. Bloch[42], C. Blocker[23], W. Blum[83,*], U. Blumenschein[54], G. J. Bobbink[107], V. S. Bobrovnikov[109,c], S. S. Bocchetta[81], A. Bocci[45], C. Bock[100], M. Boehler[48], J. A. Bogaerts[30], A. G. Bogdanchikov[109], C. Bohm[147a], V. Boisvert[77], T. Bold[38a], V. Boldea[26a], A. S. Boldyrev[99], M. Bomben[80], M. Bona[76], M. Boonekamp[137], A. Borisov[130], G. Borissov[72], S. Borroni[42], J. Bortfeldt[100], V. Bortolotto[60a,60b,60c], K. Bos[107], D. Boscherini[20a], M. Bosman[12], J. Boudreau[125], J. Bouffard[2], E. V. Bouhova-Thacker[72], D. Boumediene[34], C. Bourdarios[117], N. Bousson[114], S. Boutouil[136d], A. Boveia[30], J. Boyd[30], I. R. Boyko[65], I. Bozic[13], J. Bracinik[18], A. Brandt[8], G. Brandt[15], O. Brandt[58a], U. Bratzler[157],

B. Brau[86], J. E. Brau[116], H. M. Braun[176,*], S. F. Brazzale[165a,165c], K. Brendlinger[122], A. J. Brennan[88], L. Brenner[107], R. Brenner[167], S. Bressler[173], K. Bristow[146c], T. M. Bristow[46], D. Britton[53], D. Britzger[42], F. M. Brochu[28], I. Brock[21], R. Brock[90], J. Bronner[101], G. Brooijmans[35], T. Brooks[77], W. K. Brooks[32b], J. Brosamer[15], E. Brost[116], J. Brown[55], P. A. Bruckman de Renstrom[39], D. Bruncko[145b], R. Bruneliere[48], A. Bruni[20a], G. Bruni[20a], M. Bruschi[20a], L. Bryngemark[81], T. Buanes[14], Q. Buat[143], P. Buchholz[142], A. G. Buckley[53], S. I. Buda[26a], I. A. Budagov[65], F. Buehrer[48], L. Bugge[119], M. K. Bugge[119], O. Bulekov[98], H. Burckhart[30], S. Burdin[74], B. Burghgrave[108], S. Burke[131], I. Burmeister[43], E. Busato[34], D. Büscher[48], V. Büscher[83], P. Bussey[53], C. P. Buszello[167], J. M. Butler[22], A. I. Butt[3], C. M. Buttar[53], J. M. Butterworth[78], P. Butti[107], W. Buttinger[25], A. Buzatu[53], R. Buzykaev[109,c], S. Cabrera Urbán[168], D. Caforio[128], O. Cakir[4a], P. Calafiura[15], A. Calandri[137], G. Calderini[80], P. Calfayan[100], L. P. Caloba[24a], D. Calvet[34], S. Calvet[34], R. Camacho Toro[49], S. Camarda[42], D. Cameron[119], L. M. Caminada[15], R. Caminal Armadans[12], S. Campana[30], M. Campanelli[78], A. Campoverde[149], V. Canale[104a,104b], A. Canepa[160a], M. Cano Bret[76], J. Cantero[82], R. Cantrill[126a], T. Cao[40], M. D. M. Capeans Garrido[30], I. Caprini[26a], M. Caprini[26a], M. Capua[37a,37b], R. Caputo[83], R. Cardarelli[134a], T. Carli[30], G. Carlino[104a], L. Carminati[91a,91b], S. Caron[106], E. Carquin[32a], G. D. Carrillo-Montoya[8], J. R. Carter[28], J. Carvalho[126a,126c], D. Casadei[78], M. P. Casado[12], M. Casolino[12], E. Castaneda-Miranda[146b], A. Castelli[107], V. Castillo Gimenez[168], N. F. Castro[126a,g], P. Catastini[57], A. Catinaccio[30], J. R. Catmore[119], A. Cattai[30], J. Caudron[83], V. Cavaliere[166], D. Cavalli[91a], M. Cavalli-Sforza[12], V. Cavasinni[124a,124b], F. Ceradini[135a,135b], B. C. Cerio[45], K. Cerny[129], A. S. Cerqueira[24b], A. Cerri[150], L. Cerrito[76], F. Cerutti[15], M. Cerv[30], A. Cervelli[17], S. A. Cetin[19b], A. Chafaq[136a], D. Chakraborty[108], I. Chalupkova[129], P. Chang[166], B. Chapleau[87], J. D. Chapman[28], D. G. Charlton[18], C. C. Chau[159], C. A. Chavez Barajas[150], S. Cheatham[153], A. Chegwidden[90], S. Chekanov[6], S. V. Chekulaev[160a], G. A. Chelkov[65,h], M. A. Chelstowska[89], C. Chen[64], H. Chen[25], K. Chen[149], L. Chen[33d,i], S. Chen[33c], X. Chen[33f], Y. Chen[67], H. C. Cheng[89], Y. Cheng[31], A. Cheplakov[65], E. Cheremushkina[130], R. Cherkaoui El Moursli[136e], V. Chernyatin[25,*], E. Cheu[7], L. Chevalier[137], V. Chiarella[47], J. T. Childers[6], G. Chiodini[73a], A. S. Chisholm[18], R. T. Chislett[78], A. Chitan[26a], M. V. Chizhov[65], K. Choi[61], S. Chouridou[9], B. K. B. Chow[100], V. Christodoulou[78], D. Chromek-Burckhart[30], M. L. Chu[152], J. Chudoba[127], A. J. Chuinard[87], J. J. Chwastowski[39], L. Chytka[115], G. Ciapetti[133a,133b], A. K. Ciftci[4a], D. Cinca[53], V. Cindro[75], I. A. Cioara[21], A. Ciocio[15], Z. H. Citron[173], M. Ciubancan[26a], A. Clark[49], B. L. Clark[57], P. J. Clark[46], R. N. Clarke[15], W. Cleland[125], C. Clement[147a,147b], Y. Coadou[85], M. Cobal[165a,165c], A. Coccaro[139], J. Cochran[64], L. Coffey[23], J. G. Cogan[144], B. Cole[35], S. Cole[108], A. P. Colijn[107], J. Collot[55], T. Colombo[58c], G. Compostella[101], P. Conde Muiño[126a,126b], E. Coniavitis[48], S. H. Connell[146b], I. A. Connelly[77], S. M. Consonni[91a,91b], V. Consorti[48], S. Constantinescu[26a], C. Conta[121a,121b], G. Conti[30], F. Conventi[104a,j], M. Cooke[15], B. D. Cooper[78], A. M. Cooper-Sarkar[120], K. Copic[15], T. Cornelissen[176], M. Corradi[20a], F. Corriveau[87,k], A. Corso-Radu[164], A. Cortes-Gonzalez[12], G. Cortiana[101], G. Costa[91a], M. J. Costa[168], D. Costanzo[140], D. Côté[8], G. Cottin[28], G. Cowan[77], B. E. Cox[84], K. Cranmer[110], G. Cree[29], S. Crépé-Renaudin[55], F. Crescioli[80], W. A. Cribbs[147a,147b], M. Crispin Ortuzar[120], M. Cristinziani[21], V. Croft[106], G. Crosetti[37a,37b], T. Cuhadar Donszelmann[140], J. Cummings[177], M. Curatolo[47], C. Cuthbert[151], H. Czirr[142], P. Czodrowski[3], S. D'Auria[53], M. D'Onofrio[74], M. J. Da Cunha Sargedas De Sousa[126a,126b], C. Da Via[84], W. Dabrowski[38a], A. Dafinca[120], T. Dai[89], O. Dale[14], F. Dallaire[95], C. Dallapiccola[86], M. Dam[36], J. R. Dandoy[31], A. C. Daniells[18], M. Danninger[169], M. Dano Hoffmann[137], V. Dao[48], G. Darbo[50a], S. Darmora[8], J. Dassoulas[3], A. Dattagupta[61], W. Davey[21], C. David[170], T. Davidek[129], E. Davies[120,l], M. Davies[154], P. Davison[78], Y. Davygora[58a], E. Dawe[88], I. Dawson[140], R. K. Daya-Ishmukhametova[86], K. De[8], R. de Asmundis[104a], S. De Castro[20a,20b], S. De Cecco[80], N. De Groot[106], P. de Jong[107], H. De la Torre[82], F. De Lorenzi[64], L. De Nooij[107], D. De Pedis[133a], A. De Salvo[133a], U. De Sanctis[150], A. De Santo[150], J. B. De Vivie De Regie[117], W. J. Dearnaley[72], R. Debbe[25], C. Debenedetti[138], D. V. Dedovich[65], I. Deigaard[107], J. Del Peso[82], T. Del Prete[124a,124b], D. Delgove[117], F. Deliot[137], C. M. Delitzsch[49], M. Deliyergiyev[75], A. Dell'Acqua[30], L. Dell'Asta[22], M. Dell'Orso[124a,124b], M. Della Pietra[104a,j], D. della Volpe[49], M. Delmastro[5], P. A. Delsart[55], C. Deluca[107], D. A. DeMarco[159], S. Demers[177], M. Demichev[65], A. Demilly[80], S. P. Denisov[130], D. Derendarz[39], J. E. Derkaoui[136d], F. Derue[80], P. Dervan[74], K. Desch[21], C. Deterre[42], P. O. Deviveiros[30], A. Dewhurst[131], S. Dhaliwal[107], A. Di Ciaccio[134a,134b], L. Di Ciaccio[5], A. Di Domenico[133a,133b], C. Di Donato[104a,104b], A. Di Girolamo[30], B. Di Girolamo[30], A. Di Mattia[153], B. Di Micco[135a,135b], R. Di Nardo[47], A. Di Simone[48], R. Di Sipio[159], D. Di Valentino[29], C. Diaconu[85], M. Diamond[159], F. A. Dias[46], M. A. Diaz[32a], E. B. Diehl[89], J. Dietrich[16], S. Diglio[85], A. Dimitrievska[13], J. Dingfelder[21], P. Dita[26a], S. Dita[26a], F. Dittus[30], F. Djama[85], T. Djobava[51b], J. I. Djuvsland[58a], M. A. B. do Vale[24c], D. Dobos[30], M. Dobre[26a], C. Doglioni[49], T. Dohmae[156], J. Dolejsi[129], Z. Dolezal[129], B. A. Dolgoshein[98,*], M. Donadelli[24d], S. Donati[124a,124b], P. Dondero[121a,121b], J. Donini[34], J. Dopke[131], A. Doria[104a], M. T. Dova[71], A. T. Doyle[53], E. Drechsler[54], M. Dris[10], E. Dubreuil[34], E. Duchovni[173], G. Duckeck[100], O. A. Ducu[26a,85], D. Duda[176], A. Dudarev[30], L. Duflot[117], L. Duguid[77], M. Dührssen[30], M. Dunford[58a], H. Duran Yildiz[4a], M. Düren[52], A. Durglishvili[51b], D. Duschinger[44], M. Dwuznik[38a], M. Dyndal[38a], C. Eckardt[42], K. M. Ecker[101], W. Edson[2], N. C. Edwards[46], W. Ehrenfeld[21], T. Eifert[30],

G. Eigen[14], K. Einsweiler[15], T. Ekelof[167], M. El Kacimi[136c], M. Ellert[167], S. Elles[5], F. Ellinghaus[83], A. A. Elliot[170], N. Ellis[30], J. Elmsheuser[100], M. Elsing[30], D. Emeliyanov[131], Y. Enari[156], O. C. Endner[83], M. Endo[118], R. Engelmann[149], J. Erdmann[43], A. Ereditato[17], G. Ernis[176], J. Ernst[2], M. Ernst[25], S. Errede[166], E. Ertel[83], M. Escalier[117], H. Esch[43], C. Escobar[125], B. Esposito[47], A. I. Etienvre[137], E. Etzion[154], H. Evans[61], A. Ezhilov[123], L. Fabbri[20a,20b], G. Facini[31], R. M. Fakhrutdinov[130], S. Falciano[133a], R. J. Falla[78], J. Faltova[129], Y. Fang[33a], M. Fanti[91a,91b], A. Farbin[8], A. Farilla[135a], T. Farooque[12], S. Farrell[15], S. M. Farrington[171], P. Farthouat[30], F. Fassi[136e], P. Fassnacht[30], D. Fassouliotis[9], A. Favareto[50a,50b], L. Fayard[117], P. Federic[145a], O. L. Fedin[123,m], W. Fedorko[169], S. Feigl[30], L. Feligioni[85], C. Feng[33d], E. J. Feng[6], H. Feng[89], A. B. Fenyuk[130], P. Fernandez Martinez[168], S. Fernandez Perez[30], S. Ferrag[53], J. Ferrando[53], A. Ferrari[167], P. Ferrari[107], R. Ferrari[121a], D. E. Ferreira de Lima[53], A. Ferrer[168], D. Ferrere[49], C. Ferretti[89], A. Ferretto Parodi[50a,50b], M. Fiascaris[31], F. Fiedler[83], A. Filipčič[75], M. Filipuzzi[42], F. Filthaut[106], M. Fincke-Keeler[170], K. D. Finelli[151], M. C. N. Fiolhais[126a,126c], L. Fiorini[168], A. Firan[40], A. Fischer[2], C. Fischer[12], J. Fischer[176], W. C. Fisher[90], E. A. Fitzgerald[23], M. Flechl[48], I. Fleck[142], P. Fleischmann[89], S. Fleischmann[176], G. T. Fletcher[140], G. Fletcher[76], T. Flick[176], A. Floderus[81], L. R. Flores Castillo[60a], M. J. Flowerdew[101], A. Formica[137], A. Forti[84], D. Fournier[117], H. Fox[72], S. Fracchia[12], P. Francavilla[80], M. Franchini[20a,20b], D. Francis[30], L. Franconi[119], M. Franklin[57], M. Fraternali[121a,121b], D. Freeborn[78], S. T. French[28], F. Friedrich[44], D. Froidevaux[30], J. A. Frost[120], C. Fukunaga[157], E. Fullana Torregrosa[83], B. G. Fulsom[144], J. Fuster[168], C. Gabaldon[55], O. Gabizon[176], A. Gabrielli[20a,20b], A. Gabrielli[133a,133b], S. Gadatsch[107], S. Gadomski[49], G. Gagliardi[50a,50b], P. Gagnon[61], C. Galea[106], B. Galhardo[126a,126c], E. J. Gallas[120], B. J. Gallop[131], P. Gallus[128], G. Galster[36], K. K. Gan[111], J. Gao[33b,85], Y. Gao[46], Y. S. Gao[144,e], F. M. Garay Walls[46], F. Garberson[177], C. García[168], J. E. García Navarro[168], M. Garcia-Sciveres[15], R. W. Gardner[31], N. Garelli[144], V. Garonne[119], C. Gatti[47], A. Gaudiello[50a,50b], G. Gaudio[121a], B. Gaur[142], L. Gauthier[95], P. Gauzzi[133a,133b], I. L. Gavrilenko[96], C. Gay[169], G. Gaycken[21], E. N. Gazis[10], P. Ge[33d], Z. Gecse[169], C. N. P. Gee[131], D. A. A. Geerts[107], Ch. Geich-Gimbel[21], M. P. Geisler[58a], C. Gemme[50a], M. H. Genest[55], S. Gentile[133a,133b], M. George[54], S. George[77], D. Gerbaudo[164], A. Gershon[154], H. Ghazlane[136b], N. Ghodbane[34], B. Giacobbe[20a], S. Giagu[133a,133b], V. Giangiobbe[12], P. Giannetti[124a,124b], B. Gibbard[25], S. M. Gibson[77], M. Gilchriese[15], T. P. S. Gillam[28], D. Gillberg[30], G. Gilles[34], D. M. Gingrich[3,d], N. Giokaris[9], M. P. Giordani[165a,165c], F. M. Giorgi[20a], F. M. Giorgi[16], P. F. Giraud[137], P. Giromini[47], D. Giugni[91a], C. Giuliani[48], M. Giulini[58b], B. K. Gjelsten[119], S. Gkaitatzis[155], I. Gkialas[155], E. L. Gkougkousis[117], L. K. Gladilin[99], C. Glasman[82], J. Glatzer[30], P. C. F. Glaysher[46], A. Glazov[42], M. Goblirsch-Kolb[101], J. R. Goddard[76], J. Godlewski[39], S. Goldfarb[89], T. Golling[49], D. Golubkov[130], A. Gomes[126a,126b,126d], R. Gonçalo[126a], J. Goncalves Pinto Firmino Da Costa[137], L. Gonella[21], S. González de la Hoz[168], G. Gonzalez Parra[12], S. Gonzalez-Sevilla[49], L. Goossens[30], P. A. Gorbounov[97], H. A. Gordon[25], I. Gorelov[105], B. Gorini[30], E. Gorini[73a,73b], A. Gorišek[75], E. Gornicki[39], A. T. Goshaw[45], C. Gössling[43], M. I. Gostkin[65], D. Goujdami[136c], A. G. Goussiou[139], N. Govender[146b], H. M. X. Grabas[138], L. Graber[54], I. Grabowska-Bold[38a], P. Grafström[20a,20b], K-J. Grahn[42], J. Gramling[49], E. Gramstad[119], S. Grancagnolo[16], V. Grassi[149], V. Gratchev[123], H. M. Gray[30], E. Graziani[135a], Z. D. Greenwood[79,n], K. Gregersen[78], I. M. Gregor[42], P. Grenier[144], J. Griffiths[8], A. A. Grillo[138], K. Grimm[72], S. Grinstein[12,o], Ph. Gris[34], J.-F. Grivaz[117], J. P. Grohs[44], A. Grohsjean[42], E. Gross[173], J. Grosse-Knetter[54], G. C. Grossi[79], Z. J. Grout[150], L. Guan[33b], J. Guenther[128], F. Guescini[49], D. Guest[177], O. Gueta[154], E. Guido[50a,50b], T. Guillemin[117], S. Guindon[2], U. Gul[53], C. Gumpert[44], J. Guo[33e], S. Gupta[120], P. Gutierrez[113], N. G. Gutierrez Ortiz[53], C. Gutschow[44], C. Guyot[137], C. Gwenlan[120], C. B. Gwilliam[74], A. Haas[110], C. Haber[15], H. K. Hadavand[8], N. Haddad[136e], P. Haefner[21], S. Hageböck[21], Z. Hajduk[39], H. Hakobyan[178], M. Haleem[42], J. Haley[114], D. Hall[120], G. Halladjian[90], G. D. Hallewell[85], K. Hamacher[176], P. Hamal[115], K. Hamano[170], M. Hamer[54], A. Hamilton[146a], S. Hamilton[162], G. N. Hamity[146c], P. G. Hamnett[42], L. Han[33b], K. Hanagaki[118], K. Hanawa[156], M. Hance[15], P. Hanke[58a], R. Hanna[137], J. B. Hansen[36], J. D. Hansen[36], M. C. Hansen[21], P. H. Hansen[36], K. Hara[161], A. S. Hard[174], T. Harenberg[176], F. Hariri[117], S. Harkusha[92], R. D. Harrington[46], P. F. Harrison[171], F. Hartjes[107], M. Hasegawa[67], S. Hasegawa[103], Y. Hasegawa[141], A. Hasib[113], S. Hassani[137], S. Haug[17], R. Hauser[90], L. Hauswald[44], M. Havranek[127], C. M. Hawkes[18], R. J. Hawkings[30], A. D. Hawkins[81], T. Hayashi[161], D. Hayden[90], C. P. Hays[120], J. M. Hays[76], H. S. Hayward[74], S. J. Haywood[131], S. J. Head[18], T. Heck[83], V. Hedberg[81], L. Heelan[8], S. Heim[122], T. Heim[176], B. Heinemann[15], L. Heinrich[110], J. Hejbal[127], L. Helary[22], S. Hellman[147a,147b], D. Hellmich[21], C. Helsens[30], J. Henderson[120], R. C. W. Henderson[72], Y. Heng[174], C. Hengler[42], A. Henrichs[177], A. M. Henriques Correia[30], S. Henrot-Versille[117], G. H. Herbert[16], Y. Hernández Jiménez[168], R. Herrberg-Schubert[16], G. Herten[48], R. Hertenberger[100], L. Hervas[30], G. G. Hesketh[78], N. P. Hessey[107], J. W. Hetherly[40], R. Hickling[76], E. Higón-Rodriguez[168], E. Hill[170], J. C. Hill[28], K. H. Hiller[42], S. J. Hillier[18], I. Hinchliffe[15], E. Hines[122], R. R. Hinman[15], M. Hirose[158], D. Hirschbuehl[176], J. Hobbs[149], N. Hod[107], M. C. Hodgkinson[140], P. Hodgson[140], A. Hoecker[30], M. R. Hoeferkamp[105], F. Hoenig[100], M. Hohlfeld[83], D. Hohn[21], T. R. Holmes[15], T. M. Hong[122], L. Hooft van Huysduynen[110], W. H. Hopkins[116], Y. Horii[103], A. J. Horton[143], J-Y. Hostachy[55], S. Hou[152], A. Hoummada[136a], J. Howard[120], J. Howarth[42], M. Hrabovsky[115],

I. Hristova[16], J. Hrivnac[117], T. Hryn'ova[5], A. Hrynevich[93], C. Hsu[146c], P. J. Hsu[152,p], S.-C. Hsu[139], D. Hu[35], Q. Hu[33b], X. Hu[89], Y. Huang[42], Z. Hubacek[30], F. Hubaut[85], F. Huegging[21], T. B. Huffman[120], E. W. Hughes[35], G. Hughes[72], M. Huhtinen[30], T. A. Hülsing[83], N. Huseynov[65,b], J. Huston[90], J. Huth[57], G. Iacobucci[49], G. Iakovidis[25], I. Ibragimov[142], L. Iconomidou-Fayard[117], E. Ideal[177], Z. Idrissi[136e], P. Iengo[30], O. Igonkina[107], T. Iizawa[172], Y. Ikegami[66], K. Ikematsu[142], M. Ikeno[66], Y. Ilchenko[31,q], D. Iliadis[155], N. Ilic[159], Y. Inamaru[67], T. Ince[101], P. Ioannou[9], M. Iodice[135a], K. Iordanidou[9], V. Ippolito[57], A. Irles Quiles[168], C. Isaksson[167], M. Ishino[68], M. Ishitsuka[158], R. Ishmukhametov[111], C. Issever[120], S. Istin[19a], J. M. Iturbe Ponce[84], R. Iuppa[134a,134b], J. Ivarsson[81], W. Iwanski[39], H. Iwasaki[66], J. M. Izen[41], V. Izzo[104a], S. Jabbar[3], B. Jackson[122], M. Jackson[74], P. Jackson[1], M. R. Jaekel[30], V. Jain[2], K. Jakobs[48], S. Jakobsen[30], T. Jakoubek[127], J. Jakubek[128], D. O. Jamin[152], D. K. Jana[79], E. Jansen[78], R. W. Jansky[62], J. Janssen[21], M. Janus[171], G. Jarlskog[81], N. Javadov[65,b], T. Javůrek[48], L. Jeanty[15], J. Jejelava[51a,r], G.-Y. Jeng[151], D. Jennens[88], P. Jenni[48,s], J. Jentzsch[43], C. Jeske[171], S. Jézéquel[5], H. Ji[174], J. Jia[149], Y. Jiang[33b], S. Jiggins[78], J. Jimenez Pena[168], S. Jin[33a], A. Jinaru[26a], O. Jinnouchi[158], M. D. Joergensen[36], P. Johansson[140], K. A. Johns[7], K. Jon-And[147a,147b], G. Jones[171], R. W. L. Jones[72], T. J. Jones[74], J. Jongmanns[58a], P. M. Jorge[126a,126b], K. D. Joshi[84], J. Jovicevic[160a], X. Ju[174], C. A. Jung[43], P. Jussel[62], A. Juste Rozas[12,o], M. Kaci[168], A. Kaczmarska[39], M. Kado[117], H. Kagan[111], M. Kagan[144], S. J. Kahn[85], E. Kajomovitz[45], C. W. Kalderon[120], S. Kama[40], A. Kamenshchikov[130], N. Kanaya[156], M. Kaneda[30], S. Kaneti[28], V. A. Kantserov[98], J. Kanzaki[66], B. Kaplan[110], A. Kapliy[31], D. Kar[53], K. Karakostas[10], A. Karamaoun[3], N. Karastathis[10,107], M. J. Kareem[54], M. Karnevskiy[83], S. N. Karpov[65], Z. M. Karpova[65], K. Karthik[110], V. Kartvelishvili[72], A. N. Karyukhin[130], L. Kashif[174], R. D. Kass[111], A. Kastanas[14], Y. Kataoka[156], A. Katre[49], J. Katzy[42], K. Kawagoe[70], T. Kawamoto[156], G. Kawamura[54], S. Kazama[156], V. F. Kazanin[109,c], M. Y. Kazarinov[65], R. Keeler[170], R. Kehoe[40], J. S. Keller[42], J. J. Kempster[77], H. Keoshkerian[84], O. Kepka[127], B. P. Kerševan[75], S. Kersten[176], R. A. Keyes[87], F. Khalil-zada[11], H. Khandanyan[147a,147b], A. Khanov[114], A. G. Kharlamov[109,c], T. J. Khoo[28], V. Khovanskiy[97], E. Khramov[65], J. Khubua[51b,t], H. Y. Kim[8], H. Kim[147a,147b], S. H. Kim[161], Y. Kim[31], N. Kimura[155], O. M. Kind[16], B. T. King[74], M. King[168], R. S. B. King[120], S. B. King[169], J. Kirk[131], A. E. Kiryunin[101], T. Kishimoto[67], D. Kisielewska[38a], F. Kiss[48], K. Kiuchi[161], O. Kivernyk[137], E. Kladiva[145b], M. H. Klein[35], M. Klein[74], U. Klein[74], K. Kleinknecht[83], P. Klimek[147a,147b], A. Klimentov[25], R. Klingenberg[43], J. A. Klinger[84], T. Klioutchnikova[30], P. F. Klok[106], E.-E. Kluge[58a], P. Kluit[107], S. Kluth[101], E. Kneringer[62], E. B. F. G. Knoops[85], A. Knue[53], D. Kobayashi[158], T. Kobayashi[156], M. Kobel[44], M. Kocian[144], P. Kodys[129], T. Koffas[29], E. Koffeman[107], L. A. Kogan[120], S. Kohlmann[176], Z. Kohout[128], T. Kohriki[66], T. Koi[144], H. Kolanoski[16], I. Koletsou[5], A. A. Komar[96,*], Y. Komori[156], T. Kondo[66], N. Kondrashova[42], K. Köneke[48], A. C. König[106], S. König[83], T. Kono[66,u], R. Konoplich[110,v], N. Konstantinidis[78], R. Kopeliansky[153], S. Koperny[38a], L. Köpke[83], A. K. Kopp[48], K. Korcyl[39], K. Kordas[155], A. Korn[78], A. A. Korol[109,c], I. Korolkov[12], E. V. Korolkova[140], O. Kortner[101], S. Kortner[101], T. Kosek[129], V. V. Kostyukhin[21], V. M. Kotov[65], A. Kotwal[45], A. Kourkoumeli-Charalampidi[155], C. Kourkoumelis[9], V. Kouskoura[25], A. Koutsman[160a], R. Kowalewski[170], T. Z. Kowalski[38a], W. Kozanecki[137], A. S. Kozhin[130], V. A. Kramarenko[99], G. Kramberger[75], D. Krasnopevtsev[98], A. Krasznahorkay[30], J. K. Kraus[21], A. Kravchenko[25], S. Kreiss[110], M. Kretz[58c], J. Kretzschmar[74], K. Kreutzfeldt[52], P. Krieger[159], K. Krizka[31], K. Kroeninger[43], H. Kroha[101], J. Kroll[122], J. Kroseberg[21], J. Krstic[13], U. Kruchonak[65], H. Krüger[21], N. Krumnack[64], Z. V. Krumshteyn[65], A. Kruse[174], M. C. Kruse[45], M. Kruskal[22], T. Kubota[88], H. Kucuk[78], S. Kuday[4c], S. Kuehn[48], A. Kugel[58c], F. Kuger[175], A. Kuhl[138], T. Kuhl[42], V. Kukhtin[65], Y. Kulchitsky[92], S. Kuleshov[32b], M. Kuna[133a,133b], T. Kunigo[68], A. Kupco[127], H. Kurashige[67], Y. A. Kurochkin[92], R. Kurumida[67], V. Kus[127], E. S. Kuwertz[148], M. Kuze[158], J. Kvita[115], T. Kwan[170], D. Kyriazopoulos[140], A. La Rosa[49], J. L. La Rosa Navarro[24d], L. La Rotonda[37a,37b], C. Lacasta[168], F. Lacava[133a,133b], J. Lacey[29], H. Lacker[16], D. Lacour[80], V. R. Lacuesta[168], E. Ladygin[65], R. Lafaye[5], B. Laforge[80], T. Lagouri[177], S. Lai[48], L. Lambourne[78], S. Lammers[61], C. L. Lampen[7], W. Lampl[7], E. Lançon[137], U. Landgraf[48], M. P. J. Landon[76], V. S. Lang[58a], J. C. Lange[12], A. J. Lankford[164], F. Lanni[25], K. Lantzsch[30], S. Laplace[80], C. Lapoire[30], J. F. Laporte[137], T. Lari[91a], F. Lasagni Manghi[20a,20b], M. Lassnig[30], P. Laurelli[47], W. Lavrijsen[15], A. T. Law[138], P. Laycock[74], O. Le Dortz[80], E. Le Guirriec[85], E. Le Menedeu[12], M. LeBlanc[170], T. LeCompte[6], F. Ledroit-Guillon[55], C. A. Lee[146b], S. C. Lee[152], L. Lee[1], G. Lefebvre[80], M. Lefebvre[170], F. Legger[100], C. Leggett[15], A. Lehan[74], G. Lehmann Miotto[30], X. Lei[7], W. A. Leight[29], A. Leisos[155], A. G. Leister[177], M. A. L. Leite[24d], R. Leitner[129], D. Lellouch[173], B. Lemmer[54], K. J. C. Leney[78], T. Lenz[21], B. Lenzi[30], R. Leone[7], S. Leone[124a,124b], C. Leonidopoulos[46], S. Leontsinis[10], C. Leroy[95], C. G. Lester[28], M. Levchenko[123], J. Levêque[5], D. Levin[89], L. J. Levinson[173], M. Levy[18], A. Lewis[120], A. M. Leyko[21], M. Leyton[41], B. Li[33b,w], H. Li[149], H. L. Li[31], L. Li[45], L. Li[33e], S. Li[45], Y. Li[33c,x], Z. Liang[138], H. Liao[34], B. Liberti[134a], A. Liblong[159], P. Lichard[30], K. Lie[166], J. Liebal[21], W. Liebig[14], C. Limbach[21], A. Limosani[151], S. C. Lin[152,y], T. H. Lin[83], F. Linde[107], B. E. Lindquist[149], J. T. Linnemann[90], E. Lipeles[122], A. Lipniacka[14], M. Lisovyi[42], T. M. Liss[166], D. Lissauer[25], A. Lister[169], A. M. Litke[138], B. Liu[152,z], D. Liu[152], J. Liu[85], J. B. Liu[33b], K. Liu[85], L. Liu[166], M. Liu[45], M. Liu[33b], Y. Liu[33b], M. Livan[121a,121b], A. Lleres[55], J. Llorente Merino[82], S. L. Lloyd[76], F. Lo Sterzo[152], E. Lobodzinska[42],

P. Loch[7], W. S. Lockman[138], F. K. Loebinger[84], A. E. Loevschall-Jensen[36], A. Loginov[177], T. Lohse[16], K. Lohwasser[42], M. Lokajicek[127], B. A. Long[22], J. D. Long[89], R. E. Long[72], K. A. Looper[111], L. Lopes[126a], D. Lopez Mateos[57], B. Lopez Paredes[140], I. Lopez Paz[12], J. Lorenz[100], N. Lorenzo Martinez[61], M. Losada[163], P. Loscutoff[15], P. J. Lösel[100], X. Lou[33a], A. Lounis[117], J. Love[6], P. A. Love[72], N. Lu[89], H. J. Lubatti[139], C. Luci[133a,133b], A. Lucotte[55], F. Luehring[61], W. Lukas[62], L. Luminari[133a], O. Lundberg[147a,147b], B. Lund-Jensen[148], M. Lungwitz[83], D. Lynn[25], R. Lysak[127], E. Lytken[81], H. Ma[25], L. L. Ma[33d], G. Maccarrone[47], A. Macchiolo[101], C. M. Macdonald[140], J. Machado Miguens[122,126b], D. Macina[30], D. Madaffari[85], R. Madar[34], H. J. Maddocks[72], W. F. Mader[44], A. Madsen[167], S. Maeland[14], T. Maeno[25], A. Maevskiy[99], E. Magradze[54], K. Mahboubi[48], J. Mahlstedt[107], C. Maiani[137], C. Maidantchik[24a], A. A. Maier[101], T. Maier[100], A. Maio[126a,126b,126d], S. Majewski[116], Y. Makida[66], N. Makovec[117], B. Malaescu[80], Pa. Malecki[39], V. P. Maleev[123], F. Malek[55], U. Mallik[63], D. Malon[6], C. Malone[144], S. Maltezos[10], V. M. Malyshev[109], S. Malyukov[30], J. Mamuzic[42], G. Mancini[47], B. Mandelli[30], L. Mandelli[91a], I. Mandić[75], R. Mandrysch[63], J. Maneira[126a,126b], A. Manfredini[101], L. Manhaes de Andrade Filho[24b], J. Manjarres Ramos[160b], A. Mann[100], P. M. Manning[138], A. Manousakis-Katsikakis[9], B. Mansoulie[137], R. Mantifel[87], M. Mantoani[54], L. Mapelli[30], L. March[146c], G. Marchiori[80], M. Marcisovsky[127], C. P. Marino[170], M. Marjanovic[13], F. Marroquim[24a], S. P. Marsden[84], Z. Marshall[15], L. F. Marti[17], S. Marti-Garcia[168], B. Martin[90], T. A. Martin[171], V. J. Martin[46], B. Martin dit Latour[14], M. Martinez[12,o], S. Martin-Haugh[131], V. S. Martoiu[26a], A. C. Martyniuk[78], M. Marx[139], F. Marzano[133a], A. Marzin[30], L. Masetti[83], T. Mashimo[156], R. Mashinistov[96], J. Masik[84], A. L. Maslennikov[109,c], I. Massa[20a,20b], L. Massa[20a,20b], N. Massol[5], P. Mastrandrea[149], A. Mastroberardino[37a,37b], T. Masubuchi[156], P. Mättig[176], J. Mattmann[83], J. Maurer[26a], S. J. Maxfield[74], D. A. Maximov[109,c], R. Mazini[152], S. M. Mazza[91a,91b], L. Mazzaferro[134a,134b], G. Mc Goldrick[159], S. P. Mc Kee[89], A. McCarn[89], R. L. McCarthy[149], T. G. McCarthy[29], N. A. McCubbin[131], K. W. McFarlane[56,*], J. A. Mcfayden[78], G. Mchedlidze[54], S. J. McMahon[131], R. A. McPherson[170,k], M. Medinnis[42], S. Meehan[146a], S. Mehlhase[100], A. Mehta[74], K. Meier[58a], C. Meineck[100], B. Meirose[41], B. R. Mellado Garcia[146c], F. Meloni[17], A. Mengarelli[20a,20b], S. Menke[101], E. Meoni[162], K. M. Mercurio[57], S. Mergelmeyer[21], P. Mermod[49], L. Merola[104a,104b], C. Meroni[91a], F. S. Merritt[31], A. Messina[133a,133a], J. Metcalfe[25], A. S. Mete[164], C. Meyer[83], C. Meyer[122], J-P. Meyer[137], J. Meyer[107], R. P. Middleton[131], S. Miglioranzi[165a,165c], L. Mijović[21], G. Mikenberg[173], M. Mikestikova[127], M. Mikuž[75], M. Milesi[88], A. Milic[30], D. W. Miller[31], C. Mills[46], A. Milov[173], D. A. Milstead[147a,147b], A. A. Minaenko[130], Y. Minami[156], I. A. Minashvili[65], A. I. Mincer[110], B. Mindur[38a], M. Mineev[65], Y. Ming[174], L. M. Mir[12], T. Mitani[172], J. Mitrevski[100], V. A. Mitsou[168], A. Miucci[49], P. S. Miyagawa[140], J. U. Mjörnmark[81], T. Moa[147a,147b], K. Mochizuki[85], S. Mohapatra[35], W. Mohr[48], S. Molander[147a,147b], R. Moles-Valls[168], K. Mönig[42], C. Monini[55], J. Monk[36], E. Monnier[85], J. Montejo Berlingen[12], F. Monticelli[71], S. Monzani[133a,133b], R. W. Moore[3], N. Morange[117], D. Moreno[163], M. Moreno Llácer[54], P. Morettini[50a], M. Morgenstern[44], M. Morii[57], V. Morisbak[119], S. Moritz[83], A. K. Morley[148], G. Mornacchi[30], J. D. Morris[76], S. S. Mortensen[36], A. Morton[53], L. Morvaj[103], M. Mosidze[51b], J. Moss[111], K. Motohashi[158], R. Mount[144], E. Mountricha[25], S. V. Mouraviev[96,*], E. J. W. Moyse[86], S. Muanza[85], R. D. Mudd[18], F. Mueller[101], J. Mueller[125], K. Mueller[21], R. S. P. Mueller[100], T. Mueller[28], D. Muenstermann[49], P. Mullen[53], Y. Munwes[154], J. A. Murillo Quijada[18], W. J. Murray[171,131], H. Musheghyan[54], E. Musto[153], A. G. Myagkov[130,aa], M. Myska[128], O. Nackenhorst[54], J. Nadal[54], K. Nagai[120], R. Nagai[158], Y. Nagai[85], K. Nagano[66], A. Nagarkar[111], Y. Nagasaka[59], K. Nagata[161], M. Nagel[101], E. Nagy[85], A. M. Nairz[30], Y. Nakahama[30], K. Nakamura[66], T. Nakamura[156], I. Nakano[112], H. Namasivayam[41], R. F. Naranjo Garcia[42], R. Narayan[58b], T. Naumann[42], G. Navarro[163], R. Nayyar[7], H. A. Neal[89], P. Yu. Nechaeva[96], T. J. Neep[84], P. D. Nef[144], A. Negri[121a,121b], M. Negrini[20a], S. Nektarijevic[106], C. Nellist[117], A. Nelson[164], S. Nemecek[127], P. Nemethy[110], A. A. Nepomuceno[24a], M. Nessi[30,ab], M. S. Neubauer[166], M. Neumann[176], R. M. Neves[110], P. Nevski[25], P. R. Newman[18], D. H. Nguyen[6], R. B. Nickerson[120], R. Nicolaidou[137], B. Nicquevert[30], J. Nielsen[138], N. Nikiforou[35], A. Nikiforov[16], V. Nikolaenko[130,aa], I. Nikolic-Audit[80], K. Nikolopoulos[18], J. K. Nilsen[119], P. Nilsson[25], Y. Ninomiya[156], A. Nisati[133a], R. Nisius[101], T. Nobe[158], M. Nomachi[118], I. Nomidis[29], T. Nooney[76], S. Norberg[113], M. Nordberg[30], O. Novgorodova[44], S. Nowak[101], M. Nozaki[66], L. Nozka[115], K. Ntekas[10], G. Nunes Hanninger[88], T. Nunnemann[100], E. Nurse[78], F. Nuti[88], B. J. O'Brien[46], F. O'grady[7], D. C. O'Neil[143], V. O'Shea[53], F. G. Oakham[29,d], H. Oberlack[101], T. Obermann[21], J. Ocariz[80], A. Ochi[67], I. Ochoa[78], J. P. Ochoa-Ricoux[32a], S. Oda[70], S. Odaka[66], H. Ogren[61], A. Oh[84], S. H. Oh[45], C. C. Ohm[15], H. Ohman[167], H. Oide[30], W. Okamura[118], H. Okawa[161], Y. Okumura[31], T. Okuyama[156], A. Olariu[26a], S. A. Olivares Pino[46], D. Oliveira Damazio[25], E. Oliver Garcia[168], A. Olszewski[39], J. Olszowska[39], A. Onofre[126a,126e], P. U. E. Onyisi[31,q], C. J. Oram[160a], M. J. Oreglia[31], Y. Oren[154], D. Orestano[135a,135b], N. Orlando[155], C. Oropeza Barrera[53], R. S. Orr[159], B. Osculati[50a,50b], R. Ospanov[84], G. Otero y Garzon[27], H. Otono[70], M. Ouchrif[136d], E. A. Ouellette[170], F. Ould-Saada[119], A. Ouraou[137], K. P. Oussoren[107], Q. Ouyang[33a], A. Ovcharova[15], M. Owen[53], R. E. Owen[18], V. E. Ozcan[19a], N. Ozturk[8], K. Pachal[120], A. Pacheco Pages[12], C. Padilla Aranda[12], M. Pagáčová[48], S. Pagan Griso[15], E. Paganis[140], C. Pahl[101], F. Paige[25], P. Pais[86], K. Pajchel[119], G. Palacino[160b], S. Palestini[30], M. Palka[38b], D. Pallin[34], A. Palma[126a,126b], Y. B. Pan[174], E. Panagiotopoulou[10],

C. E. Pandini[80], J. G. Panduro Vazquez[77], P. Pani[147a,147b], S. Panitkin[25], D. Pantea[26a], L. Paolozzi[134a,134b], Th. D. Papadopoulou[10], K. Papageorgiou[155], A. Paramonov[6], D. Paredes Hernandez[155], M. A. Parker[28], K. A. Parker[140], F. Parodi[50a,50b], J. A. Parsons[35], U. Parzefall[48], E. Pasqualucci[133a], S. Passaggio[50a], F. Pastore[135a,135b,*], Fr. Pastore[77], G. Pásztor[29], S. Pataraia[176], N. D. Patel[151], J. R. Pater[84], T. Pauly[30], J. Pearce[170], B. Pearson[113], L. E. Pedersen[36], M. Pedersen[119], S. Pedraza Lopez[168], R. Pedro[126a,126b], S. V. Peleganchuk[109], D. Pelikan[167], H. Peng[33b], B. Penning[31], J. Penwell[61], D. V. Perepelitsa[25], E. Perez Codina[160a], M. T. Pérez García-Estañ[168], L. Perini[91a,91b], H. Pernegger[30], S. Perrella[104a,104b], R. Peschke[42], V. D. Peshekhonov[65], K. Peters[30], R. F. Y. Peters[84], B. A. Petersen[30], T. C. Petersen[36], E. Petit[42], A. Petridis[147a,147b], C. Petridou[155], E. Petrolo[133a], F. Petrucci[135a,135b], N. E. Pettersson[158], R. Pezoa[32b], P. W. Phillips[131], G. Piacquadio[144], E. Pianori[171], A. Picazio[49], E. Piccaro[76], M. Piccinini[20a,20b], M. A. Pickering[120], R. Piegaia[27], D. T. Pignotti[111], J. E. Pilcher[31], A. D. Pilkington[84], J. Pina[126a,126b,126d], M. Pinamonti[165a,165c,ac], J. L. Pinfold[3], A. Pingel[36], B. Pinto[126a], S. Pires[80], M. Pitt[173], C. Pizio[91a,91b], L. Plazak[145a], M. -A. Pleier[25], V. Pleskot[129], E. Plotnikova[65], P. Plucinski[147a,147b], D. Pluth[64], R. Poettgen[83], L. Poggioli[117], D. Pohl[21], G. Polesello[121a], A. Policicchio[37a,37b], R. Polifka[159], A. Polini[20a], C. S. Pollard[53], V. Polychronakos[25], K. Pommès[30], L. Pontecorvo[133a], B. G. Pope[90], G. A. Popeneciu[26b], D. S. Popovic[13], A. Poppleton[30], S. Pospisil[128], K. Potamianos[15], I. N. Potrap[65], C. J. Potter[150], C. T. Potter[116], G. Poulard[30], J. Poveda[30], V. Pozdnyakov[65], P. Pralavorio[85], A. Pranko[15], S. Prasad[30], S. Prell[64], D. Price[84], J. Price[74], L. E. Price[6], M. Primavera[73a], S. Prince[87], M. Proissl[46], K. Prokofiev[60c], F. Prokoshin[32b], E. Protopapadaki[137], S. Protopopescu[25], J. Proudfoot[6], M. Przybycien[38a], E. Ptacek[116], D. Puddu[135a,135b], E. Pueschel[86], D. Puldon[149], M. Purohit[25,ad], P. Puzo[117], J. Qian[89], G. Qin[53], Y. Qin[84], A. Quadt[54], D. R. Quarrie[15], W. B. Quayle[165a,165b], M. Queitsch-Maitland[84], D. Quilty[53], S. Raddum[119], V. Radeka[25], V. Radescu[42], S. K. Radhakrishnan[149], P. Radloff[116], P. Rados[88], F. Ragusa[91a,91b], G. Rahal[179], S. Rajagopalan[25], M. Rammensee[30], C. Rangel-Smith[167], F. Rauscher[100], S. Rave[83], T. Ravenscroft[53], M. Raymond[30], A. L. Read[119], N. P. Readioff[74], D. M. Rebuzzi[121a,121b], A. Redelbach[175], G. Redlinger[25], R. Reece[138], K. Reeves[41], L. Rehnisch[16], H. Reisin[27], M. Relich[164], C. Rembser[30], H. Ren[33a], A. Renaud[117], M. Rescigno[133a], S. Resconi[91a], O. L. Rezanova[109,c], P. Reznicek[129], R. Rezvani[95], R. Richter[101], S. Richter[78], E. Richter-Was[38b], O. Ricken[21], M. Ridel[80], P. Rieck[16], C. J. Riegel[176], J. Rieger[54], M. Rijssenbeek[149], A. Rimoldi[121a,121b], L. Rinaldi[20a], B. Ristić[49], E. Ritsch[62], I. Riu[12], F. Rizatdinova[114], E. Rizvi[76], S. H. Robertson[87,k], A. Robichaud-Veronneau[87], D. Robinson[28], J. E. M. Robinson[84], A. Robson[53], C. Roda[124a,124b], S. Roe[30], O. Røhne[119], S. Rolli[162], A. Romaniouk[98], M. Romano[20a,20b], S. M. Romano Saez[34], E. Romero Adam[168], N. Rompotis[139], M. Ronzani[48], L. Roos[80], E. Ros[168], S. Rosati[133a], K. Rosbach[48], P. Rose[138], P. L. Rosendahl[14], O. Rosenthal[142], V. Rossetti[147a,147b], E. Rossi[104a,104b], L. P. Rossi[50a], R. Rosten[139], M. Rotaru[26a], I. Roth[173], J. Rothberg[139], D. Rousseau[117], C. R. Royon[137], A. Rozanov[85], Y. Rozen[153], X. Ruan[146c], F. Rubbo[144], I. Rubinskiy[42], V. I. Rud[99], C. Rudolph[44], M. S. Rudolph[159], F. Rühr[48], A. Ruiz-Martinez[30], Z. Rurikova[48], N. A. Rusakovich[65], A. Ruschke[100], H. L. Russell[139], J. P. Rutherfoord[7], N. Ruthmann[48], Y. F. Ryabov[123], M. Rybar[129], G. Rybkin[117], N. C. Ryder[120], A. F. Saavedra[151], G. Sabato[107], S. Sacerdoti[27], A. Saddique[3], H. F-W. Sadrozinski[138], R. Sadykov[65], F. Safai Tehrani[133a], M. Saimpert[137], H. Sakamoto[156], Y. Sakurai[172], G. Salamanna[135a,135b], A. Salamon[134a], M. Saleem[113], D. Salek[107], P. H. Sales De Bruin[139], D. Salihagic[101], A. Salnikov[144], J. Salt[168], D. Salvatore[37a,37b], F. Salvatore[150], A. Salvucci[106], A. Salzburger[30], D. Sampsonidis[155], A. Sanchez[104a,104b], J. Sánchez[168], V. Sanchez Martinez[168], H. Sandaker[14], R. L. Sandbach[76], H. G. Sander[83], M. P. Sanders[100], M. Sandhoff[176], C. Sandoval[163], R. Sandstroem[101], D. P. C. Sankey[131], M. Sannino[50a,50b], A. Sansoni[47], C. Santoni[34], R. Santonico[134a,134b], H. Santos[126a], I. Santoyo Castillo[150], K. Sapp[125], A. Sapronov[65], J. G. Saraiva[126a,126d], B. Sarrazin[21], O. Sasaki[66], Y. Sasaki[156], K. Sato[161], G. Sauvage[5,*], E. Sauvan[5], G. Savage[77], P. Savard[159,d], C. Sawyer[120], L. Sawyer[79,n], J. Saxon[31], C. Sbarra[20a], A. Sbrizzi[20a,20b], T. Scanlon[78], D. A. Scannicchio[164], M. Scarcella[151], V. Scarfone[37a,37b], J. Schaarschmidt[173], P. Schacht[101], D. Schaefer[30], R. Schaefer[42], J. Schaeffer[83], S. Schaepe[21], S. Schaetzel[58b], U. Schäfer[83], A. C. Schaffer[117], D. Schaile[100], R. D. Schamberger[149], V. Scharf[58a], V. A. Schegelsky[123], D. Scheirich[129], M. Schernau[164], C. Schiavi[50a,50b], C. Schillo[48], M. Schioppa[37a,37b], S. Schlenker[30], E. Schmidt[48], K. Schmieden[30], C. Schmitt[83], S. Schmitt[58b], S. Schmitt[42], B. Schneider[160a], Y. J. Schnellbach[74], U. Schnoor[44], L. Schoeffel[137], A. Schoening[58b], B. D. Schoenrock[90], E. Schopf[21], A. L. S. Schorlemmer[54], M. Schott[83], D. Schouten[160a], J. Schovancova[8], S. Schramm[159], M. Schreyer[175], C. Schroeder[83], N. Schuh[83], M. J. Schultens[21], H.-C. Schultz-Coulon[58a], H. Schulz[16], M. Schumacher[48], B. A. Schumm[138], Ph. Schune[137], C. Schwanenberger[84], A. Schwartzman[144], T. A. Schwarz[89], Ph. Schwegler[101], Ph. Schwemling[137], R. Schwienhorst[90], J. Schwindling[137], T. Schwindt[21], M. Schwoerer[5], F. G. Sciacca[17], E. Scifo[117], G. Sciolla[23], F. Scuri[124a,124b], F. Scutti[21], J. Searcy[89], G. Sedov[42], E. Sedykh[123], P. Seema[21], S. C. Seidel[105], A. Seiden[138], F. Seifert[128], J. M. Seixas[24a], G. Sekhniaidze[104a], S. J. Sekula[40], K. E. Selbach[46], D. M. Seliverstov[123,*], N. Semprini-Cesari[20a,20b], C. Serfon[30], L. Serin[117], L. Serkin[165a,165b], T. Serre[85], R. Seuster[160a], H. Severini[113], T. Sfiligoj[75], F. Sforza[101], A. Sfyrla[30], E. Shabalina[54], M. Shamim[116], L. Y. Shan[33a], R. Shang[166], J. T. Shank[22], M. Shapiro[15], P. B. Shatalov[97], K. Shaw[165a,165b],

A. Shcherbakova[147a,147b], C. Y. Shehu[150], P. Sherwood[78], L. Shi[152,ae], S. Shimizu[67], C. O. Shimmin[164], M. Shimojima[102], M. Shiyakova[65], A. Shmeleva[96], D. Shoaleh Saadi[95], M. J. Shochet[31], S. Shojaii[91a,91b], S. Shrestha[111], E. Shulga[98], M. A. Shupe[7], S. Shushkevich[42], P. Sicho[127], O. Sidiropoulou[175], D. Sidorov[114], A. Sidoti[20a,20b], F. Siegert[44], Dj. Sijacki[13], J. Silva[126a,126d], Y. Silver[154], S. B. Silverstein[147a], V. Simak[128], O. Simard[5], Lj. Simic[13], S. Simion[117], E. Simioni[83], B. Simmons[78], D. Simon[34], R. Simoniello[91a,91b], P. Sinervo[159], N. B. Sinev[116], G. Siragusa[175], A. N. Sisakyan[65,*], S. Yu. Sivoklokov[99], J. Sjölin[147a,147b], T. B. Sjursen[14], M. B. Skinner[72], H. P. Skottowe[57], P. Skubic[113], M. Slater[18], T. Slavicek[128], M. Slawinska[107], K. Sliwa[162], V. Smakhtin[173], B. H. Smart[46], L. Smestad[14], S. Yu. Smirnov[98], Y. Smirnov[98], L. N. Smirnova[99,af], O. Smirnova[81], M. N. K. Smith[35], M. Smizanska[72], K. Smolek[128], A. A. Snesarev[96], G. Snidero[76], S. Snyder[25], R. Sobie[170,k], F. Socher[44], A. Soffer[154], D. A. Soh[152,ae], C. A. Solans[30], M. Solar[128], J. Solc[128], E. Yu. Soldatov[98], U. Soldevila[168], A. A. Solodkov[130], A. Soloshenko[65], O. V. Solovyanov[130], V. Solovyev[123], P. Sommer[48], H. Y. Song[33b], N. Soni[1], A. Sood[15], A. Sopczak[128], B. Sopko[128], V. Sopko[128], V. Sorin[12], D. Sosa[58b], M. Sosebee[8], C. L. Sotiropoulou[155], R. Soualah[165a,165c], P. Soueid[95], A. M. Soukharev[109,c], D. South[42], S. Spagnolo[73a,73b], M. Spalla[124a,124b], F. Spanò[77], W. R. Spearman[57], F. Spettel[101], R. Spighi[20a], G. Spigo[30], L. A. Spiller[88], M. Spousta[129], T. Spreitzer[159], R. D. St. Denis[53,*], S. Staerz[44], J. Stahlman[122], R. Stamen[58a], S. Stamm[16], E. Stanecka[39], C. Stanescu[135a], M. Stanescu-Bellu[42], M. M. Stanitzki[42], S. Stapnes[119], E. A. Starchenko[130], J. Stark[55], P. Staroba[127], P. Starovoitov[42], R. Staszewski[39], P. Stavina[145a,*], P. Steinberg[25], B. Stelzer[143], H. J. Stelzer[30], O. Stelzer-Chilton[160a], H. Stenzel[52], S. Stern[101], G. A. Stewart[53], J. A. Stillings[21], M. C. Stockton[87], M. Stoebe[87], G. Stoicea[26a], P. Stolte[54], S. Stonjek[101], A. R. Stradling[8], A. Straessner[44], M. E. Stramaglia[17], J. Strandberg[148], S. Strandberg[147a,147b], A. Strandlie[119], E. Strauss[144], M. Strauss[113], P. Strizenec[145b], R. Ströhmer[175], D. M. Strom[116], R. Stroynowski[40], A. Strubig[106], S. A. Stucci[17], B. Stugu[14], N. A. Styles[42], D. Su[144], J. Su[125], R. Subramaniam[79], A. Succurro[12], Y. Sugaya[118], C. Suhr[108], M. Suk[128], V. V. Sulin[96], S. Sultansoy[4d], T. Sumida[68], S. Sun[57], X. Sun[33a], J. E. Sundermann[48], K. Suruliz[150], G. Susinno[37a,37b], M. R. Sutton[150], S. Suzuki[66], Y. Suzuki[66], M. Svatos[127], S. Swedish[169], M. Swiatlowski[144], I. Sykora[145a], T. Sykora[129], D. Ta[90], C. Taccini[135a,135b], K. Tackmann[42], J. Taenzer[159], A. Taffard[164], R. Tafirout[160a], N. Taiblum[154], H. Takai[25], R. Takashima[69], H. Takeda[67], T. Takeshita[141], Y. Takubo[66], M. Talby[85], A. A. Talyshev[109,c], J. Y. C. Tam[175], K. G. Tan[88], J. Tanaka[156], R. Tanaka[117], S. Tanaka[132], S. Tanaka[66], B. B. Tannenwald[111], N. Tannoury[21], S. Tapprogge[83], S. Tarem[153], F. Tarrade[29], G. F. Tartarelli[91a], P. Tas[129], M. Tasevsky[127], T. Tashiro[68], E. Tassi[37a,37b], A. Tavares Delgado[126a,126b], Y. Tayalati[136d], F. E. Taylor[94], G. N. Taylor[88], W. Taylor[160b], F. A. Teischinger[30], M. Teixeira Dias Castanheira[76], P. Teixeira-Dias[77], K. K. Temming[48], H. Ten Kate[30], P. K. Teng[152], J. J. Teoh[118], F. Tepel[176], S. Terada[66], K. Terashi[156], J. Terron[82], S. Terzo[101], M. Testa[47], R. J. Teuscher[159,k], J. Therhaag[21], T. Theveneaux-Pelzer[34], J. P. Thomas[18], J. Thomas-Wilsker[77], E. N. Thompson[35], P. D. Thompson[18], R. J. Thompson[84], A. S. Thompson[53], L. A. Thomsen[36], E. Thomson[122], M. Thomson[28], R. P. Thun[89,*], M. J. Tibbetts[15], R. E. Ticse Torres[85], V. O. Tikhomirov[96,ag], Yu. A. Tikhonov[109,c], S. Timoshenko[98], E. Tiouchichine[85], P. Tipton[177], S. Tisserant[85], T. Todorov[5,*], S. Todorova-Nova[129], J. Tojo[70], S. Tokár[145a], K. Tokushuku[66], K. Tollefson[90], E. Tolley[57], L. Tomlinson[84], M. Tomoto[103], L. Tompkins[144,ah], K. Toms[105], E. Torrence[116], H. Torres[143], E. Torró Pastor[168], J. Toth[85,ai], F. Touchard[85], D. R. Tovey[140], T. Trefzger[175], L. Tremblet[30], A. Tricoli[30], I. M. Trigger[160a], S. Trincaz-Duvoid[80], M. F. Tripiana[12], W. Trischuk[159], B. Trocmé[55], C. Troncon[91a], M. Trottier-McDonald[15], M. Trovatelli[135a,135b], P. True[90], M. Trzebinski[39], A. Trzupek[39], C. Tsarouchas[30], J. C-L. Tseng[120], P. V. Tsiareshka[92], D. Tsionou[155], G. Tsipolitis[10], N. Tsirintanis[9], S. Tsiskaridze[12], V. Tsiskaridze[48], E. G. Tskhadadze[51a], I. I. Tsukerman[97], V. Tsulaia[15], S. Tsuno[66], D. Tsybychev[149], A. Tudorache[26a], V. Tudorache[26a], A. N. Tuna[122], S. A. Tupputi[20a,20b], S. Turchikhin[99,af], D. Turecek[128], R. Turra[91a,91b], A. J. Turvey[40], P. M. Tuts[35], A. Tykhonov[49], M. Tylmad[147a,147b], M. Tyndel[131], I. Ueda[156], R. Ueno[29], M. Ughetto[147a,147b], M. Ugland[14], M. Uhlenbrock[21], F. Ukegawa[161], G. Unal[30], A. Undrus[25], G. Unel[164], F. C. Ungaro[48], Y. Unno[66], C. Unverdorben[100], J. Urban[145b], P. Urquijo[88], P. Urrejola[83], G. Usai[8], A. Usanova[62], L. Vacavant[85], V. Vacek[128], B. Vachon[87], C. Valderanis[83], N. Valencic[107], S. Valentinetti[20a,20b], A. Valero[168], L. Valery[12], S. Valkar[129], E. Valladolid Gallego[168], S. Vallecorsa[49], J. A. Valls Ferrer[168], W. Van Den Wollenberg[107], P. C. Van Der Deijl[107], R. van der Geer[107], H. van der Graaf[107], R. Van Der Leeuw[107], N. van Eldik[153], P. van Gemmeren[6], J. Van Nieuwkoop[143], I. van Vulpen[107], M. C. van Woerden[30], M. Vanadia[133a,133b], W. Vandelli[30], R. Vanguri[122], A. Vaniachine[6], F. Vannucci[80], G. Vardanyan[178], R. Vari[133a], E. W. Varnes[7], T. Varol[40], D. Varouchas[80], A. Vartapetian[8], K. E. Varvell[151], F. Vazeille[34], T. Vazquez Schroeder[87], J. Veatch[7], F. Veloso[126a,126c], T. Velz[21], S. Veneziano[133a], A. Ventura[73a,73b], D. Ventura[86], M. Venturi[170], N. Venturi[159], A. Venturini[23], V. Vercesi[121a], M. Verducci[133a,133b], W. Verkerke[107], J. C. Vermeulen[107], A. Vest[44], M. C. Vetterli[143,d], O. Viazlo[81], I. Vichou[166], T. Vickey[140], O. E. Vickey Boeriu[140], G. H. A. Viehhauser[120], S. Viel[15], R. Vigne[30], M. Villa[20a,20b], M. Villaplana Perez[91a,91b], E. Vilucchi[47], M. G. Vincter[29], V. B. Vinogradov[65], I. Vivarelli[150], F. Vives Vaque[3], S. Vlachos[10], D. Vladoiu[100], M. Vlasak[128], M. Vogel[32a], P. Vokac[128], G. Volpi[124a,124b], M. Volpi[88], H. von der Schmitt[101], H. von Radziewski[48], E. von Toerne[21], V. Vorobel[129], K. Vorobev[98], M. Vos[168], R. Voss[30],

J. H. Vossebeld[74], N. Vranjes[13], M. Vranjes Milosavljevic[13], V. Vrba[127], M. Vreeswijk[107], R. Vuillermet[30], I. Vukotic[31], Z. Vykydal[128], P. Wagner[21], W. Wagner[176], H. Wahlberg[71], S. Wahrmund[44], J. Wakabayashi[103], J. Walder[72], R. Walker[100], W. Walkowiak[142], C. Wang[33c], F. Wang[174], H. Wang[15], H. Wang[40], J. Wang[42], J. Wang[33a], K. Wang[87], R. Wang[6], S. M. Wang[152], T. Wang[21], X. Wang[177], C. Wanotayaroj[116], A. Warburton[87], C. P. Ward[28], D. R. Wardrope[78], M. Warsinsky[48], A. Washbrook[46], C. Wasicki[42], P. M. Watkins[18], A. T. Watson[18], I. J. Watson[151], M. F. Watson[18], G. Watts[139], S. Watts[84], B. M. Waugh[78], S. Webb[84], M. S. Weber[17], S. W. Weber[175], J. S. Webster[31], A. R. Weidberg[120], B. Weinert[61], J. Weingarten[54], C. Weiser[48], H. Weits[107], P. S. Wells[30], T. Wenaus[25], T. Wengler[30], S. Wenig[30], N. Wermes[21], M. Werner[48], P. Werner[30], M. Wessels[58a], J. Wetter[162], K. Whalen[29], A. M. Wharton[72], A. White[8], M. J. White[1], R. White[32b], S. White[124a,124b], D. Whiteson[164], F. J. Wickens[131], W. Wiedenmann[174], M. Wielers[131], P. Wienemann[21], C. Wiglesworth[36], L. A. M. Wiik-Fuchs[21], A. Wildauer[101], H. G. Wilkens[30], H. H. Williams[122], S. Williams[107], C. Willis[90], S. Willocq[86], A. Wilson[89], J. A. Wilson[18], I. Wingerter-Seez[5], F. Winklmeier[116], B. T. Winter[21], M. Wittgen[144], J. Wittkowski[100], S. J. Wollstadt[83], M. W. Wolter[39], H. Wolters[126a,126c], B. K. Wosiek[39], J. Wotschack[30], M. J. Woudstra[84], K. W. Wozniak[39], M. Wu[55], M. Wu[31], S. L. Wu[174], X. Wu[49], Y. Wu[89], T. R. Wyatt[84], B. M. Wynne[46], S. Xella[36], D. Xu[33a], L. Xu[33b,aj], B. Yabsley[151], S. Yacoob[146b,ak], R. Yakabe[67], M. Yamada[66], Y. Yamaguchi[118], A. Yamamoto[66], S. Yamamoto[156], T. Yamanaka[156], K. Yamauchi[103], Y. Yamazaki[67], Z. Yan[22], H. Yang[33e], H. Yang[174], Y. Yang[152], L. Yao[33a], W-M. Yao[15], Y. Yasu[66], E. Yatsenko[42], K. H. Yau Wong[21], J. Ye[40], S. Ye[25], I. Yeletskikh[65], A. L. Yen[57], E. Yildirim[42], K. Yorita[172], R. Yoshida[6], K. Yoshihara[122], C. Young[144], C. J. S. Young[30], S. Youssef[22], D. R. Yu[15], J. Yu[8], J. M. Yu[89], J. Yu[114], L. Yuan[67], A. Yurkewicz[108], I. Yusuff[28,al], B. Zabinski[39], R. Zaidan[63], A. M. Zaitsev[130,aa], J. Zalieckas[14], A. Zaman[149], S. Zambito[23], L. Zanello[133a,133b], D. Zanzi[88], C. Zeitnitz[176], M. Zeman[128], A. Zemla[38a], K. Zengel[23], O. Zenin[130], T. Ženiš[145a], D. Zerwas[117], D. Zhang[89], F. Zhang[174], J. Zhang[6], L. Zhang[48], R. Zhang[33b], X. Zhang[33d], Z. Zhang[117], X. Zhao[40], Y. Zhao[33d,117], Z. Zhao[33b], A. Zhemchugov[65], J. Zhong[120], B. Zhou[89], C. Zhou[45], L. Zhou[35], L. Zhou[40], N. Zhou[164], C. G. Zhu[33d], H. Zhu[33a], J. Zhu[89], Y. Zhu[33b], X. Zhuang[33a], K. Zhukov[96], A. Zibell[175], D. Zieminska[61], N. I. Zimine[65], C. Zimmermann[83], R. Zimmermann[21], S. Zimmermann[48], Z. Zinonos[54], M. Zinser[83], M. Ziolkowski[142], L. Živković[13], G. Zobernig[174], A. Zoccoli[20a,20b], M. zur Nedden[16], G. Zurzolo[104a,104b], L. Zwalinski[30]

1 Department of Physics, University of Adelaide, Adelaide, Australia

2 Physics Department, SUNY Albany, Albany, NY, USA

3 Department of Physics, University of Alberta, Edmonton, AB, Canada

4 (a) Department of Physics, Ankara University, Ankara, Turkey; (b) Istanbul Aydin University, Istanbul, Turkey; (c) Division of Physics, TOBB University of Economics and Technology, Ankara, Turkey

5 LAPP, CNRS/IN2P3 and Université Savoie Mont Blanc, Annecy-le-Vieux, France

6 High Energy Physics Division, Argonne National Laboratory, Argonne, IL, USA

7 Department of Physics, University of Arizona, Tucson, AZ, USA

8 Department of Physics, The University of Texas at Arlington, Arlington, TX, USA

9 Physics Department, University of Athens, Athens, Greece

10 Physics Department, National Technical University of Athens, Zografou, Greece

11 Institute of Physics, Azerbaijan Academy of Sciences, Baku, Azerbaijan

12 Institut de Física d'Altes Energies and Departament de Física de la Universitat Autònoma de Barcelona, Barcelona, Spain

13 Institute of Physics, University of Belgrade, Belgrade, Serbia

14 Department for Physics and Technology, University of Bergen, Bergen, Norway

15 Physics Division, Lawrence Berkeley National Laboratory and University of California, Berkeley, CA, USA

16 Department of Physics, Humboldt University, Berlin, Germany

17 Albert Einstein Center for Fundamental Physics and Laboratory for High Energy Physics, University of Bern, Bern, Switzerland

18 School of Physics and Astronomy, University of Birmingham, Birmingham, UK

19 (a) Department of Physics, Bogazici University, Istanbul, Turkey; (b) Department of Physics, Dogus University, Istanbul, Turkey; (c) Department of Physics Engineering, Gaziantep University, Gaziantep, Turkey

20 (a) INFN Sezione di Bologna, Bologna, Italy; (b) Dipartimento di Fisica e Astronomia, Università di Bologna, Bologna, Italy

21 Physikalisches Institut, University of Bonn, Bonn, Germany

22 Department of Physics, Boston University, Boston, MA, USA

23 Department of Physics, Brandeis University, Waltham, MA, USA

24 (a) Universidade Federal do Rio De Janeiro COPPE/EE/IF, Rio de Janeiro, Brazil; (b) Electrical Circuits Department, Federal University of Juiz de Fora (UFJF), Juiz de Fora, Brazil; (c) Federal University of Sao Joao del Rei (UFSJ), Sao Joao del Rei, Brazil; (d) Instituto de Fisica, Universidade de Sao Paulo, São Paulo, Brazil

25 Physics Department, Brookhaven National Laboratory, Upton, NY, USA

26 (a) National Institute of Physics and Nuclear Engineering, Bucharest, Romania; (b) Physics Department, National Institute for Research and Development of Isotopic and Molecular Technologies, Cluj Napoca, Romania; (c) University Politehnica Bucharest, Bucharest, Romania; (d) West University in Timisoara, Timisoara, Romania

27 Departamento de Física, Universidad de Buenos Aires, Buenos Aires, Argentina

28 Cavendish Laboratory, University of Cambridge, Cambridge, UK

29 Department of Physics, Carleton University, Ottawa, ON, Canada

30 CERN, Geneva, Switzerland

31 Enrico Fermi Institute, University of Chicago, Chicago, IL, USA

32 (a) Departamento de Física, Pontificia Universidad Católica de Chile, Santiago, Chile; (b) Departamento de Física, Universidad Técnica Federico Santa María, Valparaiso, Chile

33 (a) Institute of High Energy Physics, Chinese Academy of Sciences, Beijing, China; (b) Department of Modern Physics, University of Science and Technology of China, Anhui, China; (c) Department of Physics, Nanjing University, Jiangsu, China; (d) School of Physics, Shandong University, Shandong, China; (e) Department of Physics and Astronomy, Shanghai Key Laboratory for Particle Physics and Cosmology, Shanghai Jiao Tong University, Shanghai, China; (f) Physics Department, Tsinghua University, 100084 Beijing, China

34 Laboratoire de Physique Corpusculaire, Clermont Université and Université Blaise Pascal and CNRS/IN2P3, Clermont-Ferrand, France

35 Nevis Laboratory, Columbia University, Irvington, NY, USA

36 Niels Bohr Institute, University of Copenhagen, Copenhagen, Denmark

37 (a) INFN Gruppo Collegato di Cosenza, Laboratori Nazionali di Frascati, Frascati, Italy; (b) Dipartimento di Fisica, Università della Calabria, Rende, Italy

38 (a) Faculty of Physics and Applied Computer Science, AGH University of Science and Technology, Kraków, Poland; (b) Marian Smoluchowski Institute of Physics, Jagiellonian University, Kraków, Poland

39 Institute of Nuclear Physics, Polish Academy of Sciences, Kraków, Poland

40 Physics Department, Southern Methodist University, Dallas, TX, USA

41 Physics Department, University of Texas at Dallas, Richardson, TX, USA

42 DESY, Hamburg and Zeuthen, Germany

43 Institut für Experimentelle Physik IV, Technische Universität Dortmund, Dortmund, Germany

44 Institut für Kern- und Teilchenphysik, Technische Universität Dresden, Dresden, Germany

45 Department of Physics, Duke University, Durham, NC, USA

46 SUPA-School of Physics and Astronomy, University of Edinburgh, Edinburgh, UK

47 INFN Laboratori Nazionali di Frascati, Frascati, Italy

48 Fakultät für Mathematik und Physik, Albert-Ludwigs-Universität, Freiburg, Germany

49 Section de Physique, Université de Genève, Geneva, Switzerland

50 (a) INFN Sezione di Genova, Genova, Italy; (b) Dipartimento di Fisica, Università di Genova, Genova, Italy

51 (a) E. Andronikashvili Institute of Physics, Iv. Javakhishvili Tbilisi State University, Tbilisi, Georgia; (b) High Energy Physics Institute, Tbilisi State University, Tbilisi, Georgia

52 II Physikalisches Institut, Justus-Liebig-Universität Giessen, Giessen, Germany

53 SUPA-School of Physics and Astronomy, University of Glasgow, Glasgow, UK

54 II Physikalisches Institut, Georg-August-Universität, Göttingen, Germany

55 Laboratoire de Physique Subatomique et de Cosmologie, Université Grenoble-Alpes, CNRS/IN2P3, Grenoble, France

56 Department of Physics, Hampton University, Hampton, VA, USA

57 Laboratory for Particle Physics and Cosmology, Harvard University, Cambridge, MA, USA

58 (a) Kirchhoff-Institut für Physik, Ruprecht-Karls-Universität Heidelberg, Heidelberg, Germany; (b) Physikalisches Institut, Ruprecht-Karls-Universität Heidelberg, Heidelberg, Germany; (c) ZITI Institut für technische Informatik, Ruprecht-Karls-Universität Heidelberg, Mannheim, Germany

59 Faculty of Applied Information Science, Hiroshima Institute of Technology, Hiroshima, Japan

60 (a) Department of Physics, The Chinese University of Hong Kong, Shatin, NT, Hong Kong; (b) Department of Physics, The University of Hong Kong, Pok Fu Lam, Hong Kong; (c) Department of Physics, The Hong Kong University of Science and Technology, Clear Water Bay, Kowloon, Hong Kong, China

61 Department of Physics, Indiana University, Bloomington, IN, USA

62 Institut für Astro- und Teilchenphysik, Leopold-Franzens-Universität, Innsbruck, Austria

63 University of Iowa, Iowa City, IA, USA

64 Department of Physics and Astronomy, Iowa State University, Ames, IA, USA

65 Joint Institute for Nuclear Research, JINR Dubna, Dubna, Russia

66 KEK, High Energy Accelerator Research Organization, Tsukuba, Japan

67 Graduate School of Science, Kobe University, Kobe, Japan

68 Faculty of Science, Kyoto University, Kyoto, Japan

69 Kyoto University of Education, Kyoto, Japan

70 Department of Physics, Kyushu University, Fukuoka, Japan

71 Instituto de Física La Plata, Universidad Nacional de La Plata and CONICET, La Plata, Argentina

72 Physics Department, Lancaster University, Lancaster, UK

73 (a) INFN Sezione di Lecce, Lecce, Italy; (b) Dipartimento di Matematica e Fisica, Università del Salento, Lecce, Italy

74 Oliver Lodge Laboratory, University of Liverpool, Liverpool, UK

75 Department of Physics, Jožef Stefan Institute and University of Ljubljana, Ljubljana, Slovenia

76 School of Physics and Astronomy, Queen Mary University of London, London, UK

77 Department of Physics, Royal Holloway University of London, Surrey, UK

78 Department of Physics and Astronomy, University College London, London, UK

79 Louisiana Tech University, Ruston, LA, USA

80 Laboratoire de Physique Nucléaire et de Hautes Energies, UPMC and Université Paris-Diderot and CNRS/IN2P3, Paris, France

81 Fysiska institutionen, Lunds universitet, Lund, Sweden

82 Departamento de Fisica Teorica C-15, Universidad Autonoma de Madrid, Madrid, Spain

83 Institut für Physik, Universität Mainz, Mainz, Germany

84 School of Physics and Astronomy, University of Manchester, Manchester, UK

85 CPPM, Aix-Marseille Université and CNRS/IN2P3, Marseille, France

86 Department of Physics, University of Massachusetts, Amherst, MA, USA

87 Department of Physics, McGill University, Montreal, QC, Canada

88 School of Physics, University of Melbourne, Melbourne, VIC, Australia

89 Department of Physics, The University of Michigan, Ann Arbor, MI, USA

90 Department of Physics and Astronomy, Michigan State University, East Lansing, MI, USA

91 (a) INFN Sezione di Milano, Milan, Italy; (b) Dipartimento di Fisica, Università di Milano, Milan, Italy

92 B.I. Stepanov Institute of Physics, National Academy of Sciences of Belarus, Minsk, Republic of Belarus

93 National Scientific and Educational Centre for Particle and High Energy Physics, Minsk, Republic of Belarus

94 Department of Physics, Massachusetts Institute of Technology, Cambridge, MA, USA

95 Group of Particle Physics, University of Montreal, Montreal, QC, Canada

96 P.N. Lebedev Institute of Physics, Academy of Sciences, Moscow, Russia

97 Institute for Theoretical and Experimental Physics (ITEP), Moscow, Russia

98 National Research Nuclear University MEPhI, Moscow, Russia

99 D.V. Skobeltsyn Institute of Nuclear Physics, M.V. Lomonosov Moscow State University, Moscow, Russia

100 Fakultät für Physik, Ludwig-Maximilians-Universität München, Munich, Germany

101 Max-Planck-Institut für Physik (Werner-Heisenberg-Institut), Munich, Germany

102 Nagasaki Institute of Applied Science, Nagasaki, Japan

103 Graduate School of Science and Kobayashi-Maskawa Institute, Nagoya University, Nagoya, Japan

104 (a) INFN Sezione di Napoli, Naples, Italy; (b) Dipartimento di Fisica, Università di Napoli, Naples, Italy

105 Department of Physics and Astronomy, University of New Mexico, Albuquerque, NM, USA

106 Institute for Mathematics, Astrophysics and Particle Physics, Radboud University Nijmegen/Nikhef, Nijmegen, The Netherlands

107 Nikhef National Institute for Subatomic Physics and University of Amsterdam, Amsterdam, The Netherlands

108 Department of Physics, Northern Illinois University, De Kalb, IL, USA

[109] Budker Institute of Nuclear Physics, SB RAS, Novosibirsk, Russia

[110] Department of Physics, New York University, New York, NY, USA

[111] Ohio State University, Columbus, OH, USA

[112] Faculty of Science, Okayama University, Okayama, Japan

[113] Homer L. Dodge Department of Physics and Astronomy, University of Oklahoma, Norman, OK, USA

[114] Department of Physics, Oklahoma State University, Stillwater, OK, USA

[115] Palacký University, RCPTM, Olomouc, Czech Republic

[116] Center for High Energy Physics, University of Oregon, Eugene, OR, USA

[117] LAL, Université Paris-Sud and CNRS/IN2P3, Orsay, France

[118] Graduate School of Science, Osaka University, Osaka, Japan

[119] Department of Physics, University of Oslo, Oslo, Norway

[120] Department of Physics, Oxford University, Oxford, UK

[121] [a] INFN Sezione di Pavia, Pavia, Italy; [b] Dipartimento di Fisica, Università di Pavia, Pavia, Italy

[122] Department of Physics, University of Pennsylvania, Philadelphia, PA, USA

[123] Petersburg Nuclear Physics Institute, Gatchina, Russia

[124] [a] INFN Sezione di Pisa, Pisa, Italy; [b] Dipartimento di Fisica E. Fermi, Università di Pisa, Pisa, Italy

[125] Department of Physics and Astronomy, University of Pittsburgh, Pittsburgh, PA, USA

[126] [a] Laboratorio de Instrumentacao e Fisica Experimental de Particulas-LIP, Lisbon, Portugal; [b] Faculdade de Ciências, Universidade de Lisboa, Lisbon, Portugal; [c] Department of Physics, University of Coimbra, Coimbra, Portugal; [d] Centro de Física Nuclear da Universidade de Lisboa, Lisbon, Portugal; [e] Departamento de Fisica, Universidade do Minho, Braga, Portugal; [f] Departamento de Fisica Teorica y del Cosmos and CAFPE, Universidad de Granada, Granada, Spain; [g] Dep Fisica and CEFITEC of Faculdade de Ciencias e Tecnologia, Universidade Nova de Lisboa, Caparica, Portugal

[127] Institute of Physics, Academy of Sciences of the Czech Republic, Prague, Czech Republic

[128] Czech Technical University in Prague, Prague, Czech Republic

[129] Faculty of Mathematics and Physics, Charles University in Prague, Prague, Czech Republic

[130] State Research Center Institute for High Energy Physics, Protvino, Russia

[131] Particle Physics Department, Rutherford Appleton Laboratory, Didcot, UK

[132] Ritsumeikan University, Kusatsu, Shiga, Japan

[133] [a] INFN Sezione di Roma, Rome, Italy; [b] Dipartimento di Fisica, Sapienza Università di Roma, Rome, Italy

[134] [a] INFN Sezione di Roma Tor Vergata, Rome, Italy; [b] Dipartimento di Fisica, Università di Roma Tor Vergata, Rome, Italy

[135] [a] INFN Sezione di Roma Tre, Rome, Italy; [b] Dipartimento di Matematica e Fisica, Università Roma Tre, Rome, Italy

[136] [a] Faculté des Sciences Ain Chock, Réseau Universitaire de Physique des Hautes Energies-Université Hassan II, Casablanca, Morocco; [b] Centre National de l'Energie des Sciences Techniques Nucleaires, Rabat, Morocco; [c] Faculté des Sciences Semlalia, Université Cadi Ayyad, LPHEA-Marrakech, Marrakech, Morocco; [d] Faculté des Sciences, Université Mohamed Premier and LPTPM, Oujda, Morocco; [e] Faculté des Sciences, Université Mohammed V-Agdal, Rabat, Morocco

[137] DSM/IRFU (Institut de Recherches sur les Lois Fondamentales de l'Univers), CEA Saclay (Commissariat à l'Energie Atomique et aux Energies Alternatives), Gif-sur-Yvette, France

[138] Santa Cruz Institute for Particle Physics, University of California Santa Cruz, Santa Cruz, CA, USA

[139] Department of Physics, University of Washington, Seattle, WA, USA

[140] Department of Physics and Astronomy, University of Sheffield, Sheffield, UK

[141] Department of Physics, Shinshu University, Nagano, Japan

[142] Fachbereich Physik, Universität Siegen, Siegen, Germany

[143] Department of Physics, Simon Fraser University, Burnaby, BC, Canada

[144] SLAC National Accelerator Laboratory, Stanford, CA, USA

[145] [a] Faculty of Mathematics, Physics and Informatics, Comenius University, Bratislava, Slovak Republic; [b] Department of Subnuclear Physics, Institute of Experimental Physics of the Slovak Academy of Sciences, Kosice, Slovak Republic

[146] [a] Department of Physics, University of Cape Town, Cape Town, South Africa; [b] Department of Physics, University of Johannesburg, Johannesburg, South Africa; [c] School of Physics, University of the Witwatersrand, Johannesburg, South Africa

[147] [a] Department of Physics, Stockholm University, Stockholm, Sweden; [b] The Oskar Klein Centre, Stockholm, Sweden

[148] Physics Department, Royal Institute of Technology, Stockholm, Sweden

[149] Departments of Physics and Astronomy and Chemistry, Stony Brook University, Stony Brook, NY, USA

[150] Department of Physics and Astronomy, University of Sussex, Brighton, UK

[151] School of Physics, University of Sydney, Sydney, Australia

[152] Institute of Physics, Academia Sinica, Taipei, Taiwan

[153] Department of Physics, Technion: Israel Institute of Technology, Haifa, Israel

[154] Raymond and Beverly Sackler School of Physics and Astronomy, Tel Aviv University, Tel Aviv, Israel

[155] Department of Physics, Aristotle University of Thessaloniki, Thessaloniki, Greece

[156] International Center for Elementary Particle Physics and Department of Physics, The University of Tokyo, Tokyo, Japan

[157] Graduate School of Science and Technology, Tokyo Metropolitan University, Tokyo, Japan

[158] Department of Physics, Tokyo Institute of Technology, Tokyo, Japan

[159] Department of Physics, University of Toronto, Toronto, ON, Canada

[160] (a) TRIUMF, Vancouver, BC, Canada; (b) Department of Physics and Astronomy, York University, Toronto, ON, Canada

[161] Faculty of Pure and Applied Sciences, University of Tsukuba, Tsukuba, Japan

[162] Department of Physics and Astronomy, Tufts University, Medford, MA, USA

[163] Centro de Investigaciones, Universidad Antonio Narino, Bogota, Colombia

[164] Department of Physics and Astronomy, University of California Irvine, Irvine, CA, USA

[165] (a) INFN Gruppo Collegato di Udine, Sezione di Trieste, Udine, Italy; (b) ICTP, Trieste, Italy; (c) Dipartimento di Chimica, Fisica e Ambiente, Università di Udine, Udine, Italy

[166] Department of Physics, University of Illinois, Urbana, IL, USA

[167] Department of Physics and Astronomy, University of Uppsala, Uppsala, Sweden

[168] Instituto de Física Corpuscular (IFIC) and Departamento de Física Atómica, Molecular y Nuclear and Departamento de Ingeniería Electrónica and Instituto de Microelectrónica de Barcelona (IMB-CNM), University of Valencia and CSIC, Valencia, Spain

[169] Department of Physics, University of British Columbia, Vancouver, BC, Canada

[170] Department of Physics and Astronomy, University of Victoria, Victoria, BC, Canada

[171] Department of Physics, University of Warwick, Coventry, UK

[172] Waseda University, Tokyo, Japan

[173] Department of Particle Physics, The Weizmann Institute of Science, Rehovot, Israel

[174] Department of Physics, University of Wisconsin, Madison, WI, USA

[175] Fakultät für Physik und Astronomie, Julius-Maximilians-Universität, Würzburg, Germany

[176] Fachbereich C Physik, Bergische Universität Wuppertal, Wuppertal, Germany

[177] Department of Physics, Yale University, New Haven, CT, USA

[178] Yerevan Physics Institute, Yerevan, Armenia

[179] Centre de Calcul de l'Institut National de Physique Nucléaire et de Physique des Particules (IN2P3), Villeurbanne, France

[a] Also at Department of Physics, King's College London, London, UK

[b] Also at Institute of Physics, Azerbaijan Academy of Sciences, Baku, Azerbaijan

[c] Also at Novosibirsk State University, Novosibirsk, Russia

[d] Also at TRIUMF, Vancouver, BC, Canada

[e] Also at Department of Physics, California State University, Fresno, CA, USA

[f] Also at Department of Physics, University of Fribourg, Fribourg, Switzerland

[g] Also at Departamento de Fisica e Astronomia, Faculdade de Ciencias, Universidade do Porto, Porto, Portugal

[h] Also at Tomsk State University, Tomsk, Russia

[i] Also at CPPM, Aix-Marseille Université and CNRS/IN2P3, Marseille, France

[j] Also at Università di Napoli Parthenope, Naples, Italy

[k] Also at Institute of Particle Physics (IPP), Victoria, Canada

[l] Also at Particle Physics Department, Rutherford Appleton Laboratory, Didcot, UK

[m] Also at Department of Physics, St. Petersburg State Polytechnical University, St. Petersburg, Russia

[n] Also at Louisiana Tech University, Ruston, LA, USA

[o] Also at Institucio Catalana de Recerca i Estudis Avancats, ICREA, Barcelona, Spain

[p] Also at Department of Physics, National Tsing Hua University, Hsinchu, Taiwan

[q] Also at Department of Physics, The University of Texas at Austin, Austin, TX, USA

[r] Also at Institute of Theoretical Physics, Ilia State University, Tbilisi, Georgia

[s] Also at CERN, Geneva, Switzerland

[t] Also at Georgian Technical University (GTU), Tbilisi, Georgia

[u] Also at Ochadai Academic Production, Ochanomizu University, Tokyo, Japan

[v] Also at Manhattan College, New York, NY, USA

[w] Also at Institute of Physics, Academia Sinica, Taipei, Taiwan

[x] Also at LAL, Université Paris-Sud and CNRS/IN2P3, Orsay, France

[y] Also at Academia Sinica Grid Computing, Institute of Physics, Academia Sinica, Taipei, Taiwan

[z] Also at School of Physics, Shandong University, Shandong, China

[aa] Also at Moscow Institute of Physics and Technology State University, Dolgoprudny, Russia

[ab] Also at Section de Physique, Université de Genève, Geneva, Switzerland

[ac] Also at International School for Advanced Studies (SISSA), Trieste, Italy

[ad] Also at Department of Physics and Astronomy, University of South Carolina, Columbia, SC, USA

[ae] Also at School of Physics and Engineering, Sun Yat-sen University, Guangzhou, China

[af] Also at Faculty of Physics, M.V. Lomonosov Moscow State University, Moscow, Russia

[ag] Also at National Research Nuclear University MEPhI, Moscow, Russia

[ah] Also at Department of Physics, Stanford University, Stanford, CA, USA

[ai] Also at Institute for Particle and Nuclear Physics, Wigner Research Centre for Physics, Budapest, Hungary

[aj] Also at Department of Physics, The University of Michigan, Ann Arbor, MI, USA

[ak] Also at Discipline of Physics, University of KwaZulu-Natal, Durban, South Africa

[al] Also at University of Malaya, Department of Physics, Kuala Lumpur, Malaysia

[*] Deceased